Ultrafast light-induced dynamics of spins and lattice

in iron oxides

Alexandra Mikhailovna Kalashnikova

Printed by Ipskamp Drukkers, Enschede, The Netherlands
ISBN/EAN 978-90-9024041-1

Illustrated with references.
Cover design by A. M. Kalashnikova.

Ultrafast light-induced dynamics of spins and lattice

in iron oxides

Een wetenschappelijke proeve op het gebied van
de Natuurwetenschappen, Wiskunde & Informatica

Proefschrift

ter verkrijging van de graad van doctor
aan de Radboud Universiteit Nijmegen
op gezag van de rector magnificus prof. mr. S. C. J. J. Kortmann,
volgens besluit van het college van decanen
in het openbaar te verdedigen op woensdag 1 april 2009
om 15:30 uur precies

door

Alexandra Mikhailovna Kalashnikova

geboren op 12 mei 1980
te Leningrad, Sovjetunie

Promotores	: Prof. dr. Th. Rasing	
	: Prof. dr. R. V. Pisarev	Ioffe Physico-Technical Institute of the Russian Academy of Sciences, St.-Petersburg, Russia
Copromotores	: Dr. A. Kirilyuk	
	: Dr. A. V. Kimel	

Manuscriptcommissie:

Prof. dr. J. C. Maan	
Prof. dr. R. Merlin	Department of Physics University of Michigan
Prof. dr. P. M. Oppeneer	Department of Physics and Material Science Uppsala University

The work described in this thesis was financially supported by the Dutch Nanotechnology Network Nanoned and the Russian Foundation for Basic Research.

to my parents and grandparents with love and gratitude

Preface

Well, it is almost done! And now it is the time to summarize four years of my ph.d. studies and ph.d. life in Nijmegen. In brief, it was great! And on the next couple of pages I'll try to explain why...

Well, this all started long time ago - in spring 2002, and quite far away from here - in my home city of St. Petersburg, where I joined the group of prof. dr. Roman Pisarev in Ioffe Institute during my undergraduate studies, and where a year later I stared my ph.d. study. Despite of the difficult financial situation, in which Ioffe Institute was at that time, prof. Pisarev was looking for every possibility for his co-workers, and me in particular, to collaborate with European researchers and to do a scientific research on a high level. Let is how one day I've got to Nijmegen, where I was invited to visit for three month the group of prof. Theo Rasing. And then I got a kind of offer, which was difficult to refuse. A continuation of my ph.d. studies here in Nijmegen was a very tempting idea because of very good opportunities, provided by this group, and, which is equally important, because of the people, who are working here. So, I agreed to stay and finish my study in two years. At the end, it turned out to be four years instead of two, but it is not a point now...

First of all, I would like to thank prof. Theo Rasing for giving me an opportunity to work here and for being such an enthusiastic and active supervisor and also very interesting and kind person. Also, I thank prof. Roman Pisarev for letting me stay in Nijmegen and for continuing helping me with advises, guidance and criticism. In the lab, the supervision of dr. Alexey Kimel and dr. Andrey Kirilyuk can not be overestimated. But also, they helped me a lot with settling down in this group and in Nijmegen in general.

I'm very happy that I got an opportunity to work in the group of Spectroscopy of Solids and Interfaces (former Experimental Physics of Solid State II) and in particular, in the part, working on a light-induced magnetization dynamics. One of the reasons for this is a spirit, a combination of curiosity, enthusiasm and persistence, by which I was impressed when I came to Nijmegen for a first time. It appeared to be both challenging and pleasant to work with people who have, besides high expertise, also a high determination towards what they are doing. First of all, it concerns my supervisors from Nijmegen Theo Rasing, Andrey Kirilyuk and Alexey Kimel and prof. Roman Pisarev from Ioffe Institute. During these four years I had to learn a lot about science. About everything in science: how to perform a proper and fruitful experiment, how to treat and explain data, how to write something convincing about it and, finally, how to present you research in such a way, that it will be interesting and fascinating for a broad scientific community. And here in Nijmegen I was given an opportunity to learn all these. I would like to thank Alexey Kimel for guiding me and explaining me a lot of tiny but very important details about pump-probe experiments and Andrey Kirilyuk for sharing with me his expertise in second harmonic generation

experiments and magnetic domain imaging. Also I would like to thank Theo, Andrey and Alexey for patiently teaching me how to give a good presentation, which was and still is a big challenge for me. I also highly appreciate all help, criticism and advises which I got from all my supervisors during a long and difficult process of writing articles and this thesis. I specially acknowledge an effort Theo made to translate the summary of this thesis into Dutch.

I also learned a lot from our collaboration with dr. Valery Gridnev from Ioffe Institute in St. Petersburg, with whom we were working out a theoretical explanation of results, obtained in our experiments. I think that it is a critical opinion of dr. Gridnev that helped a lot in a thorough understanding of our experimental observations and bringing our work to a high scientific level.

I would like to express my gratitude to the technicians of SSI and SPM groups. I thank Albert van Etteger for pointing out all mistakes that I was making in the lab and for explaining patiently how to work with laser technics in such a way that nothing would be broken. I'm grateful to Tonnie Toonen for his kind and prompt help with all necessary mechanical details. I thank Jan Hermsen for the help with a vacuum equipment and Jan Gerritsen for solving internet connection problems when I just arrived.

It was always interesting and useful to discuss problems and ideas during dynamics meetings with Alexey, Andrey, Fredrik, Daniel, Loic and Jan, who were there when I just joined the group, and new people such as Kadir, Alex, Fred, Ilie, Addis, Johan de Jong, Johan Mentink and Dimitry.

It was very interesting to work in a lab with Victor Pavlov from Ioffe Institute, who taught me basics of experimental work and of LabView programming long time ago during my undergraduate studies, Andrej Stupakiewicz from University of Bialystok, Roman Khramovskikh, who was a master student in our group, Pavel Usachev from Ioffe Institute, Kadir Vahaplar, Alex Reid, Ilie Radu, Elena Mishina and Oleg Shklyarevsky. I also appreciated working with Chris van Dijk during a construction of a "chaos and order"setup.

This world, at least its big part, would turn into a chaos for me without two very important ladies - Marilou and Riki. Marilou, thanks a lot for you kindness and patience in helping with all kind of troubles and never-ending "what should I do if...."and "whom should I call if...". And Riki, it was always amazing how fast and precise you could give an answer or at least a hint regarding a lot of different administrative issues, which looked extremely complicated for me. I also thank Marilou for taking care about Dutch translation of the summary of this thesis.

Another important reason, why I enjoyed so much my ph.d. life here in Nijmegen is the people from SSI and SPM groups, who's attitude and optimism could make even such a terrifying event as a moving to a new building relaxed and funny! I always enjoyed our group activities, such as gluhwijn parties supervised by Oleg Shklyarevskii; days-out organized by Jan Versluis (and me), and Fresia and Johan and Marilou

(who is always responsible for a musical part!); traditional beginning-of-summer barbeques, organized by Theo and Maria; season-food parties at Marilou's place and a lot of other events, where all people from SSI and SPM groups were getting together. It was always fun!

The work in the big international group might be difficult sometimes, but it is never boring and most of the time it is a great fun and unforgettable experience. Where else can you every day drink a coffee with people from Netherlands, Cameroon, Australia, Serbia, Ukraine, Romania, China, Norway, Poland, Russia, France, Ireland, Germany, Ethiopia, Turkey, Costa Rica, Bulgaria, White Russia, Japan, Korea... Incredible! It takes some effort regarding a level of your English language (hi, Chris!), but this experience worth a lot! Thanks to all people who are or were around all these four years.

I'm very happy to express my appreciation to the people with whom I was shearing the office during all these years. I thank you all, Fred, Duncan, Natascha, Sergiy, Eric, Weizhe, Grzegorz, for being such interesting people. I enjoyed so much our discussions about everything one can imagine: physics, politics (hi, Sergiy!), relationships ...and a bit of gossiping, of cause.

It was very interesting and absolutely new experience for me to be involved in filming the Cribs episode for Riki The Movie. It was a lot of fun, thanks to script-writers Duncan and Joris, director Tim, film crew Minko, Albert and Tonnie and invited star Theo. By the way, talking about arts, it was great to visit the play directed by Duncan, to enjoy Christmas and Easter songs performed by choir of Marilou, to attend the concerts given by the orchestra in which Joris plays, and even to take part in the performance of the orchestra of Jan Gerritsen. It was a lot of fun to go to concerts with Roman and Loic and, of cause, how can I forget three-days camping under the rain at PinkPop festival with Jelena and Loic!

A lot of unforgettable events, such as skiing, kanou trip, carting, paintball, bike trips, picnics, barbecues wouldn't be possible without people, who at different time were organizing them. Roman, Chris, Gabi, Jelena, Loic, Sergiy, Marina, it is great that you have enough will and energy to look for a new adventures, push thing forward and fight a boredom. And something would be missing without going out on Thursday, Friday, Saturday end even sometimes Monday nights with Kadir, Jelena, Fresia, Chris, Loic, Roman, Gabi, Fred, Sergiy, Lucian, Steven, Marina, Jing, Michiel, Minko, Sondes, Delphine, Gerald, Edgar, Matheuw, and many other people who sometimes were joining us. It was also always nice to have dinners together with Gabi and Gwilherm, Marina and Erdni, Jing and Bas.

When I made a decision to leave St. Petersburg and to come to Nijmegen for Ph.D. studies, it looked quite easy - just a pleasant adventure few thousands kilometers away from home. But it would turn out to be much more difficult, than I thought, without the hospitality and warm welcome from Andrey and Viktoria Kirilyuk, Alexey and Olga Kimel, and Roman and Oksana Shantyr. I would like also to thank Theo and

Maria for their kind hospitality!

And I cannot miss the opportunity to thank girls of SSI and SPM groups without whom my Nijmegen experience would not be so great and would be, most probably, more difficult. It was a big pleasure to meet such interesting personalities like you, Gabi, Jelena, Marina, Fresia, Jing, Natascha! I really enjoyed your company. I thank you all for your support, understanding and friendship!

In the end I would like to thank the most important people in my life - my parents and my grandparents, who were taking care about my education during my school studies. And also I would like to thank them for their love and support which were always important and valuable for me. And this work became possible also because of all that they gave me. And the last but not the least, I want to thank a very special man, my boyfriend Andrey, for his love, patience, trust and support.

Alexandra Kalashnikova
Nijmegen, February 9, 2009.

Contents

CHAPTER 1

Ultrafast light-induced spin dynamics: achievements and challenges

In this chapter the recent developments in modern magnetism, in particular, ultrafast spin dynamics, are discussed as an introduction for the main topic of this thesis: the ultrafast excitation of coherent spin dynamics by polarized subpicosecond laser pulses.

1.1 Problems of modern magnetism

The role of processing, recording and storage of data is increasing continuously and rapidly in all fields of life, from daily needs to laboratory experiments at frontiers of science. Nowadays one of the basic concepts for data storage is a magnetic hard disc drive, where bits of information are stored in oppositely oriented domains in the magnetically ordered material [1]. The unique properties of magnets are, furthermore, not only used for storage of data. Nowadays, the reading process in a conventional hard-disk drive is based on the phenomenon of giant magnetoresistivity [2, 3], which is the difference of the electric resistivity of a structure consisting of nanometer thin metallic layers with parallel or antiparallel orientation of the magnetization. For the further development of magnetic storage devices, however, researchers and engineers are facing a number of challenges, the overcoming of which requires the deepest understanding of the physics of magnetism and the related fundamental limits for dynamical processes in a magnetic medium.

One of these challenges is the increase of the data density of storage devices.

Indeed, the size of a single domain in a conventional magnetic memory device is approaching the so-called "superparamagnetic limit"[4], below which the orientation of the magnetic moment of the domain is instable due to thermal fluctuations. Therefore, there is an intensive search for new recording media which properties would allow to decrease the bit size without hitting this limit [5]. Parallel to this are the development of perpendicular magnetic recording instead of longitudinal [6] and heat assisted magnetic recording [7]. Moreover, in order to decrease the bit size, not only a proper medium should be found but also a proper way to write data in such tiny domains is required. Indeed, the writing process should be realized in such a way that only one bit is written without affecting the neighboring ones. The latter problem is closely related to the another challenge in data recording, which is the speed limit for data writing. While the approaches mentioned above in principle will allow a further decrease of the bit size, the problem of increase of the data recording speed is still open.

Applying a magnetic field is a straightforward way to manipulate and, in particular, reverse the magnetization of a medium. The speed of this process is limited by the strength and duration of the magnetic field pulse and the response time of the magnetization to this pulse. The generation of well defined (with sharp front and back edges) magnetic field pulses of sufficient amplitude, with duration below 100 ps (1 ns in current devices) is still a challenge nowadays [1]. Meanwhile, competing technologies, such as solid state memory, are much ahead in what concerns the writing speed [8]. Therefore, alternative ways of changing and controlling the magnetization on an ultrafast time scale are subject of intense studies during the last decade. Along with alternative techniques to generate short magnetic field pulses, such as electro-optical current switches [9, 10, 11] or relativistic electron bunches [12], searches and studies of fundamentally different mechanisms to influence spins are actively conducted.

One of these "alternative"mechanisms is the excitation of a spin state or even switching of the magnetization of a multilayer element by a spin-polarized current [13], first proposed theoretically in 1996 [14, 15]. This method is very well compatible with the spin-valve concept for a magnetic random access memory (MRAM) [16]. In principle, it allows not only to increase the speed of data recording, but to decrease the bit size as well [17]. Nevertheless, the time scale is still much longer than 100 ps. Interestingly, the latter time has been proposed [1] to be the limit below which the processes in a magnetic medium can be referred to as *"ultrafast magnetization dynamics*". Indeed, this time is a typical intrinsic spin-lattice relaxation time [18]. At this and longer timescales, thermodynamical models can be applied to explain the subsequent processes.

Therefore, the exploration of the spin dynamics at time scales below 100 ps is a most challenging and intriguing issue. Remarkable experimental results were published in 1996, showing the picosecond demagnetization of a Ni film induced by 60 fs laser pulses [19]. This evidence of demagnetization taking place within the first pi-

cosecond after the laser excitation triggered a surge of experimental and theoretical studies of laser induced magnetization dynamics, the ultimate goal of which is the all-optical ultrafast control of magnetization by short (tens of femtoseconds) laser pulses. The experimental observations [19, 20] suggest that, when studying ultrafast light-induced magnetization dynamics, one has to deal with time scales which are orders of magnitude shorter than 1 ps. As will be shown in the following overview, "*ultrafast light-induced spin dynamics*" operates at much shorter time scales than magnetic field-induced and even current-induced ones, and its understanding is far from complete due to a number of unresolved fundamental issues. These issues, discussed below, involve the mechanisms and time scales of the transfer of energy and angular momentum in the magnetic medium subjected to the short laser pulses.

Since 1996 studies of ultrafast light-induced magnetization dynamics resulted in a large number of experimental observations and a somewhat smaller number of theoretical attempts to describe these observations and to predict new effects. In the following Section 1.2 we briefly discuss which types of spin dynamics can be induced by laser pulses, starting from ultrafast demagnetization, which is the most known and studied process, to the recently observed and intriguing all-optical magnetization reversal. There are different microscopic mechanisms that lead to the excitation of spin dynamics. Moreover, different microscopic mechanisms can manifest themselves in similar experimental observations. In particular, coherent spin precession is known to be the result of at least four different microscopic processes, depending on such conditions as electronic and magnetic structure and the optical properties of the medium. The main objective of this thesis is to study the most interesting and the least understood process, which is often referred to as *non-thermal* or *opto-magnetic*. The present understanding of such a mechanism and the questions connected with it are discussed in Section 1.3. Other known or proposed mechanisms of light-induced spin dynamics are also briefly described in that Section, where we present a summary regarding the type of medium in which they can be observed. This thesis focuses on spin dynamics in dielectric materials, which are the best candidates to reach our objectives.

1.2 From ultrafast demagnetization to all-optical switching

After the pioneering experiments on ultrafast light-induced demagnetization [19], experimental and theoretical efforts of many research groups resulted in the discovery of a large number of light-induced ultrafast processes in magnetic media. Thus, along with ultrafast demagnetization it was found that ultrashort laser pulses can induce coherent spin precession, phase transitions of various kinds, such as spin reorientation or transition between phases with different types of the magnetic ordering, and even a full 180° magnetization reorientation. There are, however, several important issues which should be addressed before it would be possible to claim that the interactions

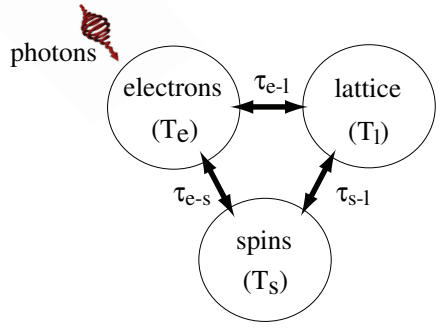

Figure 1.1: (a) Three-temperature model for the light-induced spin dynamics suggested for a ferromagnetic metal (after [1]). T_e, T_s and T_l are the effective temperatures of electron, spin and lattice reservoirs, respectively. τ are the relaxation times for the equilibration between the electrons and spins (τ_{e-s}), electrons and lattice (τ_{e-l}) and spins and lattice(τ_{s-l}).

of subpicosecond laser pulses with a magnetic medium are understood.

1.2.1 Ultrafast demagnetization and the three-temperature model

As it was mentioned above, the first successful experimental demonstration of ultrafast light-induced spin dynamics was the picosecond demagnetization of a Ni film [19], although attempts to observe this had been made before [21]. The loss of magnetic ordering caused by the interaction of a laser pulse with a metallic ferromagnetic film was explained on the basis of a so-called *three-temperature model* (Fig. 1.1). This became since then one of the standard concepts in the discussions of the effects of laser pulses on a spin system [1, 19, 22]. In brief, the idea behind this model is the following. For the excitation of spin dynamics, energy and angular momentum should be transferred to or from the spin subsystem. The energy transfer is considered in terms of an increase of the spin temperature ΔT_s and intense laser pulses serve as a source of the required energy. Generally speaking, this energy can be deposited into all three reservoirs, depicted in Fig. 1.1. However, in the spectral range where laser sources of sub-picosecond pulses typically work (near infrared and visible range), optical transitions possess an electric-dipole character and, therefore, do not lead to a change of the electron (or hole) spin. Besides this, the direct deposition of photon energy to the lattice is effective only in the far-infrared spectral range, where excitation of phonons via absorption is observed [23]. Therefore, the energy supplied by a laser

pulse has to be first deposited into the electron reservoir, causing an increase of its effective temperature T_e, as depicted in Fig. 1.1. Then the energy can be transferred to the spin reservoir via electron-spin interaction or first to the lattice and then to the spins via electron-lattice and spin-lattice interactions.

The scheme in Fig. 1.1 reflects only the channels for energy transfer. The flow of the angular momentum to and from the spin system, required for the demagnetization and for the excitation of spin dynamics in general, must end up in the lattice, but the specific channels involved, their efficiency and characteristic times are still under discussion nowadays [1, 20, 22, 24, 25, 26]. It remains controversial, what are the sources and/or sinks of angular momentum in the experiments on light-induced demagnetization. Can *circularly* polarized photons play a role? Or, instead, can light may be serve as a mediator for the angular momentum transfer between the spin, electron and lattice reservoirs?

Due to the short duration of the laser pulses used in modern experiments on spin dynamics, and the intriguing experimental observations, demonstrating response of the spins on subpicosecond time scales, the characteristic times of these interactions are of particular interest. Moreover, the response of electrons, spins and lattice to the intense and very short impact of the laser pulses is well beyond the framework of a thermodynamical approach. Indeed, the characteristic equilibration times of each subsystem [27] after excitation, as well as the times of their mutual interactions, are different and can be much longer than the typical time resolution of the pump-probe magneto-optical measurements. Therefore, the interpretation of the experimental data using standard magneto-optical theory, developed for systems in thermodynamical equilibrium, may not be valid anymore [24, 28, 29]. Consequently, developing novel approaches for the interpretation of the experimental data and new methods of measuring the ultrafast spin dynamics [20, 30] are a major challenge nowadays and a focus of the present thesis.

1.2.2 Light-induced phase transitions

Ultrafast light-induced demagnetization can be considered as a light-induced phase transition from the magnetically-ordered to the paramagnetic phase. During recent years a number of other phase transitions driven by subpicosecond laser pulses were observed experimentally [31, 32, 33, 34, 35].

For example, in the metallic antiferromagnet FeRh a light-induced appearance and growth of a ferromagnetic phase was observed and actively studied. This material is known to possess a transition from an antiferromagnetic to a ferromagnetic phase, as the temperature is increased across the transition point T_p. It was shown by two groups independently [31, 32], that the onset of ferromagnetism takes place on the sub-picosecond time scale after the excitation by a short laser pulse and is followed by a slower $\sim$30 ps increase. It is driven by the increase of the spin temperature accom-

panied by a change of local exchange interactions between the Fe and Rh magnetic moments.

Another type of light-induced phase transition has been observed in the dielectric antiferromagnet $TmFeO_3$. In this material, a 90° spin reorientation takes place as the temperature is increased from 80 to 91 K, which is related to the strong dependence of the magneto-crystalline anisotropy on temperature. Therefore, if the material is in this temperature range, an increase of the lattice temperature caused by a short laser pulse can lead to the spin reorientation, as was experimentally demonstrated in [33].

1.2.3 Light-induced coherent spin precession: beyond the three-temperature model

The processes described above are often accompanied by an excitation of coherent spin precession. Various mechanisms can lead to this. For example, the ultrafast demagnetization in thin metallic films leads to a decrease of the shape anisotropy [36]. This, in turn, changes the net effective field defining the orientation of the magnetization in the sample and, therefore, leads to the excitation of magnetization precession, as schematically shown in Fig. 1.2 (a). The inverse process, i.e. the excitation of coherent spin precession due to the increase of the demagnetizing field, accompanying the light-induced buildup of ferromagnetic ordering, was observed in FeRh [35]. In general, laser-induced heating can affect both shape and magneto-crystalline anisotropy in magnetic films and, thus, excite magnetization precession [37]. The spin reorientation phase transition in the dielectric $TmFeO_3$ also manifests itself in coherent precession of the spins around the new equilibrium, as shown in Fig.1.2(b) [33]. These excitation mechanisms of spin precession rely on the increase of the temperature of electron, spin and/or lattice reservoirs, depicted in Fig.1.1. Because of this, they are often referred to as *thermal* mechanisms of excitation of spin precession.

Recently, however, a few experimental observations revealed that short laser pulses can have an impact on a magnetic system that is beyond the framework of the three-temperature model. In a ferrimagnetic garnet film the magnetization precession was shown to be excited via the light-induced modification of the magneto-crystalline anisotropy, as shown in Fig. 1.2(c) [39, 41]. In contrast to the effects observed in metallic films [37] and orthoferrites [33], the change of the magneto-crystalline anisotropy in garnets results from electronic transitions between different ions and not from the change of lattice or spin temperatures. This effect is thus an example of a *non-thermal* mechanism of the excitation of spin precession. An important feature and advantage of non-thermal mechanisms is the sensitivity to the polarization of light.

Even earlier than the observation reported in [39], it was shown that circularly-polarized laser pulses can non-thermally excite coherent spin precession in the dielectric antiferromagnet $DyFeO_3$ [40]. A remarkable result of that experiment was the sensitivity of the excited precession for the helicity of the laser pulses. It had been

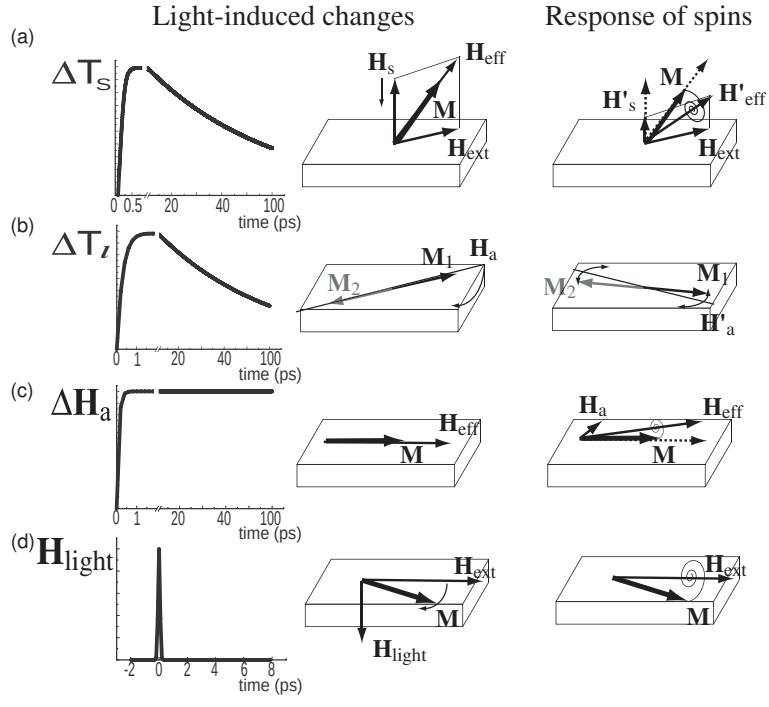

Figure 1.2: Schematic representation of various excitation processes of light-induced coherent spin precession. Left column shows the time dependences of the parameters of the medium modified by light. Central column shows the light-induced changes and the right column shows the response of the spins to these changes after the end of the pump pulse action.
(a) In a metallic ferromagnetic film: ultrafast demagnetization (ΔT_s) leads to decrease of the shape anisotropy, which, in turn, changes the direction of the effective field [36].
(b) In an antiferromagnetic dielectric with spin reorientation phase transition: ultrafast heating of the lattice (ΔT_l) leads to a change of anisotropy constants and, consequently, drives the sample to a phase with different equilibrium orientation of the spins [38].
(c) In a dielectric films with a strong photomagnetic effect: a light pulse induces a quasi-stationary additional magneto-crystalline anisotropy (ΔH_a) and, therefore, changes the direction of the effective field [39].
(d) In dielectric and metallic films: a light pulse acts on the spins as a pulse of effective magnetic field and deviates them from their equilibrium position. After the pulse the spins start to precess around the applied magnetic field [40].

proposed that a circularly polarized laser pulse acts on the spins as a magnetic field pulse (see Fig. 1.2(d)), which direction is defined by the wavevector and the helicity of the light. This effect has been called the *ultrafast inverse Faraday effect* (IFE). Later, evidence of this effect was found in ferrimagnetic garnet films [39, 41, 42], another rare-earth orthoferrite [38] and metallic GdFeCo films [43]. As a microscopical mechanism of this effect stimulated Raman scattering has been proposed. However, no thorough analysis has been given so far. From the present understanding of the ultrafast IFE it follows that the action of photons upon the spins has an instantaneous character. As discussed in the next Section and in Chapters 5 and 6 of this thesis, such process, in contrast to the processes considered above, does not involve any intermediate energy reservoirs apart from the orbitals, or change of the potential energy of electrons during the optical transition. Therefore, this mechanism might be a key to the all-optical ultrafast magnetization control of magnetism. Its understanding is therefore crucial and is the main subject of the present thesis.

1.2.4 All-optical magnetization switching

The ultimate practical goal of the studies of ultrafast light-induced spin dynamics is to realize control of the spins by means of subpicosecond laser pulses. Recently, it was demonstrated experimentally that all-optical switching of the magnetization in a GdFeCo metallic film is feasible with circularly polarized 40 fs laser pulses [25]. Though the actual time scale of this process and the microscopical mechanism are still left to be clarified, it was proposed that the underlying mechanism is a combination of thermal (demagnetization) and instantaneous non-thermal (IFE) effects. Thus, the understanding of the actual physical picture behind instantaneous non-thermal effects is important from this point of view as well.

1.3 Mechanisms of light-induced spin dynamics

As follows from the brief overview of the recent achievements in the field of ultrafast light-induced spin dynamics, in order to understand and, possibly, control the spin dynamics by laser pulses, we have to reveal the channels for the energy and angular momentum transfer between photons and the various reservoirs in magnetic media. The scheme, shown in Fig. 1.1 is only suitable for the discussion of so-called thermal mechanisms. More universal models of light-induced spin dynamics have to be quite complicated because of the various contributions to the energy of the electron, lattice and spin reservoirs which have to be disclosed. Thus, in the optical spectral range, the energy of the photons will increase the potential energy of the electrons, the efficiency of which is defined by the optical properties of a medium. Further channels of energy transfer are determined by the properties of a material, such as the structure of the conduction and valence bands and the mechanism of magnetic ordering. Therefore,

the medium defines which of the possible channels of energy and angular momentum transfer will be most efficient.

In view of this we have proposed a straightforward way to classify the mechanisms of light-induced spin dynamics [44]. Mechanisms of one type, which are called *indirect*, do not involve changes in the spin subsystem during the optical transition. Instead, the electric field of light causes changes of the energies of the electrons and/or lattice, which are consequently transferred to the spins without the presence of the electric field of light. Typically, for the realization of such a mechanism, optical absorption in the medium is required in order to deposit part of the light energy into the electrons and/or lattice. The other - *direct* - type of mechanisms, in contrast, directly depends on the electric field of light for the generation of the excitation in the spin subsystem. Obviously, in this case the excitation takes place while the light pulse is present and, therefore, may not require absorption, as we consider below and in Chapters 5 and 6. In Tables 1.1,1.2 various experimental observations of laser-induced ultrafast spin dynamics in metals, half-metals, semiconductors and dielectrics are summarized and assigned to either a direct or indirect type of microscopical excitation mechanism.

We note that it is quite common nowadays to divide the mechanisms of light-induced spin dynamics in thermal or non-thermal, as was described above. This, however, might be rather confusing, because the temperature is, strictly speaking, a thermodynamical concept and is not well defined at times shorter than the time of equilibration of all reservoirs in Fig. 1.1. Moreover, the use of a spin temperature as a measure of demagnetization was questioned lately [45].

1.3.1 Direct mechanisms of light-induced spin dynamics

In a *direct* mechanism of light-magnetic matter interactions, the perturbation of the spin system happens directly during the light pulse via optical transitions. These mechanisms are very sensitive to optical selection rules and, therefore, light polarization, that provides the possibility to control their efficiency. The optical spin orientation in semiconductors is an example of such a mechanism [57]. In magnetically ordered metals and dielectrics, however, experimental studies of direct mechanisms on the subpicosecond time scale are rare [25, 40, 41, 61].

One of the possible direct mechanisms of the excitation of coherent spin precession in a transparent medium was proposed in the 1960s [62]. It is stimulated Raman scattering (SRS) from magnons. The theory developed for this process considers continuous wave (CW) laser radiation [62, 63]. However, when subpicosecond pulses are involved the SRS process should acquire new features, related to the short duration and broad spectral width of the pulse, as was observed in the studies of the generation of coherent phonons (coherent lattice vibrations)[64, 65, 66].

The subpicosecond SRS from magnons was already proposed to be responsible for the excitation of coherent spin precession in $DyFeO_3$ by 100 fs circularly polarized laser

Table 1.1: Direct and indirect mechanisms of excitation of light-induced spin dynamics in metals (M), half-metals (HM), semiconductors (SC) and dielectrics (D). Letters in parenthesis refer to (t) thermal and (n) nonthermal type of mechanism. Note that processes, such as spin polarization or magnon squeezing, which do not involve dynamics of the macroscopic magnetization, are also included.

medium	indirect	direct
M	• ultrafast demagnetization (t) [19, 20, 24, 28, 46, 47] [26, 30, 48, 49, 50] • spin waves via change of magnetic shape anisotropy (t) [36] • creation of magnetic moment and spin waves via light-induced antiferromagnet-ferromagnet phase transition (t) [31, 32, 35] • spin waves via transition over the compensation point (t) [37]	• spin-polarization of excited electrons (n) [51, 52] • spin waves via ultrafast IFE (n) [43]
	magnetization switching by 40 fs single pulse (t+n ?)[25]	
HM	• spin waves via change of magnetic anisotropy (t) [53]	
SC	• magnetization reorientation via light-induced coercivity change (t) [54] • demagnetization in $Ga_{1-x}Mn_xAs$ and dynamical hole polarization via $p-d$ scattering of hot holes (t) [55] • spin waves via changes of magnetic anisotropy (t) [56]	• optical orientation (n) [57] • spin manipulation via optical Stark effect (n) [58, 59]

Table 1.2: Continuation of Table 1.1.

medium	indirect	direct
D	• spin waves via light-induced spin-reorientation phase transition (t) [33, 34] • magnetization quenching via phonon-magnon interaction (t) [60] • spin waves via photomagnetic effect (n) [39]	• spin waves via ultrafast IFE (n) [40, 41] • magnon squeezing via 2^{nd} order ISRS (n) [61]

pulses [40], through without a thorough analysis. At the same time, this experimental observations was explained in terms of the so-called *ultrafast inverse Faraday effect*, which is an example of an *opto-magnetic* effect. The impact of a circularly polarized laser pulse on the spins was considered as the action of an effective light-induced magnetic field pulse oriented along the wavevector of light. This field can be either parallel or antiparallel to the wavevector of light, depending on the helicity of the light pulse. Therefore, the initial phase of an excited spin precession has to depend on the helicity, which was indeed observed in the experiments [40]. This effect is assumed not to have any particular requirements for the medium apart from possessing a large magneto-optical susceptibility. Later, supporting this idea, similar effects were observed in ferrimagnetic garnet films [41] as well as in thin films of the amorphous metallic alloy GdFeCo [25].

The origin of the term "inverse Faraday effect" deserves separate consideration. It originates from works in the 1960s devoted to interactions of long laser pulses or CW electromagnetic radiation with a medium [67, 68, 69]. The possibility to induce magnetization in an isotropic transparent paramagnetic medium by circularly polarized light was predicted [67, 68] and observed [69] for 30 ns circularly-polarized pulses. This effect was named the inverse Faraday effect and was phenomenologically described by the formulae

$$\mathbf{M} = K[\mathbf{E} \times \mathbf{E}^*], \tag{1.1}$$

where K is a magneto-optical susceptibility, defining also the Faraday effect, or magnetic circular birefringence. The latter results in rotation of the polarization of light propagating through a magnetic/magnetized medium. Apparently, the same optical transitions that define the Faraday effect are responsible of the IFE. In [40] an ef-

fective light-induced field existing only during the 100 fs laser excitation pulse was introduced in analogy with Eq. (1.1):

$$\mathbf{H}^{\text{eff}} = K[\mathbf{E} \times \mathbf{E}^*], \tag{1.2}$$

This led to nice qualitative agreements with the experimentally observed results. However, the correspondence between a theory developed for an isotropic paramagnet subjected to CW electromagnetic radiation and the behavior of a magnetically-ordered medium excited by ultrashort laser pulses was not completely justified[1]. This problem will be further addressed in this thesis.

First, the interaction of light with a transparent *magnetic* medium is described by the free energy F, which is more complex for a magnetically ordered than for a paramagnetic medium. For a magnetic system, generally speaking, F is a function of the electric field of light $\mathbf{E}$ and the ferromagnetic $\mathbf{M}$ and antiferromagnetic $\mathbf{L}$ vectors, characterizing the magnetic ordering of the medium [71] (See Table 1.3). For example, it is known that the conventional Faraday effect can, in the case of a multi-sublattice magnetic medium, include a so-called antiferromagnetic part, originating from the antiferromagnetically aligned magnetic moments [72]. Thus, it is natural to expect that the inverse effect in such systems could be also rather different from the one observed in paramagnets.

Second, as can be seen from Table 1.3, one can also expect an effect of linearly polarized light on a magnetic medium. In magneto-optics the Cotton-Mouton (or Voigt) effect, or magnetic linear birefringence, is known [71, 73]. The authors of reference [74] indeed predicted the inverse effect, i.e the magnetization induced by linearly polarized light in a paramagnetic medium placed in an external magnetic field $\mathbf{H}$. This effect was observed for an atomic gas placed in crossed external DC magnetic and AC electric fields [75]. Attempts to observe a similar effect in a magnetically-ordered medium, namely ferrimagnetic garnets, were reported in [76]. However, most probably, thermal demagnetization dominated the reported results. Again, the natural question arises, whether linearly polarized subpicosecond laser pulses can act on spins as a light-induced effective field, in analogy with the observations for circularly polarized pulses [40, 41, 77].

Third, the expression for an effective field (1.2) gives information about the symmetry of the effect and its dependence on the magneto-optical properties of a medium. However, it does not reveal its microscopical origin. Indeed, effective magnetic fields are commonly used to present in a more pictorial way a number of different processes affecting the spin system but having different microscopical origins. Thus, the change of magneto-crystalline anisotropy in [39, 41] and the optical Stark effect in [58, 59] were described by effective magnetic fields, although their microscopical origins are essentially different. Therefore, a true microscopical mechanism, phenomenologically

[1] This fact has been noticed, for example, in [70].

Table 1.3: Magneto-optics and opto-magnetism. The question marks denote the issues considered in the present work.

Free energy term		Linear in M or L	Quadratic in M or L or bilinear in ML
Magneto-optics		Magnetic *circular* birefringence or Faraday effect (ferro- and antiferromagnetic parts)	Magnetic *linear* birefringence or Voigt effect: (ferro- and antiferromagnetic parts)
Opto-magnetism	CW light	Inverse Faraday effect (IFE): magnetization induced by *circularly* polarized light	Inverse Cotton-Mouton effect: magnetization induced by *linearly* polarized light
	Sub-ps pulses	Effective field induced by *circularly* polarized light (?)	Effective field induced by *linearly* polarized light (?)

described by a light-induced field (1.2), has to be found. While the processes leading to the CW opto-magnetic effects were analyzed in great detail [63], novel aspects in light-medium interactions can dominate for sub-picosecond excitation pulses. In [40, 41] SRS was proposed to be a microscopical mechanism of coherent spin precession excitation, described by the field (1.2), but no clear evidence for this was given.

Finally, it is worth to note that the combination of direct and indirect mechanisms is of practical interest because it could lead to the control of the magnetic state by light, as shown experimentally in [25], where a helicity-dependent switching of the magnetization by 40 fs circularly-polarized pulses was observed in a metallic film. Therefore, a profound understanding of the processes taking place during and after the optical excitation by a subpicosecond laser pulse is of particular importance.

The main goal of the work presented in this thesis is to understand the direct mechanisms of the excitation of coherent spin precession triggered by ultrashort laser pulses in a transparent medium. The Chapters 5 and 6, based on recently published works [44, 78], are devoted to theoretical and experimental attempts to resolve the

controversial issues listed above in this Section, by conducting both experimental and theoretical studies.

1.3.2 Indirect mechanisms of light-induced spin dynamics

Another part of this thesis is devoted to an experimental attempt to explore possible indirect mechanisms of the excitation of spin dynamics by laser pulses in a multiferroic material.

As one can see from Table 1.1, there is a relatively large number of indirect optical effects to trigger spin dynamics. The most studied indirect process is the ultrafast light-induced demagnetization in metals, already briefly introduced above. A lot of experimental (See Table 1.1) and theoretical research [29, 45, 79, 80, 81, 82, 83] has been done in order to determine and characterize the channels of energy and angular momentum transfer in this process. We will not treat the state of the art of this subject in great detail here because processes in a metallic magnetic medium are beyond the scope of this thesis. In dielectrics, in turn, the mechanisms of ultrafast demagnetization, being so effective in metals, are often inefficient. Instead, the quenching of the magnetic moment in dielectric media was shown to take place via phonon-magnon interactions, which can be, however, as slow as 700 ps [60] and can hardly be referred to as ultrafast.

Due to this, dielectric materials are interesting to study other processes of excitation of spin dynamics, not related to and not obscured by the demagnetization and heating in general, as was demonstrated in a number of experimental works (for a review see [77]).

For an effective excitation of a spin system via indirect processes, strong interactions between the spins and other subsystems of a magnetic medium are crucial. In view of this, so-called multiferroic materials [84] are promising candidates for such studies. These materials are characterized by the presence of several order parameters in the same phase. These order parameters are the spontaneous magnetic ordering, the electric polarization and the strain [85]. While in ordinary ferroic materials (e.g. ferromagnets) the magnetization can be manipulated by an external magnetic field only, in multiferroic materials, where magnetic and ferroelelctric ordering coexist [86], the magnetization can also be controlled by an applied electric field and *vise versa*. It is worth to note that the latter, *magnetoelectric*, effect can exist not only in multiferroics [87]. However, in media possessing both magnetic and electric ordering the magnetoelectric susceptibility is expected to be higher [87, 88].

The few reports on the manifestation of the magnetoelectric effect in linear and nonlinear optics [89, 90] suggest that a study of the time induced magnetization dynamics in multiferroic materials can be quite interesting. The interaction between the various order parameters can lead to new paths for the manipulation of magnetization by light, via the intermediate interaction of light with the electric polarization.

Exploring this option is one of the subjects of this thesis (Chapter 8).

1.4 Scope of this thesis

This thesis describes a combined experimental and theoretical study of ultrafast light-induced dynamical processes in magnetic dielectric materials.

The experimental techniques used are described in Chapter 2. Then in Chapter 3 information on the crystallographic and magnetic structures of the used materials - canted antiferromagnet iron borate $FeBO_3$ and ferrimagnetic multiferroic gallium ferrite $GaFeO_3$ - is presented, forming the basis for the further discussion of the experimental results.

Chapter 4 is devoted to the characterization of the samples by means of ellipsometric and magneto-optical studies. Due to the weak linear magneto-optical response of $GaFeO_3$ we complete the characterization of it by measurements of the magnetic optical second harmonic generation. These results were published in [91, 92].

The following discussion can be separated into two major parts. Chapters 5, 6 and 7 form one part which is devoted to the excitation of coherent spin precession and lattice vibrations by subpicosecond laser pulses. In Chapter 5 we present a phenomenological description of the interaction of light pulses with a magnetic medium with specific magnetic properties. Main attention is paid to impulsive stimulated Raman scattering as the mechanism of light-induced excitation of coherent spin precession. Two approaches are considered. One of them describes the interaction of light with the spins using a so-called classical Hamiltonian approach [93], where the coherent spin excitations are treated using the normal coordinate formalism. In the second approach the magnetic excitation is seen as a precession of the ferro- and antiferromagnetic vectors and is described by the Landau-Lifshitz equations. The action of light on the magnetic system is then described in terms of light-induced effective fields. Although this approach was used earlier in a certain form to analyze various light-induced processes, we show that a more intricate situation occurs when a multisublattice magnetic medium is concerned. In Chapter 6 the experimental results are presented for the easy-plane weak ferromagnet $FeBO_3$, showing a good agreement with the theoretical predictions of Chapter 5.

This combined theoretical and experimental study allowed us to show unambiguously that impulsive stimulated Raman scattering indeed can be the mechanism of the excitation of coherent spin precession. This mechanism, in contrast to some previous ideas about the light-induced spin dynamics [1], is not restricted to the case of circularly-polarized laser pulses. In turn, it can be even more efficient for the case of linearly-polarized ones. This observation allowed us to argue that angular momentum transfer between photons and spins is not required for the excitation of spin dynamics. Moreover, we have shown theoretically and experimentally, that the efficiency of the spin precession excitation is defined by the specific magnetic anisotropy of a medium,

namely the ellipticity of the spin precession, and not only by its magneto-optical properties, as was proposed earlier [40].

Chapter 7 completes the consideration of light-induced excitations in $FeBO_3$ by dealing with the coherent phonons generated by laser pulses. The possible interplay between light-induced excitations of non-magnetic origin and the magnetic ordering is discussed. These three Chapters are based on published papers [44, 78].

The second part of the discussion (Chapter 8) concerns the light-induced processes in the multiferroic $GaFeO_3$. The main target of the experiments with this material was the detection of processes excited by subpicosecond laser pulses and related to the multiferroicity. However, no magnetic response was observed either in the linear or nonlinear pump-probe measurements. Instead, light-induced dynamics was detected in a linear optical birefringence signal. In the SHG measurement we observed light-induced changes in signals of both crystallographic and magnetic origins. However, our analysis showed that the measured dynamics of the magnetic SHG response can not be ascribed with confidence to a light-induced magnetization dynamics. This indicates that the interpretation of light-induced dynamics in the SHG response of a medium requires accurate verification and can not be directly related to the dynamics of the spin system.

References

[1] J. Stöhr and H. C. Siegmann, *Magnetism: from Fundamentals to nanoscale Dynamics* (Springer-Verlag, 2006).

[2] M. N. Baibich, J. M. Broto, A. Fert, F. Nguyen Van Dau, F. Petroff, P. Etienne, G. Creuzet, A. Friederich, and J. Chazelas, Phys. Rev. Lett. **61**, 2472 (1988).

[3] G. Binasch, P. Grünberg, F. Saurenbach, and W. Zinn, Phys. Rev. B **39**, 4828 (1989).

[4] D. Weller and A. Moser, IEEE Trans. Magn. **35**, 4423 (1999).

[5] V. Skumryev, S. Stoyanov, Y. Zhang, G. Hadjipanayis, D. Givord, and J. Nogués, IEEE Trans. Magn. **423**, 850 (2003).

[6] S. N. Piramanayagam, J. Appl. Phys. **102**, 011301 (2007).

[7] W. A. Challener, T. W. McDaniel, C. D. Mihalcea, K. R. Mountfield, K. Pelhos, and I. K. Sendur, Jpn. J. Appl. Phys. **42**, 981 (2002).

[8] W. W. Wang and J. D. Peralta, *War of the disks: Hard disk drives vs. flash solid state disks*, http://www.storagesearch.com/bitmicro-art3.html.

[9] A. Y. Elezzabi, M. R. Freeman, and M. Johnson, Phys. Rev. Lett. **77**, 3220 (2007).

[10] T. Gerrits, H. A. M. van der Berg, J. Hohlfeld, L. Bär, and T. Rasing, Nature (London) **418**, 509 (2002).

[11] Y. Acremann, M. Buess, C. H. Back, M. Dumm, G. Bayreuther, and D. Pescia, Nature (London) **414**, 51 (2001).

[12] I. Tusoda, C. Stamm, A. B. Kashuba, F. King, H. C. Siegmann, J. Stöhr, G. Ju, B. Lu, and D. Weller, Nature (London) **428**, 831 (2004).

[13] F. J. Albert, N. C. Emley, E. B. Myers, D. C. Ralph, and R. A. Buhrman, Phys. Rev. Lett. **89**, 226802 (2002).

[14] J. C. Slonczewski, J. Magn. Magn. Matter. **159**, L1 (1996).

[15] L. Berger, Phys. Rev. B **54**, 9353 (1996).

[16] W. H. Butler and A. Gupta, Nature Materials **3**, 845 (2004).

[17] S. Mangin, D. Ravelosona, J. A. Katine, M. J. Carey, B. D. Terris, and E. E. Fullerton, Nature Materials **5**, 210 (2006).

[18] A. Vaterlaus, T. Beutler, and F. Meier, Phys. Rev. Lett. **67**, 3314 (1991).

[19] E. Beaurepaire, J. C. Merle, A. Daunois, and J. Y. Bigot, Phys. Rev. Lett. **76**, 4250 (1996).

[20] C. Stamm, T. Kachel, N. Pontius, R. Mitzner, T. Quast, K. Holldack, S. Khan, C. Lupulescu, E. F. Aziz, M. Wietstruk, et al., Nature Materials **6**, 740 (2007).

[21] M. B. Agranat, S. I. Ashitkov, A. B. Granovsky, and et al., Sov. Phys. - JETP **59**, 804 (1984).

[22] B. Koopmans, Nature Materials **6**, 715 (2007).

[23] K. Nakamoto, *Infrared and Raman Spectra of Inorganic and Coordination Compounds* (John Wiley Sons, 1986).

[24] B. Koopmans, M. van Kampen, J. T. Kohlhepp, and W. J. M. de Jonge, Phys. Rev. Lett. **85**, 844 (2000).

[25] C. D. Stanciu, F. Hansteen, A. V. Kimel, A. Kirilyuk, A. Tsukamoto, A. Itoh, and T. Rasing, Phys. Rev. Lett. **99**, 047601 (2007).

[26] F. Dalla Longa, J. T. Kohlhepp, W. J. M. de Jonge, and B. Koopmans, Phys. Rev. B **75**, 224431 (2007).

[27] A. I. Akhiezer, V. G. Bar'yakhtar, and M. I. Kaganov, Sov. Phys. - Uspekhi **72**, 3 (1960).

[28] H. Regensburger, R. Vollmer, and J. Kirschner, Phys. Rev. B **61**, 14716 (2000).

[29] P. M. Oppeneer and A. Liebsch, J. Phys.: Condens. Matter **16**, 5519 (2004).

[30] J.-Y. Bigot, L. Guidoni, E. Beaurepaire, and P. N. Saeta, Phys. Rev. Lett. **93**, 077401 (2004).

[31] G. Ju, J. Hohlfeld, B. Bergman, R. J. M. van de Veerdonk, O. N. Mryasov, J.-Y. Kim, X. Wu, D. Weller, and B. Koopmans, Phys. Rev. Lett. **93**, 197403 (2004).

[32] J.-U. Thiele, M. Buesses, and C. H. Back, Appl. Phys. Lett. **85**, 2857 (2004).

[33] A. V. Kimel, A. Kirilyuk, A. Tsvetkov, R. V. Pisarev, and T. Rasing, Nature (London) **429**, 850 (2004).

[34] S. Tomimoto, M. Matsubara, T. Ogasawara, H. Okamoto, T. Kimura, and Y. Tokura, Phys. Rev. Lett. **98**, 017402 (2007).

[35] B. Bergman, G. Ju, J. Hohlfeld, R. J. M. van der Veerdonk, J.-Y.Kim, X. Wu, D. Weller, and B. Koopmans, Phys. Rev. B **73**, 060407 (2006).

[36] M. van Kampen, C. Jozsa, J. T. Kohlhepp, P. LeClair, L. Lagae, W. J. M. de Jonge, and B. Koopmans, Phys. Rev. Lett. **88**, 227201 (2002).

[37] C. D. Stanciu, A. V. Kimel, F. Hansteen, A. Tsukamoto, A. Itoh, A. Kirilyuk, and T. Rasing, Phys. Rev. B **73**, 220402 (2006).

[38] A. V. Kimel, C. D. Stanciu, P. A. Usachev, R. V. Pisarev, V. N. Gridnev, A. Kirilyuk, and T. Rasing, Phys. Rev. B **74**, 060403 (2006).

[39] F. Hansteen, A. V. Kimel, A. Kirilyuk, and T. Rasing, Phys. Rev. Lett. **95**, 047402 (2005).

[40] A. V. Kimel, A. Kirilyuk, P. A. Usachev, R. V. Pisarev, A. M. Balbashov, and T. Rasing, Nature (London) **435**, 655 (2005).

[41] F. Hansteen, A. Kimel, A. Kirilyuk, and T. Rasing, Phys. Rev. B **73**, 014421 (pages 14) (2006).

[42] A. M. Kalashnikova et al. (2007), helicity dependent excitation of weak magnetization precession in $Bi_3Fe_5O_{12}$ single crystal was recently observed at T=10 K.

[43] C. D. Stanciu, F. Hansteen, A. V. Kimel, A. Tsukamoto, A. Itoh, A. Kirilyuk, and T. Rasing, Phys. Rev. Lett. **98**, 207401 (2007).

[44] A. M. Kalashnikova, A. V. Kimel, R. V. Pisarev, V. N. Gridnev, P. A. Usachev, A. Kirilyuk, and T. Rasing, Phys. Rev. B **78**, 104301 (2008).

[45] N. Kazantseva, U. Nowak, J. H. R. W. Chantrell, and A. Rebei, Europhys. Lett. **81**, 27004 (2008).

[46] J. Hohlfeld, E. Matthias, R. Knorren, and K. H. Bennemann, Phys. Rev. Lett. **78**, 4861 (1997).

[47] E. Beaurepaire, M. Maret, V. Halté, J.-C. Merle, A. Daunois, , and J.-Y. Bigot, Phys. Rev. B **58**, 12134 (1998).

[48] L. Guidoni, E. Beaurepaire, and J.-Y. Bigot, Phys. Rev. Lett. **89**, 017401 (2002).

[49] E. Beaurepaire, G. M. Turner, S. M. Harel, M. C. Beard, J.-Y. Bigot, and C. A. Schmuttenmaer, Phys. Rev. Lett. **84**, 3465 (2004).

[50] M. Vomir, L. H. F. Andrade, E. Beaurepaire, M. Albrecht, and J.-Y. Bigot, **99**, 08A501 (2006).

[51] G. Ju, A. Vertikov, A. V. Nurmikko, C. Canady, G. Xiao, R. F. C. Farrow, and A. Cebollada, Phys. Rev. B **57**, R700 (1998).

[52] A. Winkelmann, W.-C. Lin, F. Bisio, H. Petek, and J. Kirschner, Phys. Rev. Lett. **100**, 206601 (2008).

[53] Q. Zhang, A. V. Nurmikko, A. Anguelouch, G. Xiao, and A. Gupta, Phys. Rev. Lett. **89**, 177402 (2002).

[54] G. V. Astakhov, A. V. Kimel, G. M. Schott, A. A. Tsvetkov, A. Kirilyuk, D. R. Yakovlev, G. Kerczewski, W. Ossau, G. Schidt, and L. W. Molenkamp, and Th. Rasing, Appl. Phys. Lett. **86**, 152506 (2000).

[55] J. Wang, Ł. Cywiński, C. Sun, J. Kono, H. Munekata, and L. J. Sham, Phys. Rev. B **77**, 235308 (2008).

[56] D. Wang, Y. H. Ren, X. Liu, J. K. Furgyna, M. Grimsditch, and R. Merlin, Phys. Rev. B **75**, 233308 (2007).

[57] F. Meier and B. P. Zakharchenya, *Optical orientation* (Elsevier Science Ltd, , 1984).

[58] J. A. Gupta, R. Knobel, N. Samarth, and D. D. Awschalom, Science **292**, 2458 (2001).

[59] J. Berezovsky, M. H. Mikkelsen, N. G. Stoltz, L. A. Coldren, and D. D. Awschalom, Science **320**, 349 (2008).

[60] A. V. Kimel, R. V. Pisarev, J. Hohlfeld, and T. Rasing, Phys. Rev. Lett. **89**, 287401 (2002).

[61] J. Zhao, A. V. Bragas, D. J. Lockwood, and R. Merlin, Phys. Rev. Lett. **93**, 107203 (2004).

[62] Y. R. Shen and N. Bloembergen, Phys. Rev. **143**, 372 (1966).

[63] Y. R. Shen, *The Principles of Nonlinear Optics* (John Wiley & Sons, New York, 1985).

[64] L. Dhar, J. A. Rogers, and K. A. Nelson, Chem. Phys. **94**, 157 (1994).

[65] R. Merlin, Sol. State Comm. **102**, 207 (1997).

[66] M. Cardona and G. Güntherodt, *Light Scattering in Solids VIII* (Springer, 2000).

[67] L. P. Pitaevskii, Sov. Phys. - JETP **12**, 1008 (1961).

[68] P. S. Pershan, Phys. Rev. **130**, 919 (1963).

[69] J. P. van der Ziel, P. S. Pershan, and L. D. Malmstrom, Phys. Rev. Lett. **15**, 190 (1965).

[70] S. R. Woodford, A. Bringer, and S. Blügel, J. Appl. Phys. **101**, 053912 (2007).

[71] G. A. Smolenskii, R. V. Pisarev, and I. G. Sinii, Sov. Phys. Usp. **18**, 1218 (1970).

[72] R. V. Pisarev, Sov. Phys. - JETP **31**, 761 (1970).

[73] J. Ferré and G. A. Gehring, Rep. Prog. Phys. **47**, 513 (1984).

[74] P. S.Pershan, J. P. van der Ziel, and L. D. Malmstrom, Phys. Rev. **143**, 574 (1966).

[75] S. I. Marmo and V. D. Ovsiannikov, Physics Lett. A **202**, 201 (1995).

[76] B. A. Zon, V. Y. Kupershmidt, G. V. Pakhomov, and T. T. Urazbaev, JETP Lett. **45**, 272 (1987).

[77] A. V. Kimel, A. Kirilyuk, F. Hansteen, R. V. Pisarev, and T. Rasing, J. Phys.: Cond. Matter **19**, 043201 (2007).

[78] A. M. Kalashnikova, A. V. Kimel, R. V. Pisarev, V. N. Gridnev, A. Kirilyuk, and T. Rasing, Phys. Rev. Lett. **99**, 167205 (2007).

[79] W. Hübner and G. P. Zhang, Phys. Rev. B **58**, R5920 (1998).

[80] G. Lefkidis and W. Hübner, Phys. Rev. B **76**, 014418 (2007).

[81] N. Kazantseva, D. Hinzke, U. Nowak, R. W. Chantrell, and O. Chubykalo-Fesenko, phys. stat. sol. (b) **244**, 4389 (2007).

[82] U. Atxitia, O. Chubykalo-Fesenko, N. Kazantseva, D. Hinzke, U. Nowak, and R. W. Chantrell, Appl. Phys. Lett. **91**, 232507 (2007).

[83] N. Kazantseva, D. Hinzke, U. Nowak, R. W. Chantrell, U. Atxitia, and O. Chubykalo-Fesenko, Phys. Rev. B **77**, 184428 (2008).

[84] H. Schmid, Ferroelectrics **252**, 41 (2001).

[85] M. Fiebig, J. Phys. D: Appl. Phys. **38**, R123 (2005).

[86] G. A. Smolenskiĭ and I. E. Chupis, Sov. Phys. - Uspekhi **25**, 475 (1982).

[87] W.Eerrenstein, N. D. Mathur, and J. F. Scott, Nature (London) **442**, 759 (2006).

[88] W. F. Brown, Jr., R. M. Hornreich, and S. Shtrikman, Phys. Rev. **168**, 574 (1968).

[89] B. B. van Aken, J.-P. Rivera, H. Schmidt, and M. Fiebig, Nature (London) **449**, 702 (2007).

[90] J. H. Jung, M. Matsubara, T. Arima, J. P. He, Y. Kaneko, and Y. Tokura, Phys. Rev. Lett. **93**, 037403 (2004).

[91] A. M. Kalashnikova, R. V. Pisarev, L. N. Bezmaternykh, V. L. Temerov, A. Kirilyuk, and T. Rasing, JETP Lett. **81**, 452 (2005).

[92] P. A. Markovin, A. M. Kalashnikova, R. V. Pisarev, and T. Rasing, JETP Lett. **86**, 712 (2007).

[93] V. L'vov, *Nonlinear Spin Waves (in Russian)* (Nauka, Moscow, 1987).

CHAPTER 2

Experimental techniques

In order to monitor the fast magnetization dynamics, that is a subject of this thesis, one has to have a proper "tool" that combines the required time resolution and sensitivity. The latter can be provided by magneto-optics [1]. Linear and non-linear magneto-optical effects have been known for a long time as efficient and convenient tools to study various magnetic properties of matter, from imaging the domain structure in ferromagnets [2, 3] to verifying the magnetic phase diagrams in non-collinear antiferromagnets [4].

The combination of optical and, in particular, magneto-optical effects with sufficient time resolution became possible with the invention of mode-locked lasers with pulse duration of 100 fs and below [5]. Initially, time-resolved sub-picosecond techniques were thought to simply supplement the conventional and widely used spectroscopic measurements. Indeed, the results obtained in the time domain are related to results obtained in the frequency domain via Fourier transformation. However, the important potential of such techniques for extracting unique dynamical information about various processes was recognized very soon [6]. For example, Raman spectroscopy is widely used for studying the vibrational sublevels of the ground state of media [7]. Pump-probe experiments, in turn, can provide information on the vibrational sublevels of both ground and excited states, as was demonstrated both theoretically and experimentally [8, 9]. Moreover, while the information on coherent medium excitations, i.e. phonons and magnons etc., can be obtained from conventional Raman and Brilloiun scattering, the time-resolved measurements allow to access the dynamics of a much wider spectrum of processes. Therefore, the availability of sub-picosecond

pump-probe optical techniques triggered a whole new field of the study of ultrafast processes in different media, be it the light-induced demagnetization, magnetization precession, lattice vibrations, phase transitions, molecular rotations or chemical reactions.

Several static and time-resolved optical and magneto-optical techniques were used in the experiments described in this thesis. In the present chapter the basic characteristics of the techniques and experimental setups are discussed. Although the main subject of this work was the study of the ultrafast interactions of laser pulses with magnetic media, the static measurements were also important and indispensable for the characterization of the samples.

The basic principle of all optical and magneto-optical measurements consists in detecting the change of certain parameters of light after its interaction with a sample of interest. Two types of the experiments are considered in this Chapter. In *linear* optical experiments [1] the change of polarization and intensity of light after interaction with the medium are studied at the same (*fundamental*) frequency as the incident one. In *nonlinear* optical experiments [10] the study is focused at the properties of the light emerging after the interaction with the medium, with a frequency different from the fundamental one. As will be discussed in this Chapter, the optical properties of a medium are strongly influenced by the magnetic ordering, lattice distortions etc. Moreover, according to selection rules, light is mainly affected by the orbital part of the electron wavefunctions. Therefore, optical and magneto-optical effects are powerful tools for studying spin, orbital and lattice degrees of freedom in a medium. Among various optical techniques, the choice of one or another depends not only on the purpose of the study itself, but also on the limitations of these techniques in certain cases. Although linear magneto-optical measurements are relatively easy to perform, in some materials linear magneto-optical effects can be weak. In this case magnetization induced second harmonic generation (MSHG) experiments can provide an alternative way to study the magnetic properties of the material, having, for instance, a sensitivity to the symmetry properties as an additional advantage [11].

In the following part the general phenomenological formalism describing the interactions of light with matter is introduced. This serves as a basis for the following description of experimental techniques used and for the discussions in Chapters 4-8 as well.

2.1 Linear and nonlinear optical effects

2.1.1 Free energy of a magnetic medium subjected to light

The interaction of light with a medium in the electric-dipole approximation can be described in terms of the free energy [10, 12]:

$$\Phi = -[\chi_{ij}^{(\mathrm{i})} E_i^* E_j + \chi_{ij}^{(\mathrm{c})} E_i^* E_j + \chi_{ijk}^{(\mathrm{i})} E_i^* E_j E_k + \chi_{ijk}^{(\mathrm{c})} E_i^* E_j E_k], \tag{2.1}$$

where E_i is the time dependent electric field of light $E_i = E_{0i} e^{-\mathrm{i}\omega_0 t}$ and $\hat{\chi}$ denotes the susceptibilities of various orders and origins that will be discussed below. In general, a tensor $\hat{\chi}$ can be of either (i)- or (c)-type depending on whether or not it is invariant under the time reversal operation. Also, the tensors can be either polar or axial depending on the microscopical properties of the optical transitions, described by them. The terms of higher power in E, describing a higher optical harmonic generation process, are omitted in Eq. (2.1) because they are not involved in the discussion below and comprise a separate subject of study [13]. The indices i, j, k are usually associated with certain prominent directions in the crystal, such as crystallographic and magnetic axes.

The electric field of light induces a polarization, i.e. an electric dipole moment per unit volume, in a medium. Polarization can be expressed as a derivative of the free energy (2.1) with respect to the electric field of light $\mathbf{P} = -\partial\Phi/\partial\mathbf{E}^*$. One can see that there are several terms that contribute to the induced polarization in a medium. For the discussion below we distinguish three types of terms:

$$P_i^0 = \chi_{ij}^{(\mathrm{i})0} E_j; \tag{2.2a}$$

$$P_i^{\mathrm{MO}} = \chi_{ij}^{(\mathrm{c})} E_j + \chi_{ij}^{(\mathrm{i})\mathrm{MO}} E_j; \tag{2.2b}$$

$$P_i^{(2)} = \chi_{ijk}^{(\mathrm{i})} E_j E_k + \chi_{ijk}^{(\mathrm{c})} E_j E_k. \tag{2.2c}$$

The susceptibilities entering Eqs. (2.2) are tensors, the number of independent components of which can be found from the space-time symmetry of the particular medium [14].

The first two groups of terms (2.2a,2.2b) describe the induced polarization at the same frequency ω_0 as the fundamental wave. The susceptibility $\chi^{(\mathrm{i})0}$ is the polar i-tensor of second rank, which properties are defined only by the crystallographic symmetry of the medium. This susceptibility describes such optical responses of the medium as refraction, absorption, birefringence and dichroism. The polar tensors $\chi_{ij}^{(\mathrm{c})}$ and $\chi_{ij}^{(\mathrm{i})\mathrm{MO}}$ account for the linear magneto-optical effects which are linear and quadratic in the magnetic order parameters, respectively. Their properties can be found taking into account the crystallographic and magnetic symmetry [15]. From Eq. (2.2b) it follows that the magneto-optical effects linear in M change their sign

when the orientation of the spins is reversed, while quadratic magneto-optical effects are even with respect to the spin orientation.

The third contribution (2.2c) to the polarization $\mathbf{P}$ describes the non-linear response of a medium, such as sum- or difference-frequency generation, in particular second harmonic generation. Again, as in the case of linear optics, the properties of the third-rank tensors $\chi^{(\mathrm{i})}_{ijk}$ and $\chi^{(\mathrm{c})}_{ijk}$ can be defined from the time-space symmetry of the medium.

In this Section we do not consider the specific symmetry properties of the materials used in the presented study. This is done in the Section 4, devoted to the investigation of the optical properties of gallium ferrite $GaFeO_3$ and iron borate $FeBO_3$.

2.1.2 Linear optical effects

Dielectric tensor formalism

The value which is commonly used to characterize the linear optical and magneto-optical properties of a medium is the dielectric permittivity ε, that relates the electric induction in the medium to the electric field of light $\mathbf{D} = \hat{\varepsilon}\mathbf{E} = (1 + \hat{\chi})\mathbf{E}$ [16]. The dielectric tensor can be found as

$$\varepsilon_{ij}(\omega) = 1 - \frac{\partial \Phi}{\partial E_i(\omega) \partial E_j(\omega)}. \tag{2.3}$$

The number of independent component of the tensor $\hat{\varepsilon}$ is defined by the properties of the medium. First, in a non-absorbing medium the tensor ε_{ij} is Hermitian and its components satisfy [12, 16]

$$\varepsilon_{ij} = \varepsilon^*_{ji}. \tag{2.4}$$

Symmetry of a medium in time and space further restricts the number of independent components of $\hat{\varepsilon}$. Thus, in the absence of magnetic ordering and applied magnetic field, i.e. when the medium is time-invariant, the generalized principle of the symmetry of the kinetic coefficients (Onsager principle) [17] states that [16]

$$\varepsilon_{ij} = \varepsilon_{ji}. \tag{2.5}$$

The invariance of the medium with respect to some operations of the space symmetry, such as rotations, reflections etc., results in the vanishing of some components of $\hat{\varepsilon}$ and establishes relations between the remaining ones [14].

For the description of the propagation of light through a medium the complex refraction index N is also used, which is related to the dielectric permittivity via:

$$N = n - \mathrm{i}k; \tag{2.6a}$$

$$\varepsilon = \varepsilon' - \mathrm{i}\varepsilon''; \tag{2.6b}$$

$$N_i = \sqrt{\varepsilon_{ii}}; \tag{2.6c}$$

$$\begin{array}{l} \varepsilon'_{ii} = n^2 - k^2, \\ \varepsilon''_{ii} = 2nk, \end{array} \tag{2.6d}$$

where n and k are refraction and absorption indices, respectively, and the tensor $\hat{\varepsilon}$ is diagonalized. Here and everywhere below "i" stands for the imaginary unit, while "i" - for the index of the tensor. The dielectric permittivity is a 2nd rank polar tensor, while N_i is a scalar.

Crystallographic birefringence

The dielectric permittivity tensor for a medium possessing no magnetic order satisfies Eq. (2.5). The degree of space anisotropy of the medium defines further restrictions on the number of independent components of $\hat{\varepsilon}$ [14]. Thus, in an isotropic medium only one independent component exists: $\varepsilon^0_{xx} = \varepsilon^0_{yy} = \varepsilon^0_{zz}$ ($\varepsilon^0_{ij} = 0$, $i \neq j$). However, an overwhelming number of solids possesses a certain degree of anisotropy. A large group of crystals belongs to the so-called optically uniaxial type of crystals, with their dielectric tensor having two independent components:

$$\begin{pmatrix} \varepsilon^0_{xx} & 0 & 0 \\ 0 & \varepsilon^0_{yy} = \varepsilon^0_{xx} & 0 \\ 0 & 0 & \varepsilon^0_{zz} \end{pmatrix}. \tag{2.7}$$

Two principle polarization directions can be defined for light waves propagating through such a crystal. If light is polarized either along or perpendicular to the z axis, its polarization will not change. Such waves comprise a set of two *eigenwaves* for this medium. A wave of any polarization propagating through the medium can be represented in the basis formed by these eigenwaves. For waves which polarization plane is not along one of the axes, the polarization of light will be changed depending on the difference between ε^0_{xx} and ε^0_{zz}, the path length d and the actual polarization. The refraction indices for the two eigenwaves are $n_o = \sqrt{\varepsilon^0_{xx}}$ and $n_e = \sqrt{\varepsilon^0_{zz}}$ for light polarized perpendicularly and parallel to the z axis, respectively. n_o and n_e are called *ordinary* and *extraordinary* refraction indices. If $n_o < n_e$ the crystal is referred to as a *negative* uniaxial crystal. A uniaxial crystal is called *positive* otherwise. In the notation used the z axis is called *optical axis* of the crystal. For light propagating along this axis the refraction index and, therefore, the propagation speed does not depend on the polarization. For light, which propagation direction makes a finite angle with respect to the z axis, the propagation speed for waves with the electric field polarized along and perpendicular to the z axis will be different, thus resulting in crystallographic birefringence. In the particular case of light propagating along the x or y axes and linearly polarized at 45° with respect to the z axis, the phase difference

between two orthogonally polarized components of the light wave is defined by:

$$\Delta = \frac{2\pi d}{\lambda}(n_o - n_e), \tag{2.8}$$

where d is the geometrical light path in the crystal. This phase difference results in the following parameters of *elliptical* polarization of light passed through the sample [18]

$$\phi = 45^{\circ};\ \epsilon = 2\Delta, \tag{2.9}$$

where ϕ is the angle between the major axis of the polarization ellipse and $\tan\epsilon$ is the ratio between major and minor axes of the ellipse.

As an example, the crystals belonging to the $\bar{3}m$ point group can be considered. These crystals have an optical axis that is directed along the 3-fold crystallographic axis. Iron borate $FeBO_3$, which was studied in our experiments, belongs to this symmetry group. Its particular optical properties are considered in Chapter 4.

If the symmetry of a crystal is lower, all three diagonal elements of the dielectric tensor are different and such a crystal has two optical axes, which directions are defined by the ratio between ε_{xx}, ε_{yy} and ε_{zz} and, in general, do not coincide with the directions of the crystallographic axes. Moreover, due to different spectral dependencies of dielectric permittivity tensor components, the directions of the optical axes in a biaxial crystal depend on the wavelength. Gallium ferrite GaFeO, belonging to the $m2m$ point group is an example of such a crystal (for optical properties of $GaFeO_3$ see Chapter 4).

Magnetic circular birefringence

Application of an external magnetic field or the presence of magnetic ordering removes the time-inversion symmetry of the crystal and, therefore, lowers its symmetry. According to the generalized principle of the symmetry of kinetic coefficients, the dielectric permittivity in this case satisfies [16]

$$\varepsilon_{ij}(\mathbf{M}) = \varepsilon_{ji}(-\mathbf{M}), \tag{2.10}$$

where $\mathbf{M}$ is a magnetization vector. In the absence of absorption $\hat{\varepsilon}$ is Hermitian ($\varepsilon_{ij} = \varepsilon^*_{ji}$). Therefore, the conditions for the real ε'_{ij} and imaginary ε''_{ij} parts of the dielectric permittivity tensor $\varepsilon_{ij} = \varepsilon'_{ij} - \mathrm{i}\varepsilon''_{ij}$ are

$$\begin{cases} \varepsilon'_{ij}(\mathbf{M}) = \varepsilon'_{ji}(\mathbf{M}) = \varepsilon'_{ij}(-\mathbf{M}); \\ \varepsilon''_{ij}(\mathbf{M}) = -\varepsilon''_{ji}(\mathbf{M}) = -\varepsilon''_{ij}(-\mathbf{M}) \end{cases} \tag{2.11}$$

The diagonal components of $\hat{\varepsilon}$, naturally, can be only real, while off-diagonal ones can be, in general, complex. From Eq. (2.11) it follows that there are symmetric (ε^s_{ij}) and antisymmetric ($\mathrm{i}\varepsilon^a_{ij}$) parts of the tensor ε_{ij}, which are quadratic and linear in the

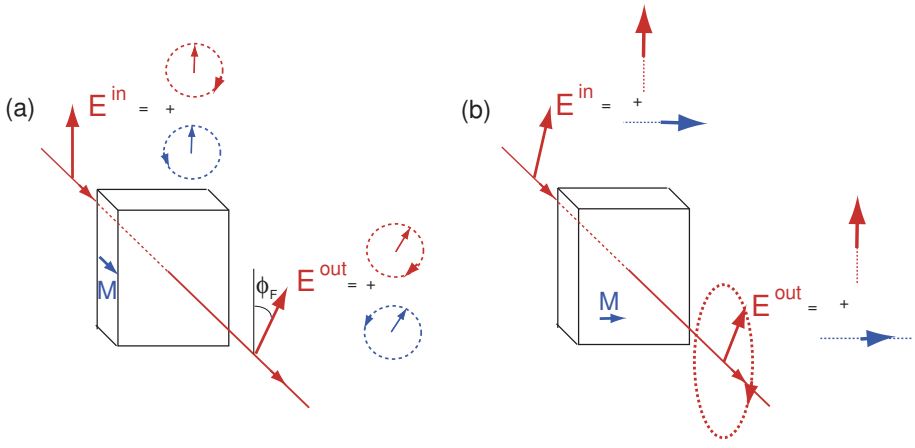

Figure 2.1: (a) Magneto-optical Faraday effect. (b) Magnetic linear birefringence.

magnetic order parameter (or external magnetic field in the case of a magnetically non-ordered medium), respectively

$$\begin{aligned} \mathrm{i}\varepsilon^a_{ij} = -\mathrm{i}\varepsilon^a_{ji} = \mathrm{i}\chi^{(\mathrm{c})}_{ij} = \mathrm{i}\chi^{(\mathrm{i})}_{ijk} M_k,\ i \neq j; \\ \varepsilon^s_{ij} = \varepsilon^s_{ji} = \chi^{(\mathrm{i})\mathrm{MO}}_{ij} = \chi^{(\mathrm{i})}_{ijkl} M_k M_l, \end{aligned} \tag{2.12}$$

where χ_{ijk} and χ_{ijkl} are axial and polar (i)-tensors, respectively. The appearance of these components in the dielectric tensor leads to the presence of *magnetic* birefringence[1].

The antisymmetric part $\mathrm{i}\varepsilon^a_{ij}$ describes the magnetic circular birefringence, or Faraday effect. If one considers an isotropic (or uniaxial) medium magnetized along the (optical) z axis, the dielectric tensor contains additional elements $\mathrm{i}\varepsilon_{xy} = -\mathrm{i}\varepsilon_{yx} = \mathrm{i}\chi_{xyz} M_z$. Two circularly polarized waves with opposite helicities propagating along the z axis will be the eigenwaves for for such a medium. It can be shown that the refraction indices for these eigenwaves are [20]

$$n_\pm = \sqrt{\varepsilon_{xx} \pm \varepsilon_{xy}}.$$

Wave of any polarization can be represented as a superposition of these two eigenwaves. For example, linearly polarized light is the superposition of two eigenwaves

[1] In the special case of a medium having more than one magnetic sublattice the expression for $\varepsilon^{a(s)}_{ij}$ and, therefore, the magneto-optical effects, becomes more complex [19]. However, a detailed consideration of this case is more appropriate for Chapter 4, where the optical properties of iron oxides are considered.

with equal amplitudes (Fig. 2.1(a)) and certain phase shift, which defines the orientation of its polarization plane. While light propagates through a medium, the phase shift between the eigenwaves changes because of their different propagation speed. Therefore, the result of the superposition of these waves after a certain distance d in a medium will be a linearly polarized wave with the polarization plane rotated with respect to the initial one. This rotation depends on the value of the off-diagonal and diagonal elements of the dielectric tensor and on the distance d traveled by light in the medium [1]

$$\phi_F = \frac{\varepsilon_{xy}}{\sqrt{\varepsilon_{xx}}} \frac{\pi d}{\lambda}, \tag{2.13}$$

where λ is the wavelength.

In the case when the crystallographic birefringence cannot be neglected, the eigenwaves are not circular anymore, but elliptical and the rotation of the polarization plane is rather a periodic than a linear function of the thickness d [21].

Magnetic linear birefringence

The symmetric part of dielectric tensor ε^s_{ij} describes magnetic linear birefringence (MLB), resulting in the change of the polarization of light propagating perpendicular to the magnetic order parameter of a medium. This effect is referred to as Cotton-Mouton effect in magnetic fluids or liquid crystals and as Voigt effect in solids. Despite of the fact that the effect on the light polarization is the same in both cases, the microscopic mechanisms of these effects are essentially different [22]. In the case of solids the application of an external magnetic field or magnetic ordering leads to a Zeeman shift of the energy levels [20, 23], while in a case of liquids and liquid crystals a reorientation of the (magnetic) molecules takes place [24], which, in turn, leads to the linear birefringence.

If one considers a medium with magnetization $\mathbf{M}$ along the x axis, the diagonal elements of the dielectric tensor have additional components

$$\varepsilon_{xx} = \varepsilon^0_{xx} + \chi^{(\mathrm{i})}_{xxxx} M_x^2 \tag{2.14}$$

$$\varepsilon_{yy} = \varepsilon^0_{yy} + \chi^{(\mathrm{i})}_{yyxx} M_x^2 \tag{2.15}$$

$$\varepsilon_{zz} = \varepsilon^0_{zz} + \chi^{(\mathrm{i})}_{zzxx} M_x^2. \tag{2.16}$$

If light propagates perpendicular to this quantization axis along, say, the z axis, then the eigenwaves are two linearly polarized waves along the x and y axes with refraction indices $n_x = \sqrt{\varepsilon_{xx}}$ and $n_y = \sqrt{\varepsilon_{yy}}$ (Fig.2.1(b)). As in the case of crystallographic birefringence, the appearance of ellipticity (2.9) will be observed for light which is initially polarized at some finite angle to the x or y axes.

2.1.3 Nonlinear optical effects

The third group of terms (2.2c) in the induced polarization P describes the non-linear optical effects [10]:

$$P_i^{(2)}(\omega_3) = \chi_{ijk}^{(i)}(\omega_3;\omega_1,\omega_2)E_j(\omega_1)E_k(\omega_2) + \chi_{ijk}^{(c)}(\omega_3;\omega_1,\omega_2)E_j(\omega_1)E_k(\omega_2). \quad (2.17)$$

First and second terms in this equation describe sum- and difference-harmonic generation if $\omega_{1,2}$ are optical frequencies, and the linear electro-optical effect if $\omega_1 \to 0$ [12] in nonmagnetic and magnetic media, respectively. In general, the second term in Eq. (2.17) can be written in a form $\chi_{ijkl}^{(i)}(\omega_3;\omega_1,\omega_2,0)E_j(\omega_1)E_k(\omega_2)M_l(0)$. This way of describing nonlinear optical effects in a magnetic medium is common when changes in a magnetic structure are considered, such as reorientation of the magnetization $\mathbf{M}$.

Second harmonic generation

A particularly interesting case of non-linear effects in a medium is second harmonic generation (SHG), when $\omega_1 = \omega_2$ and $\omega_3 = 2\omega_1$. In a medium lacking magnetic ordering only a polar (i)-tensor $\chi_{ij}^{(\mathrm{i})}$ exists. In this case Eq. (2.17) describes the *crystallographic* contribution to the SHG. The particular properties of the tensor $\chi_{ij}^{(\mathrm{i})}$ for crystals belonging to one of the 32 crystallographic classes are considered in detail in Refs.[10, 14]. In contrast to the second rank tensors $\chi_{ij}^{(\mathrm{i})}$ and $\chi_{ij}^{(\mathrm{c})}$, describing linear optical and magneto-optical effects, the tensor $\chi_{ijk}^{(i)}$ has non-zero components only in a medium lacking space inversion symmetry.

If the medium possesses one or another type of magnetic ordering, the non-linear optical polarization (2.17) has, in general, all two contributions. The polar (c)-tensor $\chi_{ijk}^{(\mathrm{c})}$ describes the *magnetic* contribution to the SHG signal. For opposite orientations of the magnetic moments, the crystallographic contribution to the SHG possesses the same sign, while the magnetic contribution has opposite sign. Moreover, these contributions to the SHG polarization (2.17) can be distinguished because of the different properties of the tensors $\chi_{ijk}^{(\mathrm{i})}$ and $\chi_{ijk}^{(\mathrm{c})}$ with respect to the symmetry operations characterizing the particular medium of interest. The properties of the tensor $\chi_{ijk}^{(\mathrm{c})}$ for all magnetic classes are considered in [14].

The sensitivity of second harmonic generation to magnetic ordering (i.e. time inversion symmetry) has been proven to be indispensable for the study of magnetic domains [3, 25] and magnetic phases of crystals [4], while the sensitivity to the crystallographic structure (i.e. space symmetry) allowed to study the properties of crystals possessing a spontaneous electric polarization [26] and the properties of surfaces and interfaces of centrosymmetric media, where this inversion is necessarily broken [10, 27]. Moreover, SHG allows one to study the interplay between the magnetic and electric types of ordering in a medium [28].

2.2 Static linear optical measurements

2.2.1 Jones matrix formalism

The polarization of light changes when light interacts with a medium, as described in Sec. 2.1. The specific changes are defined by the optical properties of the material at the frequency ω_0 of the light and by the geometry of the experiment. A convenient way to describe this process implies the use of Jones matrices, which are 2×2 matrices describing the optical properties of a medium, and the Jones vectors - 2×1 matrices describing the polarization of the incoming and outgoing light [18]

$$\begin{bmatrix} E_x \\ E_y \end{bmatrix} = \begin{bmatrix} T_{11} & T_{12} \\ T_{21} & T_{22} \end{bmatrix} \cdot \begin{bmatrix} E_{0x} \\ E_{0y} \end{bmatrix} \tag{2.18}$$

It is important to choose the proper coordinate system in which these matrices have a simple form. This choice depends on two factors: the symmetry properties of the medium and the polarization of the light itself. The most common bases are linear, when the polarization of light is represented as a superposition of two vectors along orthogonal axes x and y, and circular, when a superposition of two circularly polarized waves with opposite helicity is used. In the Cartesian coordinate system linearly and circularly polarized waves propagating along the z axis are described, respectively, by the Jones vectors [18]

$$E_0 \begin{bmatrix} \cos\xi \\ \sin\xi \end{bmatrix}; E_0 \frac{\sqrt{2}}{2} \begin{bmatrix} 1 \\ \pm \mathrm{i} \end{bmatrix}, \tag{2.19}$$

where E_0 is the amplitude of the electric field of light, ξ is the angle between the polarization plane and the x axis, i is the imaginary unit, and the sign $\pm$ corresponds to left- and right-handed helicity, respectively.

The meaning of the elements T_{ij} of the Jones matrix (2.18) can be understood considering the simplified case when the incoming light is linearly polarized along the x axis of the Cartesian coordinate system chosen ($\xi = 0$ in Eq. (2.19)). Thus, the element T_{11} describes the relative amplitude and phase of the outgoing x component of the electric field of the light itself. If the off-diagonal element T_{12} is nonzero, a y component $E_y = T_{21}E_{x0}$ appears in the Jones vector, which means that the polarization of light is rotated.

In general, the Jones matrix is complex: $\tilde{T}_{ij} = T_{ij}e^{\mathrm{i}T^a_{ij}}$. It can be easily shown that, if the diagonal element $\tilde{T}_{11} = e^{\mathrm{i}T^a_{11}}$, the outgoing x-component E_x of the light has the same amplitude as the incoming E_{0x} but its phase is delayed, i.e. only the refraction of light is observed. Contrary, a nonzero real part of T_{11} leads to a change of the amplitude of the E_x, i.e. describes the absorption.

Thus, knowing the polarization of light before and after the interaction with a medium, one can calculate the Jones matrix elements, which, in turn, are unambiguously related to the complex refractive index of the medium. If the proper basis

for the Jones matrix is chosen, the latter can have a simplified diagonal form. The propagation of light through the medium in this case is described by

$$\begin{bmatrix} e^{-\mathrm{i}N_1 kz} & 0 \\ 0 & e^{-\mathrm{i}N_2 kz} \end{bmatrix} \tag{2.20}$$

Where $N_{1,2}$ are the complex refraction indices for the two eigenwaves. The reflection from the surface of the isotropic sample is described by

$$\begin{bmatrix} R_{pp} & 0 \\ 0 & R_{ss} \end{bmatrix}, \tag{2.21}$$

where R_{pp} and R_{ss} are the Fresnel coefficients [18]

$$\begin{aligned} R_{pp} &= \frac{\cos\alpha/\sqrt{N^2-\sin^2\alpha}-1}{\cos\alpha/\sqrt{N^2-\sin^2\alpha}+1}; \\ R_{ss} &= \frac{1-N^2\cos\alpha/\sqrt{N^2-\sin^2\alpha}}{1+N^2\cos\alpha/\sqrt{N^2-\sin^2\alpha}}, \end{aligned} \tag{2.22}$$

where α is the angle of incidence.

To obtain information about the complex refractive index N in a wide range of wavelengths, *ellipsometric* measurements in reflection are used. For the investigation of birefringence of various origin, *polarimetric* measurements in transmission or reflection are performed. The incoming polarization of light is chosen different from the polarization of the eigenwaves, so that it will change and the difference $\Delta N = N_1 - N_2$ can be calculated.

2.2.2 Ellipsometric measurements

Principle of ellipsometric measurements

Ellipsometric measurements [29] in reflection allow one to obtain information on the optical constants of a material in a wide spectral range, independent of absorption, which could restrict the measurements in transmission. The typical geometry of such measurements is shown in Fig 2.2. It is natural to choose two waves linearly polarized along the crystallographic axes of the crystal waves as a basis. If the sample is isotropic, then Eq. (2.21) is applicable, and the refraction index N is the only value to be obtained from the experiment. In the case of an anisotropic medium the Jones matrix (2.21), in the basis formed by two linearly polarized waves, has off-diagonal elements. The refraction index N entering Eq. (2.22) is different for R_{pp} and R_{ss}. Therefore, two values N_1 and N_2 are to be found.

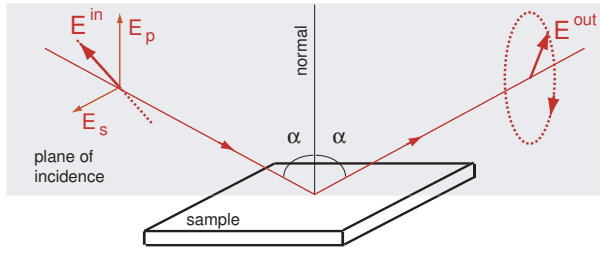

Figure 2.2: Geometry of ellipsometric measurements in reflection.

The polarization of light after reflection can be described using two parameters, or ellipsometric angles, Ψ and δ. They are related to the Fresnel coefficients via

$$\tan \Psi e^{\mathrm{i}\Delta} = \frac{R_{pp}}{R_{ss}}. \tag{2.23}$$

From this expression one can see that the angle Ψ characterizes the ratio between the real parts of the diagonal elements, i.e. describes the rotation of the polarization plane after reflection, while Δ describes the ellipticity. The values Ψ and Δ are the actual values that are obtained from the ellipsometric measurements. The procedure that is used to obtain the optical constants of the sample strongly depends on the sample itself. In the case of an isotropic bulk sample this procedure is straightforward and implies solution of Eqs. (2.22):

$$N^2 = \varepsilon = \sin^2 \alpha \left[1 + \tan^2 \alpha \left(\frac{1 - R_{pp}/R_{ss}}{1 + R_{pp}/R_{ss}} \right)^2 \right] \tag{2.24}$$

In the case of an anisotropic uniaxial crystal two refractive indices are to be obtained. It can be done by performing two sets of measurements, one with the optical axis of the sample aligned parallel to the incidence plane and another with the optical axis aligned perpendicular to this plane. It can be shown [18] that in the former case Eq. (2.24) gives the value of the extraordinary refraction index $n_e = \sqrt{\varepsilon_{zz}}$ and in the latter case it gives the value of the ordinary refraction index $n_o = \sqrt{\varepsilon_{xx}}$. If the sample is bi-axial, then the optical axes do not coincide with the crystallographic ones. However, calculating the components of the dielectric tensor ε_{xx}, ε_{yy}, and ε_{zz} and the related *principle* refraction indices $n_i = \sqrt{\varepsilon_{ii}}$ along the three crystallographic axes using Eq.(2.24) allows one to calculate the directions of the optical axes.

Rotating-analyzer variable-angle spectroscopic ellipsometry

The experimental ellipsometry results, which are presented in this thesis, were obtained using the variable angle spectrometric ellipsometer *WVASE* from the company

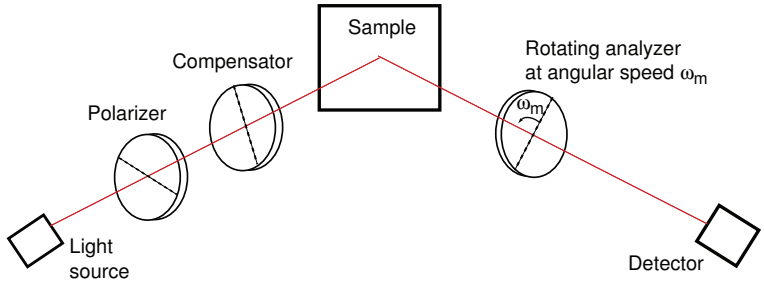

Figure 2.3: Basic optical components of a rotating-analyzer ellipsometer [30].

J.A.Woollam Co., Inc [30]. The possibility to perform measurements in a wide spectral range (0.6-5.8 eV) and in a wide range of incidence angles (40-90°), allows one to study bulk crystals as well as thin films with various optical properties. The principle scheme of operation of this *rotating-analyzer ellipsometer* is shown in Fig. 2.3

The analyzer is being rotated at the angular speed ω_m, while other optical components (compensator, which is optional, polarizer, and sample) are fixed. In this scheme, the information about the real signal, proportional to the ellipsometric angles Φ and Δ, is contained in the Fourier component with frequency ω_m present in the photocurrent from the detector.

2.2.3 Linear magneto-optical measurements

Measurements of Faraday rotation

The magneto-optical measurements, the results of which are presented in this thesis, were done in transmission experiments in the region where the absorption in the samples is low. In this case the Faraday effect consists of the rotation of the polarization plane of the linearly polarized light (2.13). In Fig. 2.4(a,b) the schemes of two kinds of polarimetric setups used to measure the Faraday rotation (2.13) are shown. In scheme (a) the light of intensity $\sim E_0^2$ from the laser source, linearly polarized along the x axis, passes through the sample along the magnetization direction. The polarization of light is rotated over a certain angle ϕ_F (2.13). To describe such a system it is convenient to use the linear basis. The Jones matrix for the sample possessing a Faraday rotation ϕ_F is

$$T_{\text{sample}} = \begin{bmatrix} \cos\phi_F & \sin\phi_F \\ -\sin\phi_F & \cos\phi_F \end{bmatrix} \tag{2.25}$$

Afterwards the light passes through the Faraday cell, which is a thick glass with a high Verdet constant placed inside a coil with AC current. This cell is used to enhance the

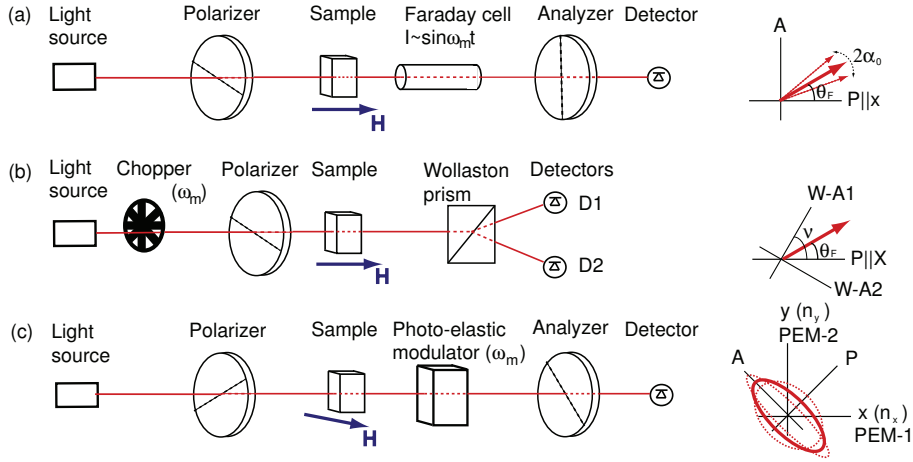

Figure 2.4: (a)-(b) Schemes used for measurements of Faraday rotation. (c) Scheme used for measurements of crystallographic and magnetic birefringence. On the right the relative orientation of the axes of the polarizer (P), analyzer (A), photo-elastic modulator (PEM-1,2), and Wollaston prism (W-A1,2) are shown.

sensitivity of the measurements by making it a modulation-based experiment. The Jones matrix for the Faraday cell rotation angle φ has, naturally, the same form as for the sample possessing a Faraday rotation (2.25), with ϕ_F replaced by φ. If the current in the coil and, consequently, the magnetic field applied to the glass, is modulated with frequency ω_m, than $\varphi = \varphi_0 \sin \omega_m t$. The Jones matrix for the Faraday cell in this case is

$$T_{\text{cell}} = \begin{bmatrix} \cos(\varphi_0 \sin \omega_m t) & \sin(\varphi_0 \sin \omega_m t) \\ -\sin(\varphi_0 \sin \omega_m t) & \cos(\varphi_0 \sin \omega_m t) \end{bmatrix}, \tag{2.26}$$

Afterwards light passes through the analyzer which axis is set to be orthogonal to the axis of the polarizer. The Jones matrix is $T_A = \begin{bmatrix} 0 & 0 \\ 0 & 1 \end{bmatrix}$. The light passed through the analyzer is described, therefore, by:

$$\begin{bmatrix} E_x \\ E_y \end{bmatrix} = T_A \cdot T_{\text{cell}} \cdot T_{\text{sample}} \cdot \begin{bmatrix} E_0 \\ 0 \end{bmatrix}$$

The intensity of light passed through the analyzer $I = |E_x|^2 + |E_y|^2$ and measured by the detector is

$$I(t) = I_0 \cos^2(\phi_F + \varphi_0 \sin \omega_m t) \approx \phi_F^2 + \frac{\varphi_0^2}{2}(1 - \cos 2\omega_m t) + 2\phi_F \varphi_0 \sin \omega_m t, \tag{2.27}$$

for small ϕ_F and φ_0. From this expression one can see that, if no Faraday rotation occurs in the sample, the photocurrent in the detector only has Fourier components at frequencies 0 and $2\omega_m$. If, however, $\phi_F \neq 0$, than the first harmonic at frequency ω_m is observed, with an amplitude that is proportional to the Faraday rotation ϕ_F. This setup is characterized by a high sensitivity ($\sim$1 mdeg) and was used to measure the Faraday rotation in the bi-axial gallium ferrite $GaFeO_3$, in which the true Faraday rotation is weak and obscured by the strong crystallographic birefringence.

The setup for measurements of the Faraday rotation shown in Fig.2.4(b) does possess somewhat lower sensitivity, which, however, is sufficient for experiments on samples with large values of Faraday rotation. After passing the sample, which Jones matrix is defined by Eq. (2.25), the beam is split into two orthogonally-polarized beams by a Wollaston prism. The signal in the Jones vector for the beam incident on one of the diodes then is

$$\begin{bmatrix} E_{1x} \\ E_{1y} \end{bmatrix} = \begin{bmatrix} 1 & 0 \\ 0 & 0 \end{bmatrix} \cdot \begin{bmatrix} \cos\nu & \sin\nu \\ -\sin\nu & \cos\nu \end{bmatrix} \cdot T_{\text{sample}} \cdot \begin{bmatrix} E_0 \\ 0 \end{bmatrix},$$

where ν is the angle between the initial polarization of light, defined by the orientation of the polarizer and the polarization of the beam in this channel after the Wollaston prism. The signal incident on the other diode is defined in a similar way

$$\begin{bmatrix} E_{2x} \\ E_{2y} \end{bmatrix} = \begin{bmatrix} 1 & 0 \\ 0 & 0 \end{bmatrix} \cdot \begin{bmatrix} \sin\nu & \cos\nu \\ -\cos\nu & \sin\nu \end{bmatrix} \cdot T_{\text{sample}} \cdot \begin{bmatrix} E_0 \\ 0 \end{bmatrix}.$$

The difference between the intensities $I_i = |E_{ix}|^2 + |E_{iy}|^2$ of the signal in the two channels is actually measured in the experiment:

$$I_1 - I_2 = E_0^2 \left[\cos(\nu - \phi_F) - \sin(\nu + \phi_F)\right]. \tag{2.28}$$

Initially the Wollaston prism is oriented in such a way that the intensities of the two beams in the absence of Faraday rotation in a sample are equal, i.e. $\nu = \pi/4$. If a Faraday rotation is present, then the measured signal is $I_1 - I_2 = \sqrt{2}E_0^2 \sin\phi_F \approx \sqrt{2}E_0^2\phi_F$. The light from a continuous wave (CW) or pulsed laser source is chopped at frequency ω_m in order to get a modulation of the signal. This increases the sensitivity by increasing the signal-to-noise ratio. The DC signal from one of the diodes, proportional to the E_0^2 value, was measured along with the AC difference signal. Therefore, the rotation angle ϕ_F could be calculated directly from these two measured values.

Measurements of linear birefringence

In the measurements of the crystallographic or magnetic birefringence the ellipticity of the light after the interaction with the medium is studied. It can be done using one of the schemes of Fig. 2.4(a,b), by adding a quarter-wave plate after the sample, which

transforms the ellipticity of light into a rotation of the polarization plane. Another technique, using the birefringent modulator as shown in Fig. 2.4(c), typically provides higher sensitivity [23]. The initial polarization of light, controlled by the polarizer, is linear and makes an angle 45° with the crystallographic or magnetic axis of the sample, which is denoted as x axis. For light propagating perpendicularly to the x axis, the Jones matrix of the sample possessing birefringence has the form

$$T_{\text{sample}} = \begin{bmatrix} e^{-\mathrm{i}n_x kd} & 0 \\ 0 & e^{-\mathrm{i}n_y kd} \end{bmatrix} = e^{-\mathrm{i}n_y kd} \begin{bmatrix} e^{-\mathrm{i}\Delta nkd} & 0 \\ 0 & 1 \end{bmatrix}, \tag{2.29}$$

where $\Delta n = n_y - n_x$ is the birefringence to be measured. The photo-elastic modulator *PEM-90* (HINDS Instruments) [31] is used to change the polarization state of light periodically between right- and left-handed circularly polarized, with a frequency ω_m

$$T_{\text{PEM}} = \begin{bmatrix} e^{-\mathrm{i}A_0 \cos \omega_m t} & 0 \\ 0 & 1 \end{bmatrix}, \tag{2.30}$$

where A_0 is the amplitude of the modulation. The light passing through the analyzer is described by the Jones matrix:

$$\begin{bmatrix} E_x \\ E_y \end{bmatrix} = \begin{bmatrix} \frac{\sqrt{2}}{2} & 0 \\ 0 & \frac{\sqrt{2}}{2} \end{bmatrix} \cdot T_{\text{PEM}} \cdot T_{\text{sample}} \cdot \frac{\sqrt{2}}{2} \begin{bmatrix} E_0 \\ E_0 \end{bmatrix}$$

The intensity of the signal measured by the photodiode is [31]

$$\begin{aligned} I(t) \sim E_0^2 [1 - \cos(\Delta nkd) \mathrm{J}_0(A_0) + \\ 2 \sin(\Delta nkd) \mathrm{J}_1(A_0) \cos(\omega_m t) + \\ 2 \cos(\Delta nkd) \mathrm{J}_2(A_0) \cos(2\omega_m t)], \end{aligned} \tag{2.31}$$

where $\mathrm{J}_i(A_0)$ are the Bessel functions. If the sample possesses no birefringence, this signal has Fourier components only at frequencies 0 and $2\omega_m$. However, if the sample is birefringent, a component at frequency ω_m appears in the measured signal, with an amplitude proportional to the birefringence Δn.

In all three setups the measurements of the signal from the photodiodes were done using the lock-in amplifier *SR830* (Stanford Research Systems). A CW He-Ne laser with a wavelength of 632.8 nm was used as a light source. For some measurements performed with setup 2.4(b), the short (40-150 fs) pulses with central wavelength 800 nm from the amplified Ti:Sapphier laser system (Spectra Physics) (See Section 2.4.1) were used. The samples were placed in a cold-finger optical cryostat *Microstate^{He}* (Oxford Instruments) that allowed to perform measurements in the range of temperatures 10-400 K.

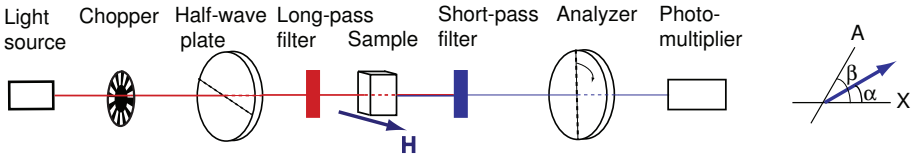

Figure 2.5: Schemes used for measurements of second harmonic generation in transmission geometry. On the right the meaning of the angles in Eq. (2.32) is illustrated.

2.3 Static second harmonic generation measurements

2.3.1 Experimental setup

The experimental setup for studying the optical second harmonic generation in transmission is shown in Fig. 2.5. As discussed in Section 2.1.3, the second harmonic signal is sensitive to the polarization of light at the fundamental frequency ω_0 as well as to the properties of the particular medium. The *Mira-900* Ti:Sapphire mode-locked laser (Coherent, Inc.) with pulses of 160 fs duration and a repetition frequency of 76 MHz was used for the fundamental excitation. The central wavelength was 800 nm. The polarization of the fundamental wave was controlled by the half wave plate, allowing to obtain linearly polarized light of any azimuthal angle ϕ. The long-pass filter was used to block possible second harmonic light generated in the optical components of the setup. After the sample the light at the fundamental frequency was blocked by the short-pass filter. The light at the doubled frequency $2\omega_0$ was passing through the analyzer, the orientation of the axis of which was controlled by a step motor. A photomultiplier and a photon counter were used to measure the intensity of the second harmonic light passing through the analyzer. Two kinds of measurements were performed: (i) the SHG-intensity of light as a function of the orientation of the analyzer axis and (ii) the SHG-intensity as a function of the applied magnetic field H. The intensity of the second harmonic light generated in a sample is a quadratic function of the intensity of the fundamental light. Therefore, the use of neutral density filters for reduction of the intensity of the fundamental beam causes a drastic decrease of the intensity of the SHG. To avoid this, a chopper was used that decreased the averaged power of the fundamental beam but not the peak intensity of the pulses. The samples were placed in the cold-finger optical cryostat *Microstate*^{He}(Oxford Instruments) to perform measurements in the temperature range of 10-400 K.

2.3.2 Principle of SHG measurements

The second harmonic optical polarization can be found from expression (2.17). Consider the SHG light with amplitude $E_{\mathrm{SHG}} \propto \chi^{(\mathrm{i})} E_0^2$ polarized at an angle ζ with

respect to the x axis of the laboratorium coordinate system. Then the light passing through the analyzer which axis makes an angle β with this axis is:

$$\begin{bmatrix} E_x \\ E_y \end{bmatrix} = \begin{bmatrix} 1 & 0 \\ 0 & 0 \end{bmatrix} \cdot \begin{bmatrix} \cos\beta & \sin\beta \\ -\sin\beta & \cos\beta \end{bmatrix} \cdot E_{\mathrm{SHG}} \begin{bmatrix} \cos\zeta \\ \sin\zeta \end{bmatrix}.$$

The intensity of light detected by the photomultiplier then is:

$$I_{\mathrm{SHG}} = E_{SHG}^2 \cos^2(\beta - \zeta). \tag{2.32}$$

Therefore, as expected, the maximum of the signal $I_{\mathrm{SHG}} = \chi^{(\mathrm{i})2} I_0^2$ is observed when the analyzer axis is parallel to the polarization direction of the SHG signal and the minimum $I_{\mathrm{SHG}} = 0$ is observed, when they are perpendicular.

If the SHG signal is of pure magnetic origin, then the intensity of SHG light passing through the analyzer is $I_{\mathrm{MSHG}} = \chi^{(\mathrm{c})2} M I_0^2 \cos(\beta - \zeta_M)$, where ζ_M is the azimuthal angle for the polarization of the MSHG signal. This means that the reorientation of the magnetic order parameter (i.e. a sign change of $\hat{\chi}_M$) does not influence the measured signal. If this information is of particular interest, then a special experimental geometry can be used, where both crystallographic and magnetic contributions to the SHG signal are observed. In this case the light passing through the analyzer is:

$$\begin{bmatrix} E_x \\ E_y \end{bmatrix} = \begin{bmatrix} 1 & 0 \\ 0 & 0 \end{bmatrix} \cdot \Big(\begin{bmatrix} \cos\beta & \sin\beta \\ -\sin\beta & \cos\beta \end{bmatrix} \cdot E_{\mathrm{SHG}} \begin{bmatrix} \cos\zeta \\ \sin\zeta \end{bmatrix} + \begin{bmatrix} \cos\beta & \sin\beta \\ -\sin\beta & \cos\beta \end{bmatrix} \cdot E_{\mathrm{MSHG}} \begin{bmatrix} \cos\zeta_M \\ \sin\zeta_M \end{bmatrix} \Big).$$

The total intensity of SHG light measured in this case is $I = I_{\mathrm{SHG}} + I_{\mathrm{MSHG}} + 2\chi_{\mathrm{cr}}\chi_M I_0^2(\cos(\beta - \zeta)\cos(\beta - \zeta_M))$. The latter term in this expression changes sign when the direction of the magnetic order parameter M is reversed. In such experiments the magnetic contrast of the SHG signal is usually measured:

$$\frac{I(+M) - I(-M)}{I(+M) + I(-M)} = \frac{2\chi_{\mathrm{cr}}\chi_M I_0^2(\cos(\beta - \zeta)\cos(\beta - \zeta_M))}{I_{\mathrm{SHG}} + I_{\mathrm{MSHG}}} \tag{2.33}$$

Such technique, based on the interference of the crystallographic and magnetic SHG signals, can be used also to distinguish the magnetic contribution to the SHG signal when it is much smaller than the crystallographic one.

2.4 Time-resolved magneto-optical techniques

The experimental setup combining time-resolved linear and SHG measurements is shown in Fig. 2.6. As a source of high intensity short laser pulses the system combining

a Ti:Sapphire mode-locked laser and an amplifier was used. In a majority of the experimental results which are presented in this thesis, a system providing 150 fs laser pulses was used. In some experiments, requiring shorter pulse duration, a 40 fs-system was used.

2.4.1 Ti:Sapphire amplified system

The Ti:Sapphire system consists of

- *Tsunami* mode-locked Ti:Sapphire laser;
- *Millennia*[2] diode-pumped continuous wave Nd:YVO_4 laser;
- *Spitfire* pulsed Ti:Sapphire regenerative amplifier;
- *Merlin*[3] Q-switched intra cavity frequency doubled Nd:YLF laser.

All components are from SpectraPhysics. The system provides a train of 40-100 fs laser pulses with a repetition frequency of 1 kHz. The average output power is 2.2 W. The central wavelength of the pulses used in the experiments was 800 nm.

The *Millennia* laser providing 4.3 W CW radiation at a wavelength of 532 nm was used to pump the *Tsunami* mode-locked laser which output delivers 60 fs pulses[4] at 82 MHz repetition frequency. The output from the *Tsunami* laser is directed into the *Spitfire* regenerative amplifier pumped by *Merlin* Q-switched intra cavity frequency doubled Nd:YLF laser at λ=527 nm. The average output power of this pump laser is 10 W at a repetition rate of 1 KHz. The pulses from the *Tsunami* are stretched temporally inside the *Spitfire* by a grating-mirror system. The timed Pockels cell is used to insure that the pulses from the pump (*Merlin*) and seed (*Tsumani*) lasers arrive in the Ti:Sapphire active laser crystal at the same time. The pulses travel several times through the crystal providing the amplification of the pulse intensity. There exists an optimal number of round trips resulting in a maximal amplification. When the maximal amplification is achieved, a voltage is applied to a second Pockels cell allowing the pulse to leave the cavity. The following compression of the pulse is adjustable allowing to obtain pulse durations from 40 fs up to several picoseconds.

2.4.2 Principles of time-resolved pump-probe experiments

The principle of *stroboscopic*, time-resolved optical measurements, independent on the specific detection technique, is as follows. The beam from the laser system is split into two beams with ratio of intensities of about 100:1. The intense part is used as a

[2] In the 40 fs system - *Millennia Pro*
[3] In the 40 fs system - *Empower*
[4] In the 40 fs system a *Tsunami* model providing a pulse length of 35 fs was used

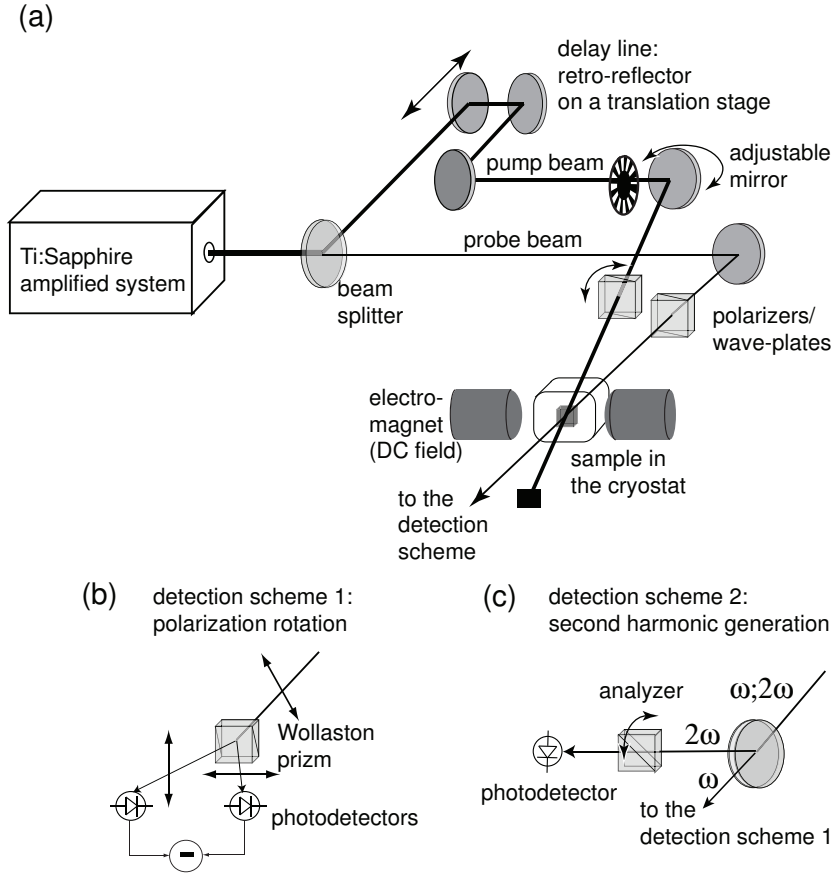

Figure 2.6: (a) The principle scheme of the pump-probe experiments. (b) Detection scheme used to measure the rotation of the probe polarization. (c) Detection scheme used to measure the intensity of the second harmonic signal.

pump beam, while the less intense one serves as a probe. The pump pulses are used to excite the dynamics of the magnetic order, electronic structure, lattice etc. The probe beam is used to monitor this dynamics as a function of time after the excitation event.

To realize the time resolution, one of the beams is sent via a delay line. In the experiments presented in this thesis, the delay line was incorporated into the pump path, as shown in Fig. 2.6(a). The delay line consists of an optical retro-reflector fixed on a movable stage driven by a step motor. The length of the delay line is 600 mm, corresponding to a maximal achievable delay time of 3.96 ns. The shortest step of the delay line is 1.5 μm, corresponding to a time resolution of 9.9 fs.

As each data point (at a given delay time) is obtained from averaging over typically 300 pulses, such stroboscopic experiments rely on the fact that between successive pump pulses the system has relaxed back to its original state. With a repetitive frequency of 1 kHz this means that the relaxation process should be faster than 1 ms, a condition that is met in all experiments presented here.

The polarization of the pump pulses is set by the half-wave plate for the experiments with linearly-polarized pulses or by a quarter-wave plate for the experiments with circularly polarized pulses. The probe beam was linearly polarized. The pump was focused to a spot of 100 μm in diameter on the sample. The probe beam was focused to a spot of smaller size to avoid the effect of small jitter of the beam on the measured signal. An adjustable mirror, providing the possibility to fine tune the position of the pump spot on the sample, was used to adjust the spatial overlap of the pump and probe pulses. In order to realize the lock-in based measurements requiring modulation, the pump beam was chopped at a frequency of 500 Hz by a synchronized chopper, which allowed to block every second pump pulse out of a 1 kHz sequence. Two sets of neutral density filters were used to control the intensity of the pump and probe beams independently.

The main subject of the work presented in this thesis was the study of coherent magnetic excitations induced by the laser pulses. The detection of these excitations was done by means of measurements of the linear magneto-optical effects or (magnetic) second harmonic generation.

Linear pump-probe measurements

The optical detection scheme shown in Fig.2.6(b) was used for the measurements of the time-resolved rotation of the probe polarization. The difference signal from the photodiodes was sent to a gated integrator and boxcar averager *SR250* (Stanford Research Systems). The trigger for the Pockells cells in the *Spitfire* amplifier was used as a trigger for the gated integrator. The gates were delayed with respect to the trigger in order to allow for the time needed for the probe pulse to reach the detector and for the delays introduced by the electronic equipment. The gate width was set to the maximal possible value for the integrator of 3 μs. This scheme allows to increase

the signal-to-noise ratio by measuring only the signal appearing at the time when the probe pulse reaches the detector. The averaged signal from the gated integrator and boxcar averager was sent to a lock-in amplifier *SR890* (Stanford Research Systems). The signal from the chopper (See Fig.2.6(a)), with a frequency of 500 Hz, was used as a reference signal for the lock-in amplifier. Therefore, only the changes in the rotation of the probe polarization appearing with the repetition frequency of the pump pulses are detected.

Nonlinear pump-probe measurements

For the measurements of the time-resolved SHG a detection scheme shown in Fig. 2.6(c) was used. The long-pass filter (not shown in Fig.2.6) was used to block parasitic SHG signal before the sample. The fundamental and SHG beams were separated using a mirror reflecting light at 400 nm and transmitting light at 800 nm. The analyzer could be rotated in order to suppress the crystallographic or magnetic contributions to the SHG signal. The SHG signal was registered using a photomultiplier. The signals from the multiplier were measured using the same principle as for the linear magneto-optical measurements described above. Typically, a SHG signal is weaker than the linear optical signals. Therefore, for the alignment of the setup - searching for the spatial and temporal overlap of pump and probe pulses - the fundamental beam was used with the detection scheme shown in Fig. 2.6(b).

References

[1] A. K. Zvezdin and V. A. Kotov, *Modern Magnetooptics and Magnetooptical Materials* (IOP Publishing Ltd., 1997).

[2] R. Szymczak, Acta Phys. Pol. A **43**, 571 (1973).

[3] V. Kirilyuk, A. Kirilyuk, and T. Rasing, Appl. Phys. Lett. **70**, 2306 (1997).

[4] M. Fiebig, D. Fröhlich, K. Kohn, S. Leute, Th. Lottermoser, V. V. Pavlov, and R. V. Pisarev, Phys. Rev. Lett. **84**, 56205623 (2000).

[5] J.-C. Diels and W. Rudolph, *Ultrashort Laser Phenomena. Fundamentals, Techniques and Applications on a Femtosecond Time Scale* (Elsevier, 2006).

[6] L. Dhar, J. A. Rogers, and K. A. Nelson, Chem. Phys. **94**, 157 (1994).

[7] K. Nakamoto, *Infrared and Raman Spectra of Inorganic and Coordination Compounds* (John Wiley & Sons, 1986).

[8] I. A. Walmsley, F. W. Wise, and C. L. Tang, Chem. Phys. Lett. **154**, 315 (1989).

[9] J. Chesnoy and A. Mokhtai, Phys. Rev. A **38**, 3566 (1988).

[10] Y. R. Shen, *The Principles of Nonlinear Optics* (John Wiley & Sons, 1985).

[11] M. Fiebig, V. V. Pavlov, and R. V. Pisarev, J. Opt. Soc. Am. B **22**, 96 (2005).

[12] P. S. Pershan, Phys. Rev. **130**, 919 (1963).

[13] T. Brabec and F. Krausz, Rev. Mod. Phys. **72**, 545 (2000).

[14] R. R. Birss, Rep. Prog. Phys. **26**, 307 (1963).

[15] E. A. Turov, Phys. Usp. **37**, 303 (1994).

[16] L. D. Landau, E. M. Lifshitz, and L. P. Pitaevskii, *Landau and Lifshits course of Theoretical Physics. Vol. 8 Electrodynamics of Continious Media* (Elsevier, 2006).

[17] L. D. Landau, E. M. Lifshitz, and L. P. Pitaevskii, *Landau and Lifshits course of Theoretical Physics. Vol. 5 Statistical Physics. Part 1* (Elsevier, 2006).

[18] R. M. A. Azzam and N. M. Bashara, *Ellipsometry and Polarized Light* (Elsevier, 1987).

[19] R. V. Pisarev, Sov. Phys. - JETP **31**, 761764 (1970).

[20] G. A. Smolenskiĭ, R. V. Pisarev, and I. G. Siniĭ, Phys. Usp. **116**, 213 (1975).

[21] W. J. Tabor and F. S. Chen, J. Appl. Phys **40**, 2760 (1969).

[22] P. S. Pershan, J. Appl. Phys. **38**, 1482 (1967).

[23] J. Ferré and G. A. Gehring, Rep. Prog. Phys. **47**, 513 (1984).

[24] M. I. Boamfă, K. Viertler, A.Wewerka, F. Stelzer, P. C. Christianen, and J. C. Maan, Phys. Rev. Lett. **90**, 025501 (2003).

[25] M. Fiebig, D. Fröhlich, G. Sluyterman v. L., and R. V. Pisarev, Appl. Phys. Lett. **66**, 2906 (1995).

[26] M. Fiebig, D. Fröhlich, Th. Lottermoser, and M. Maat, Phys. Rev. B **66**, 144102 (2002).

[27] A. Kirilyuk and T. Rasing, J. Opt. Soc. Am. B **22**, 148 (2000).

[28] M. Fiebig, Th. Lottermoser, D. Fröhlich, A. V. Goltsev, and R. V. Pisarev, Nature (London) **419**, 818 (2002).

[29] D. E. Aspnes, Thin Solis Films **455-456**, 3 (2002).

[30] *Guide to Using WVASE32*, J. A. Woolam Co., Inc., New York (2003).

[31] *PEM-90*$^{\mathrm{TM}}$ *Photoelastic Modulator*, HINDS Instruments, Inc., Hillsboro (1998).

CHAPTER 3

Iron oxides

The experimental results which are presented in this thesis, were obtained from two materials - an iron borate $FeBO_3$ and a gallium ferrite $GaFeO_3$ single crystal. Both are magnetically ordered dielectric materials relatively transparent in the vicinity of the central pulse energy of a Ti:Sapphire laser (1.5 eV or 800 nm). $FeBO_3$ represents a model example of a magnetic dielectric material consisting of several sublattices and possessing a high magneto-optical susceptibility. $GaFeO_3$ is interesting primary due to the coexistence of magnetic and electric ordering (multiferroicity) at temperatures close to room temperature. In this Chapter the crystallographic and magnetic structures of these two materials are described on a basis of the literature data.

3.1 Iron borate $FeBO_3$

Iron borate $FeBO_3$ received a lot of attention since its discovery, mainly because of the combination of a number of attractive optical and magneto-optical properties it possesses [1]. In particular, it combines high values of the Faraday rotation and a high transparency in visible and near-infrared parts of the optical spectrum. This makes $FeBO_3$ a good candidate for various magneto-optical studies. Moreover, from the magnetic point of view iron borate is a two sublattice antiferromagnet with a bulk weak magnetic moment and a highly anisotropic spin precession. These properties defined the choice of $FeBO_3$ as a model material for the study of light-induced magnetic excitations, discussed in Chapters 5 and 6.

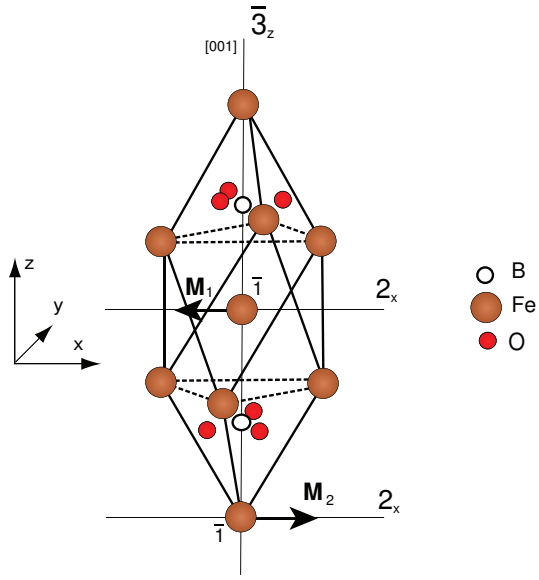

Figure 3.1: Schematic representation of the crystallographic structure of $FeBO_3$ [1]. Thin solid lines show the symmetry elements, such as rotation axes $\bar{3}_z$ and 2_x. $\mathbf{M}_{1,2}$ are the magnetic moments of the Fe^{3+} ions.

3.1.1 Crystallographic structure and growth

Iron borate $FeBO_3$, crystallizes in the rhombohedral calcite-type structure (space group $R\bar{3}c$, point group $\bar{3}m$) with two formula units per unit cell. The schematic representation of the crystallographic structure of $FeBO_3$ is shown in Fig.3.1 [1, 2, 3]. Two Fe^{3+} ions occupy identical octahedrally coordinated positions with a symmetry C_{3i} [4] along the three-fold symmetry axis, which is denoted as z axis in Fig. 3.1 and below in the discussion. Three two-fold symmetry axes are perpendicular to this axis. The positions of the iron ions coincide with the inversion symmetry centers that play an important role for the properties of the magnetic part of the dielectric tensor [5], as discussed in the next Chapter.

The samples used in the present study were grown[1] by two methods: from the flux and from the gas phase. The samples grown from the flux were thin (186 μm) samples with the normal along the crystallographic z axis. However, for the sake of completeness of our studies, also samples with the z axis lying in the sample plane

[1]The samples used in the experiments were grown by G. T. Andreeva in A. F. Ioffe Institute of Russian Academy of Sciences

were crucial. Such samples were obtained using the method of growth from the gas phase. A thin plate with the normal along the y axis with a thickness of 190 μm was cut from this sample.

3.1.2 Equilibrium magnetic properties

Below the Neel temperature T_N=348 K, the magnetic moments $\mathbf{M}_1$ and $\mathbf{M}_2$ of the two Fe^{3+} ions form two antiferromagnetically coupled sublattices, as shown in Fig. 3.1. It is common to describe this magnetic structure in terms of the ferromagnetic vector $\mathbf{M}=\mathbf{M}_1+\mathbf{M}_2$ and the antiferromagnetic vector $\mathbf{L}=\mathbf{M}_1-\mathbf{M}_2$, as shown in Fig. 3.2(a). In terms of these vectors the Hamiltonian describing the magnetic structure of $FeBO_3$ has the form (for a homogeneous case) [6]

$$\mathcal{H} = \frac{A}{2}\mathbf{M}^2 + \frac{b}{2}L_z^2 + \frac{a}{2}M_z^2 - D[\mathbf{M}\times\mathbf{L}]_z - \mathbf{MH}. \tag{3.1}$$

Often the parameters of the magnetic structure are given in terms of effective fields $\mathbf{H}^{\text{eff}} = -\partial\mathcal{H}/\partial\mathbf{M}(\mathbf{L})$. The first term in Eq. (3.1) describes the isotropic exchange interactions and corresponds to an effective exchange field[2] $H_E = A|\mathbf{M}| = 2.6\cdot 10^3$ kOe. The second and third terms describe the magneto-crystalline anisotropy. The constants a, b are positive, which corresponds to an "easy-plane" type of spin alignment, where spins of both sublattices are perpendicular to the crystallographic z axis. The effective magneto-crystalline anisotropy field is $H_A \simeq 1.7$ kOe. The presence of the fourth term in Eq. (3.1) accounts for the antisymmetric exchange interactions [8, 9], leading to a canting of the spins in the xy plane. The effective Dzyaloshinskii field is $H_D \simeq 61.9$ kOe, corresponding to a canting angle of $\sim H_D/H_E \simeq 1^{\text{o}}$ and a net magnetic moment of $4\pi M_s$=115 G at T =300 K [10] (238 G at $T\to 0$ K). The magneto-crystalline anisotropy in the xy plane is as weak as $H_{A'} \simeq 0.26$ Oe. Therefore, a small magnetic field of up to 0.5 kOe applied in the xy plane was sufficient to saturate the samples.

3.1.3 Dynamic magnetic properties

In general, the precession of a magnetic moment $\mathbf{M}_i$ around its equilibrium position, defined by intrinsic and applied fields, is described by the Landau-Lifshitz (L-L) equation [11]. In the case of $FeBO_3$, comprised of two magnetic sublattices, the spin precession is usually described as the precession (including change of length for the high-energy modes) of the ferromagnetic $\mathbf{M}(t)$ and antiferromagnetic $\mathbf{L}(t)$ vectors (Fig. 3.2(b-c)), for which the L-L equations have the form [5, 12]

$$\frac{d\mathbf{M}(t)}{dt} = -\gamma\left(\left[\mathbf{M}(t)\times\mathbf{H}^{\text{eff}}\right] + \left[\mathbf{L}(t)\times\mathbf{h}^{\text{eff}}\right]\right) + \mathbf{R}_M; \tag{3.2a}$$

[2] All values of the effective fields are given for room temperature according to [7] and references therein.

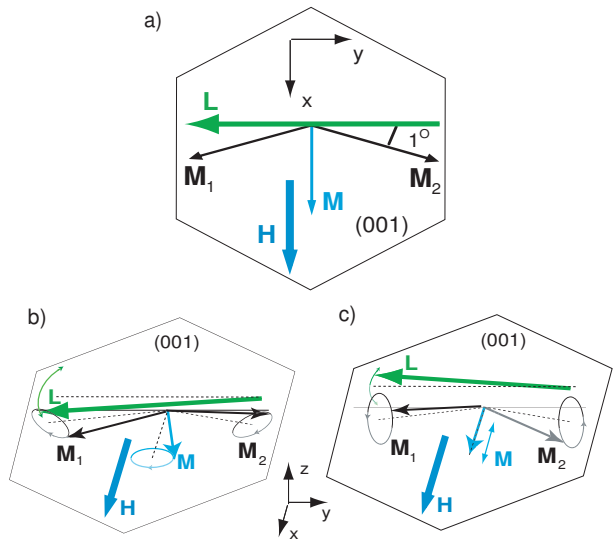

Figure 3.2: (a) Magnetic structure of the $FeBO_3$ in the xy easy-plane. Two modes of spin precession excist: (b) quasi-ferromagnetic and (c) quasi-antiferromagnetic resonance modes [1, 7].

$$\frac{d\mathbf{L}(t)}{dt} = -\gamma \left(\left[\mathbf{M}(t) \times \mathbf{h}^{\text{eff}} \right] + \left[\mathbf{L}(t) \times \mathbf{H}^{\text{eff}} \right] \right) + \mathbf{R}_L, \tag{3.2b}$$

where γ is the gyromagnetic ratio. The effective fields $\mathbf{H}^{\text{eff}}$ and $\mathbf{h}^{\text{eff}}$ include the internal and applied magnetic fields and are defined as the gradients $\mathbf{H}^{\text{eff}}$=-$\partial\mathcal{H}/\partial\mathbf{M}$ and $\mathbf{h}^{\text{eff}}$=-$\partial\mathcal{H}/\partial\mathbf{L}$ of the Hamiltonian (3.1) with respect to the corresponding vectors. The terms $\mathbf{R}_{M(L)}$ account for the damping of the precession amplitude of $\mathbf{M}$ and $\mathbf{L}$, respectively. Below we neglect the damping terms because they do not play any role in the discussion.

The two eigen-solutions of the linearized Eqs. (3.2) give two spin precession modes existing in $FeBO_3$, with the frequencies [7, 13, 14]

$$\Omega^{\text{FMR}} = \gamma\sqrt{H(H + H_D) + 2H_E H_{A'}}, \tag{3.3a}$$

$$\Omega^{\text{AFMR}} = \gamma\sqrt{H_D(H + H_D) + 2H_E H_A}. \tag{3.3b}$$

Eq.(3.3a) describes the frequency Ω^{FMR} of the low-energy quasi-ferromagnetic resonance (FMR) mode (Fig. 3.2(b)) [15]. This is a homogenous precession of the magnetic moments of the two sublattices in such a way that the angle between them does not change. Eq.(3.3b) represents the high-energy quasi-antiferromagnetic resonance

(AFMR) mode (Fig. 3.2(c)). In this mode the angle between the sublattice magnetic moments varies. The ferromagnetic and antiferromagnetic vectors can be represented as a sum of static $\mathbf{M}^{(0)}$ and $\mathbf{L}^{(0)}$ and time-dependent $\mathbf{m}(t)$ and $\mathbf{l}(t)$ components

$$\mathbf{M}(t) = \mathbf{M}^{(0)} + \mathbf{m}(t), \tag{3.4a}$$

$$\mathbf{L}(t) = \mathbf{L}^{(0)} + \mathbf{l}(t). \tag{3.4b}$$

In these terms the FMR mode involves oscillations of the l_x, m_y, and m_z components of $\mathbf{l}(t)$ and $\mathbf{m}(t)$ while the AFMR mode involves time variations of the m_x, l_y and l_z components.

The FMR mode is characterized by strong ellipticity,[3] which is related to the weakness of the in-plane magneto-crystalline anisotropy as compared to the out-of-plane one. For a magnetic field applied in the easy plane of magnetic anisotropy along the x axis, the ratios between the out-of-plane and in-plane deviations of the spins are [7]

$$\frac{m_z}{l_x} = \frac{\Omega^{\mathrm{FMR}}}{2\gamma H_E};\ \frac{m_z}{m_y} = \frac{\Omega^{\mathrm{FMR}}}{2\gamma H_D}. \tag{3.5}$$

For moderate magnetic fields around H =10 kG, this gives $m_z/l_x \sim 0.01$ and $m_z/m_y \sim 0.4$. The ellipticity of the AFMR mode [7] is, in turn,

$$\frac{l_z}{m_x} = \frac{\Omega^{\mathrm{AFMR}}}{2\gamma H_E} \sim 0.1 \tag{3.6}$$

and is weaker by an order of magnitude than that for the FMR mode.

3.2 Gallium ferrite $GaFeO_3$

The gallium ferrites $Ga_{2-x}Fe_xO_3$, in particular $GaFeO_3$ (x = 1), synthesized for the first time by Remeika [16], have attracted much attention because of the coexistence of ferrimagnetic ordering and a spontaneous electric polarization at temperatures close to room temperature and even above. It is this material that was the first ferrimagnet in which a linear magnetoelectric effect was observed [17].[4]

3.2.1 Crystallographic structure and growth

The crystallographic structure of the compounds $Ga_{2-x}Fe_xO_3$ depends on the concentration of Fe^{3+} ions. Thus, in a range of concentrations $0.7 < x < 1.4$ the compound

[3] Here we define ellipticity of the spin precession as the ratio between out-of-plane and in-plane deviations of the spins. By a strong ellipticity we mean that the in-plane deviation is much larger than the out-of plane one.

[4] Before that work the magnetoelectric effect had been observed in antiferromagnets only. Note, that $Ga_{2-x}Fe_xO_3$ was thought to be a ferromagnet in [17]. Its ferrimagnetic nature was demonstrated a year later in [18].

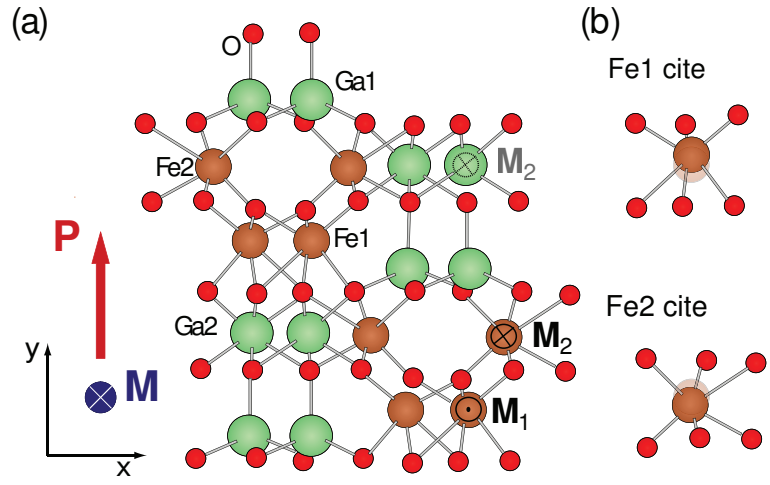

Figure 3.3: (a) Crystallographic structure of $GaFeO_3$ [19] and the direction of the magnetization **M** and the spontaneous electric polarization **P**. Fe1,2 and Ga1,2 denote four cation sites occupied predominantly by Fe^{3+} and Ga^{3+}, respectively. $\odot\mathbf{M}_1$ corresponds to the orientation of iron ion magnetic moments in Fe1 sites and $\otimes\mathbf{M}_2$ indicates the orientation of the magnetic moment of iron ions in Fe2 and Ga2 sites, antiparallel ($\odot$) and parallel ($\otimes$) to the crystallographic z axis, respectively. (b) The shift of the Fe^{3+} ions from the centra of the oxygen octahedra at sites Fe1 and Fe2.

has an orthorhombic crystallographic structure with eight formula units per unit cell [20]. In this range $Ga_{2-x}Fe_xO_3$ belongs to the $Pc2_1n$ space group ($m2m$ point group). The schematic representation of the crystallographic structure of $Ga_{2-x}Fe_xO_3$ is shown in Fig. 3.3(a). The lattice constants along the x, y and z axes are $a = 8.77\,\AA$, $b = 9.44\,\AA$ and $c = 5.08\,\AA$, respectively [16, 20]. If the concentration x of Fe^{3+} ions exceeds 1.4, the compound possesses the rhombohedral structure, similar to the one of hematite $\alpha-Fe_2O_3$.

In orthorhombic gallium ferrites four nonequivalent cation crystallographic sites, occupied by Ga^{3+} and Fe^{3+} ions, have been distinguished [21], as depicted in Fig. 3.3(a). One of the sites, denoted as Ga1, has a tetrahedral symmetry and is occupied almost exclusively by Ga^{3+} ions, while the other three octahedral sites are occupied by Fe^{3+} and Ga^{3+}. The ions in the Fe1 and Fe2 sites are located in distorted oxygen-octahedra and are shifted from the central positions along the y axis by +0.26 and -0.11 $\AA$, respectively (See Fig. 3.3(b)). These sites are occupied for the most part by Fe^{3+} ions. However, the Ga^{3+} ions access both Fe sites and *vice versa*. The degree of this occupation depends on the growth procedure used and influences the magnetic properties

of the compound [19]. In view of this, the growth procedures for gallium ferrites are considered below in some detail.

Two methods to grow $Ga_{2-x}Fe_xO_3$ crystals are reported. Initially, the flux method was used [16] to obtain single crystals of gallium ferrite. However, the size of the crystals, in particular the dimension along the y axis, is usually not sufficient for many experimental studies [19]. Therefore, the floating-zone method (FZ) was employed [19] to obtain crystals of a reasonable size. However, this growth method appeared to affect a number of the properties of the obtained single crystals. Namely, when the flux method is used, a mixture of Ga_2O_3 and Fe_2O_3 is slowly cooled from a temperature of 800^oC [16], which is significantly lower than in the case of the FZ method with a melting point of 1600^oC [19]. This temperature affects the randomness in the occupation of Fe1,2 and Ga1,2 sites by gallium and iron ions which is lower for the lower temperatures. Thus, for the single crystals $Ga_{0.85}Fe_{1.15}O_3$ grown by the flux method the Fe occupation parameters of the Fe1,2 and Ga2 sites is larger than for the ones grown by the FZ method, while for the Ga1 sites this parameter is smaller and can be equal to zero [19, 22].

The samples used in this work[5] were thin plates of 60 and 62 μm thick, with the normals along z and y axes, respectively, cut from bulk crystals grown by the flux method, which details are reported in [23]. The surface dimensions of the samples were sufficient to carry out the optical studies. The crystallographic structure and the orientation of the crystals were checked by X-ray and the obtained parameters were in a good agreement with the data from the literature [24].

3.2.2 Pyroelectric properties

The Fe^{3+} ions in the two octahedral positions Fe1 and Fe2 are displaced from the centers of the oxygen octahedrons in opposite directions along the y axis (See Fig. 3.3(b)), resulting in a spontaneous electric polarization of -0.025 C/m^2 [19] along this axis (Fig.3.3). The attempts to observe the ferroelectric hysteresis loops in this compound failed and the compound was thus proven to be pyroelectric [16].

3.2.3 Magnetic properties

From the magnetic point of view the gallium ferrite is ferrimagnetic [18] although it was initially thought to be a ferromagnet [17] or a weak ferromagnet [16, 21]. The spins of the Fe^{3+} ions in the Fe1,2 sites are aligned along the crystallographic z axis and are coupled antiferromagnetically, as shown in Fig. 3.3(a). The y axis is the hard magnetization axis [19]. Due to the different occupation numbers for Fe^{3+} at

[5]The samples were grown by L. N. Bezmaternykh and V. L. Temerov in the Institute of Physics of Siberian Branch of Russian Academy of Sciences (Krasnoyarsk).

the sites Fe1 and Fe2, a bulk magnetic moment is observed and the $Ga_{2-x}Fe_xO_3$ is ferrimagnetic.

The Curie temperature lies in the wide range of 200-345 K, depending on the concentration x and on the growth procedure. A detailed study of the relation between the concentration x and the Curie temperature of the crystals grown from the flux is presented in [25] for all range of concentrations where $Ga_{2-x}Fe_xO_3$ possesses the orthorhombic structure. The experimental trend in the dependence of the Curie temperature on the concentration x demonstrates a clear linear proportionality with the Curie temperature, being 200 K for x=0.8 and 350 for x=1.1. The low temperature magnetic moment, i. e. the one at 0 K, also follows a linear dependence on the concentration x [25]. The average magnetic moment per iron ion was determined to be 0.76 μ_B.

Crystals with the same composition but grown by different methods possess different Curie temperatures. Thus, it was shown [19] that the crystals grown by the FZ method typically have lower Curie temperatures than the crystals grown from the flux. This is explained by the different access of Fe ions to the Ga cites and *vice versa*. The superexchange interaction between the Fe^{3+} ions is affected by the Fe-O-Fe bond angle. In [19] the bond angle between Fe1-O-Fe2 is reported to be 166^o and is proposed to be responsible for the ferrimagnetic ordering. The bond angle Fe1-O-Fe(Ga2) is 164^o and is responsible for the antiferromagnetic alignment of the magnetic moments of the Fe ions in the sites F1 and Ga2. Therefore, the replacement of Ga by Fe at the site Ga2 should raise the T_C through the stronger antiferromagnetic ordering. Indeed, the samples grown by the FZ method possess a lower occupation of the Ga2 site by Fe ions and, therefore, these samples have lower Curie temperatures than the samples grown from the flux [19]. The dependence of the Curie temperature on the iron concentration x is similar for the samples grown from the flux and by the FZ method.

References

[1] Landoldt-Börnstein, *Group III Condenced Matter, vol. 27H* (Springer-Verlag GmbH, 1993).

[2] I. Bernal, C. W. Struck, and J. G. White, Acta Cryst. **16**, 849 (1963).

[3] R. Diehl, Solid State Comm. **17**, 743 (1975).

[4] B. Andlauer, O. F. Schirmer, and J. Schneider, Solid State Comm. **13**, 1655 (1973).

[5] E. A. Turov, A. V. Kolchanov, V. V. Men'shenin, I. F. Mirsaev, and V. V. Nikolaev, *Symmetry and physical properties of antiferromagnets* (Fizmatlit, Moscow, 2001).

[6] E. A. Turov, *Physical Properties of Magnetically Ordered Crystals* (Academic Press, New York, 1965).

[7] J. Schober, IEEE Trans. Magn. **12**, 401 (1976).

[8] I. Dzyaloshinsky, J. Phys. Chem. Solids **4** (1958).

[9] T. Moriya, Phys. Rev. **120** (1960).

[10] A. J. Kurtzig, R. Wolfe, R. C. LeCraw, and J. W. Nielsen, Appl. Phys. Lett. **14** (1969).

[11] L. Landau and E. Lifshitz, Phys. Z. Union **8** (1935).

[12] A. S. Borovik-Romanov and N. M. Kreines, Phys. Rep. **81** (1982).

[13] E. A. Turov and N. G. Guseĭnov, Sov. Phys. - JETP **11** (1960).

[14] W. Jantz, J. R. Sandercock, and W. Wettling, J. Phys. C **9** (1976).

[15] R. C. LeCraw, R. Wolfe, and J. W. Nielsen, Appl. Phys. Lett. **14** (1969).

[16] J. P. Remeika, J. Appl. Phys. **31**, 263S (1960).

[17] J. T. Rado, Phys. Rev. Lett. **13**, 335 (1964).

[18] R. B. Frankel, N. A. Blum, S. Foner, A. J. Freeman, and M. Schieber, Phys. Rev. Lett. **15**, 958 (1965).

[19] T. Arima, D. Higashiyama, Y. Kaneko, J. P. He, T. Goto, S. Miyasaka, T. Kimura, K. Oikawa, T. Kamiyama, R. Kimari, et al., Phys. Rev. B **70**, 064426 (2004).

[20] E. A. Wood, Acta Cryst. **13**, 628 (1960).

[21] C. S. Abrahams and J. M. Reddy, Phys. Rev. Lett **13**, 688 (1964).

[22] C. S. Abrahams and J. M. Reddy, J. Phys.: Cond. Matter **28**, 1451 (28).

[23] A. M. Kalashnikova, R. V. Pisarev, L. N. Bezmaternykh, V. L. Temerov, A. Kirilyuk, and Th. Rasing, JETP Lett. **81**, 452 (2005).

[24] C. S. Abrahams, J. M. Reddy, and J. L. Bernstein, J. Chem. Phys. **42**, 3957 (1965).

[25] C. N. Nowlin and R. V. Jones, J. Appl. Phys. **34**, 1262 (1963).

CHAPTER 4

Optical properties of iron oxides[1]

4.1 Introduction

This Chapter is devoted to the study of the optical and magneto-optical properties of iron borate $FeBO_3$ and gallium ferrite $GaFeO_3$. The linear optical characteristics of iron oxides, such as dielectric functions and optical constants and their anisotropy, are obtained in the wide spectral range of 0.6-5.6 eV. The structure of the obtained spectra was assigned to the energy levels of the iron ion in the oxygen cluster. The dependence of the optical properties below and above the band gap on the particular crystallographic structure is discussed. In the introductory part the energy levels contributing to the formation of the optical spectra of the dielectric iron oxides are considered briefly.

The study of the magneto-optical effects in the iron oxides $FeBO_3$ and $GaFeO_3$ is of particular importance for the pump-probe experiments, which are the main subject of this thesis. The results of the linear magneto-optical measurements are presented in this Chapter following a brief overview of the origin of the magneto-optical effects in iron oxides, given in the introduction. In $GaFeO_3$ the magneto-optical response appeared to be rather weak, which drastically reduces the sensitivity of the pump-probe measurements. Therefore, the non-linear magneto-optical response, magnetic

[1]Based on: A. M. Kalashnikova, R. V. Pisarev, L. N. Bezmaternykh, V. L .Temerov, A. Kirilyuk, and Th. Rasing, *JETP Lett.* **81**, 452 (2005) and P. A. Markovin, A. M. Kalashnikova, R. V. Pisarev, and Th. Rasing, *JETP Lett.* **86**, 712 (2007).

second harmonic generation (MSHG), was studied in $GaFeO_3$ as an alternative optical tool for monitoring its magnetic structure.

4.1.1 Energy level diagram of iron oxides

Crystal field splitting

The energy levels of the outer shell of a free ion are degenerate. However, when the ion is in a crystal, the specific environment creates a crystal field which lifts the degeneracy and defines the spectrum of the energy levels of the ion [1]. In the iron oxides considered in this thesis, the ion Fe^{3+} is surrounded by six ligands (O^{2-} ions), forming the octahedral complex distorted to a certain degree. To obtain the energy spectrum for the particular crystal, the spectrum of the iron ion in the ideal octahedral coordination is used as a starting point. The splitting of the energy levels of the Fe^{3+} ion in the cubic crystal field (symmetry O_h) is shown in Fig. 4.1(b). Energy level t_{2g} corresponds to the xy, xz, and yz orbitals pointing between the ligands. Since x, y and z axes are indistinguishable in the regular octahedron, energies of these orbitals are degenerate. The energy level e_g corresponds to the orbitals z^2 and x^2-y^2 pointing towards the ligands along the z axis and in the xy plane, respectively. Their energies are, again, degenerate, but higher than for the t_{2g} level.

The distortion of the octahedral complex leads to a further splitting of these two energy levels. For example, the elongation of the octahedron along the z axis leads to the degeneracy lifting between z^2 and $x^2 - y^2$ orbitals making the energy of z^2 lower (Fig. 4.1(c)). In the same manner, the energy of the xy orbital becomes higher than the energy of the xz and yz orbitals, which remain degenerate. This degeneracy would be lifted by a further distortion of the octahedron in the xy plane.

This model describes adequately an ion containing one electron in the outer shell. However, in the oxides considered in this thesis the Fe^{3+} ion contains five electrons in its outer shell. In order to construct the term diagrams and to predict the transitions for such a multi-electron system the energy levels derived for the single-electron ion can be used as a starting point [1, 2].

In the ground state five unpaired electrons of the outer shell of the Fe^{3+} ion occupy each one orbital, as shown in the Fig. 4.2 on the left-hand side. The intraband excitations, i.e. the excitations inside the d shell, known also as the $d-d$ excitations, lead to the lower spin states, some of which are shown in Fig. 4.2 on the right-hand side. The selection rules define the probability and, consequently, the intensity of the transitions from the ground state $^6A_1$ to one of the excited states. They are: (i) electric dipole transitions between states of equal parity are forbidden in this approximation. This means, in particular, that the $d - d$ transitions are forbidden. (ii) The electric-dipole transitions between wavefunctions with different spin numbers are forbidden, which, again, prohibits transitions from the high-spin ground state $^6A_1$ to the low-spin excited states. Certainly, magnetic dipole and electric quadrupole

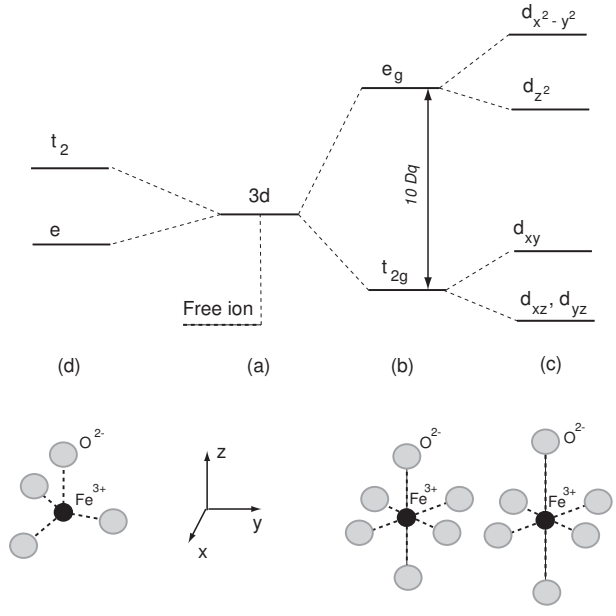

Figure 4.1: Energy levels in the point-charge approximation: (a) spherically perturbed d shell, (b) octahedral perturbation, (c) octahedron with small tetragonal perturbation (elongation along the z axis), and (d) tetrahedral perturbation.

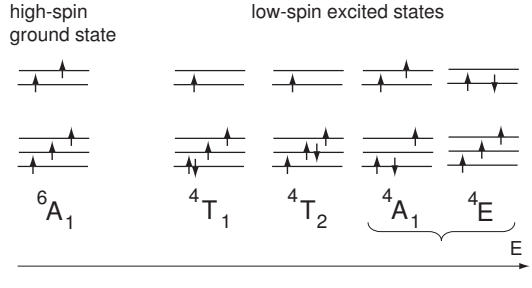

Figure 4.2: Electronic configuration for the d^5 ion in the octahedral field [1]. The order of the excited levels is given according to [2] for a moderate crystal field. The abbreviations common in the spectroscopic literature are used to mark the levels.

transitions might contribute to the optical spectra. However, as far as the transition metal oxides are concerned, these transitions have very low probability [1, 3]. The electric-dipole transitions, in turn, appear to have non-zero intensity in most of iron oxide compounds, partly because of the non-centrosymmetrical crystal fields and the phonon-assisted electronic transitions. The probability of these transitions typically exceeds the probability of the magnetic dipole and magnetic-quadrupole transitions by several orders of magnitude [2].

The position of the $d-d$ transitions depends on the crystal field parameter Dq, defining the splitting between the t_{2g} and e_g terms (Fig. 4.1) and on the other parameters defining the further splitting of these levels [1]. Typically they are located in the energy range of 1-3 eV for iron oxides.

Charge-transfer transitions

The absorption above ∼3 eV is defined by the charge-transfer transitions, which are, in a cluster model, the electron transfers from the ligand (O^{2-}) ion to the iron ion. In a band model they are seen as electronic transitions from the valence band to the conduction band, formed predominantly by the oxygen $2p$ and iron $3d$ orbitals, respectively. As intensity of the electric dipole transition is the higher the larger the change in the dipole moment, the charge-transfer (CT) transitions possess a much higher intensity than the $d-d$ transitions. Note that the CT transitions, being the $p-d$ transitions preserving the spin parity, are allowed in the electric-dipole approximation.

The scheme of the CT transitions for the FeO_6 octahedral complex was obtained from the nonempirical calculations in [4]. The following CT transitions form the optical spectrum of the FeO_6 complex: $1t_{2u}^{\downarrow}$, $6t_{1u}^{\downarrow}$, $5t_{1u}^{\downarrow} \rightarrow 2t_{2g}^{\downarrow}$, $4e_{2g}^{\downarrow}$. The superscript $\downarrow$ indicates that the electron transfers to the unoccupied d levels of the Fe^{3+} ion which are separated by a gap from the filled $2p$ states of oxygen. In Fig.4.3 the energy levels, relevant for the range of 0.6-5.6 eV, for the FeO_6 complex are shown.

It is worth to note that in dielectrics the determination of the fundamental band gap E_g is somewhat ambiguous, because they do not possess such a sharp absorption edge as, for example, semiconductors. Moreover, the $d-d$ transition ${}^6A_1 \rightarrow {}^4A_1, {}^4E$ is often very close to the first CT transition. However, the central energy of the lowest CT transition can be used as a convenient characteristic of the the band gap in oxides.

Determination of the electronic transitions in experimental spectra

The spectra of the dielectric functions presented in this Chapter are obtained from the ellipsometric measurements described in Section 2.2.2. To locate the positions of the optical transitions contributing to the dielectric susceptibility, these spectra were

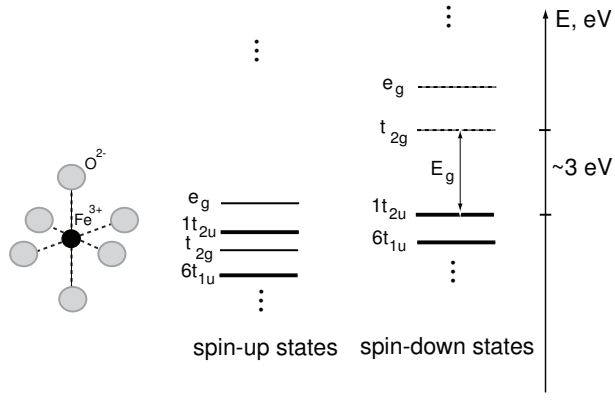

Figure 4.3: Energy level diagram for an FeO_6 complex [4]. The levels, contributing to the absorption spectrum in the range 2-6 eV are shown. Thick lines show the occupied states of the oxygen, while thin ones indicate the filled (solid) and empty (dashed) states of Fe^{3+}.

fitted[1] using a superposition of Lorentz functions

$$\varepsilon(E) = \varepsilon_1(E) - i\varepsilon_2(E) = \varepsilon(0) + bE + \sum \frac{f_j}{E_j^2 - E^2 - jE\gamma_j}, \tag{4.1}$$

where $\varepsilon(0)$ is the dielectric permittivity at zero frequency and f_j, E_j and γ_j are the oscillator strength, central energy and the broadening of the j-th transition [5]. The linear term bE is introduced to account for the transitions at energies higher than the studied range of 0.6-5.8 eV.

4.1.2 Magneto-optical effects

The large values of the magneto-optical effects observed in various iron oxide dielectrics, e.g. iron garnets and rare-earth orthoferrites, are attributed to the electric-dipole transitions from the ligands to the $3d$ shell of Fe^{3+} ion [6, 7, 8]. As an example here we consider the Faraday effect, consisting of the rotation of the polarization of light propagating along the magnetization of a medium (Eq. (2.13)).

The ground state of the Fe^{3+} ion in the iron oxide ${}^6A_{1g}$ is a singlet with orbital momentum $L = 0$. The excited states for the CT transitions have the symmetry ${}^6T_{1u}$ with orbital momentum $L = 1$. Therefore, the spin-orbit interactions λ_{SL} only split

[1] For the fit of some experimental curves the program kindly provided by V. V. Pavlov from A. F. Ioffe Institute of Russian Academy of Sciences was used.

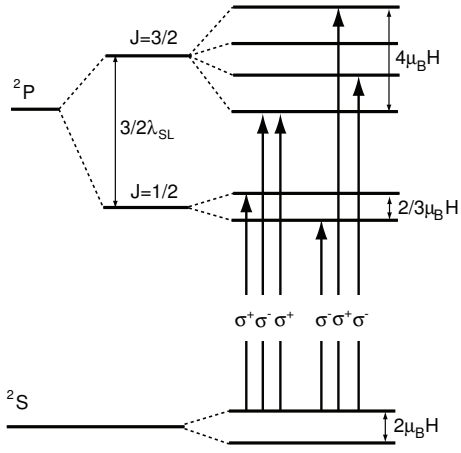

Figure 4.4: The diagram of the energy levels contributing to a formation of the magneto-optical effects in the oxides of the Fe^3+ ion and the scheme of the electric-dipole allowed transitions for the right- (σ^+) and the left-handed σ^- circularly polarized light.

the energy levels of the excited state, as shown in Fig. 4.4 for the case of the ground ^2S and excited ^2P levels. Both terms are split by the external magnetic field H.

At T=0 only the lowest sublevel of ^2S is populated. The transitions allowed in the electric-dipole approximation in this case for the right- (σ^+) and left-handed (σ^-) circularly polarized light are shown in Fig. 4.4. At finite temperatures the higher sublevel of ^2S is populated and the transitions from this level, shown in Fig. 4.4, contribute to the interaction of light with the medium. The overall matrix elements for the σ^+ and σ^- transitions are the same if one disregards the difference between the energies of these transitions and the difference between the population of the sublevels of ^2S [7, 8]. Therefore, the magnetic circular dichroism appears because of (i) the difference in the energies of these transitions and (ii) and the difference in the the population of the sublevels of ^2S. The contribution (i) to the magneto-optical effect is called diamagnetic, while the contribution (ii) - paramagnetic. The shift of the central energies of the allowed transitions and the difference in their intensities for light with opposite helicities also lead to the difference in the dispersion curves far from the resonant energy. As a consequence, the refraction indices for right- and left-handed circularly polarized light are different in the transparency region, leading to a Faraday rotation.

It is worth to note that the magnetic linear birefringence (MLB) is an effect of second order in the magnetic order parameters. Nevertheless, in a magnetically

Table 4.1: Crystallographic and magnetic contributions to the symmetric $\hat{\varepsilon}^s$ and antisymmetric $\hat{\varepsilon}^a$ parts of the dielectric permittivity tensor for $FeBO_3$.

ε^s_{ij}	Crystallographic contribution	Contribution caused by L_y, M_x	ε^a_{ij}	Contribution caused by L_y, M_x
xx	ε_{xx}	$b_2L_y^2 + c_1M_xL_y$		
yy	ε_{xx}	$b_1L_y^2 - c_2M_xL_y$		
zz	ε_{zz}	$b_3L_y^2 + c_4M_xL_y$		
xy	–	–	xy	–
xz	–	–	xz	–
yz	–	$-b_4L_y^2 + c_5M_xL_y$	yz	$iK_1M_x - iK_2L_y$

ordered medium MLB can be comparable with the Faraday effect [9, 10], which is a first order effect.

4.2 Optical properties of $FeBO_3$

4.2.1 Anisotropy of dielectric permittivity at optical frequencies

Table 4.1 lists the contributions of various origin to the dielectric permittivity tensor for $FeBO_3$. The crystallographic contribution for the $FeBO_3$ point group $\bar{3}m$ were obtained from the tables presented in [11]. The procedure to find the magnetic contribution is, however, somewhat more complex and is based on the approach developed in [12]. In brief, one should consider the transformation of the ferromagnetic $\mathbf{M}$ and antiferromagnetic $\mathbf{L}$ vectors when the symmetry operations of the space group $R\bar{3}c$ of the crystal (See Fig. 3.1) are applied and take into account that the antiferromagnetic vector does not transform as an axial vector if the certain space symmetry operation interchanges magnetic ions belonging to different sublattices. A crucial role for the properties of the antiferromagnetic vector is played by the positions of the magnetic ions Fe^{3+} relative to the inversion symmetry center. The results for $FeBO_3$ are presented in Table 4.1 for the case of ferro- and antiferromagnetic vectors being directed along the x and y axes, respectively.

4.2.2 Optical spectra

$FeBO_3$ is an optically uniaxial crystal with the optical axis being parallel to the crystallographic z axis. The dielectric permittivity tensor in the paramagnetic phase

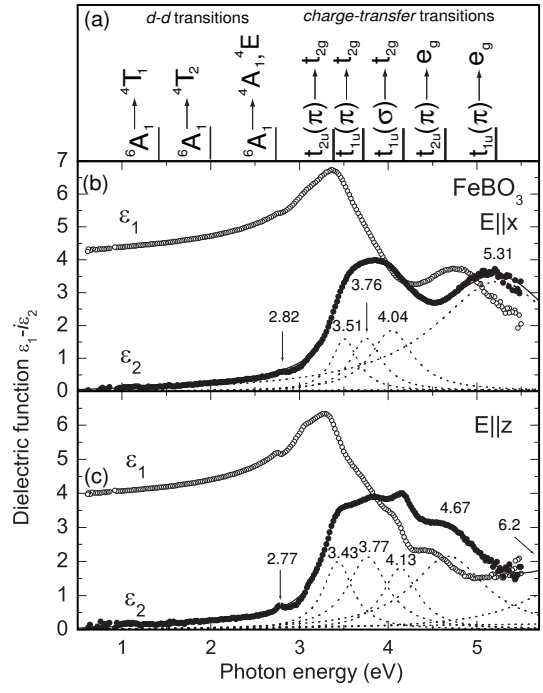

Figure 4.5: (a) Scheme of the localized *d-d* transitions and charge-transfer transitions according to [4]. Spectral dependencies (symbols) of the dielectric functions ε_1 and ε_2 of $FeBO_3$ for the light polarized perpendicular (b) and parallel (c) to the optical z axis. Solid lines are fits to the experimental data using Eq. (4.1). Dashed lines are the single Lorentz oscillators indicating the positions of the electronic transitions. The central energies E_0 of these transitions are given by numbers.

has only two non-vanishing components, as shown in Table 4.1. The spectra of the dielectric permittivity for the light polarized along (ε_{zz}) and perpendicular ($\varepsilon_{xx} = \varepsilon_{yy}$) to the optical axis are presented in Fig. 4.5(b,c). In Fig. 4.5(a) the scheme of the $d-d$ [2, 13] and CT transitions [4] is shown.

In the experimental ε_{xx} and ε_{zz} spectra (Fig. 4.5(b,c)) one can distinguish the highest $d-d$ transition ${}^6A_1 \rightarrow {}^4A_1, {}^4E$ centered at the photon energy $E \approx 2.8$ eV. Two lower $d-d$ transitions ${}^6A_1 \rightarrow {}^4T_1, {}^4T_2$ (Fig. 4.2) can not be seen in the spectrum because of their relatively low intensity of about 150 cm^{-1} at RT [13, 14, 15, 16, 17, 18]. The transition ${}^6A_1 \rightarrow {}^4A_1, {}^4E$ is, however, strongly enhanced with respect to other $d-d$ transitions. In [13] calculations of the energy structure and optical spectra of $FeBO_3$ in the framework of a model combining a one-electron description of the *sp* states of boron and oxygen and a many-electron description of the *d* states of iron ion are presented. It is shown that the high intensity of this transition is explained by a substantial contribution of CT transitions. Interestingly, the intensity of the ${}^6A_1 \rightarrow {}^4A_1, {}^4E$ transition exceeds by an order of magnitude the one in some other iron oxides where the Fe^{3+} ions are in a noticeably distorted environment, e.g $GdFe_3(BO_3)_4$ [17]. The CT transitions in $GdFe_3(BO_3)_4$ are, in turn, detected at energies much higher than in $FeBO_3$. This shows that the vicinity of the CT transitions is the dominating factor defining the enhancement of the intensity of ${}^6A_1 \rightarrow {}^4A_1, {}^4E$ transition. For a light polarized alon the x and z axes this transition is centered at 2.82 eV and 2.77 eV, respectively. The intensity of the transition also depends on the polarization. This anisotropy resembles the anisotropy of the lowest CT transition $t_{1u}(\sigma) \rightarrow t_{2g}$, as well as the anisotropy of the CT transitions lying in the range 4.5-5.5 eV.

For the CT transitions there is a qualitative agreement with calculations [4] for the FeO_6 cluster. The fundamental band gap for $FeBO_3$ was predicted theoretically to be close to 3 eV [13, 19], which is in agreement with previous experimental papers [13, 14, 15], where it was determined as the energy above which the absorption exceeds 1000 cm^{-1}. Our data confirm these conclusions. The lowest CT transition is found to be centered at 3.43 eV. However, to the best of our knowledge no theoretical or *ab initio* calculations of the electronic structure of $FeBO_3$ above the band gap are reported in literature.

The spectral dependencies of the ordinary and extraordinary refractive indices n_x, n_z and absorption indices k_x, k_z are shown in Fig. 4.6. Previously the birefringence was studied in $FeBO_3$ only at a few distinct photon energies [20]. Our data are in good agreement with those results. Below the band gap the ordinary refraction index (n_x) is larger than the extraordinary one (n_z) and the crystal, therefore, is optically negative. The crystallographic birefringence in $FeBO_3$, as can be seen in Fig. 4.6, is rather strong. Thus, for the photon energy of the Ti:Sapphire laser (E=1.54 eV), used in the pump-probe experiments, the birefringence is $\Delta n = n_x - n_z$=0.08. This strong birefringence is determined by the anisotropy of the CT transitions above 3 eV

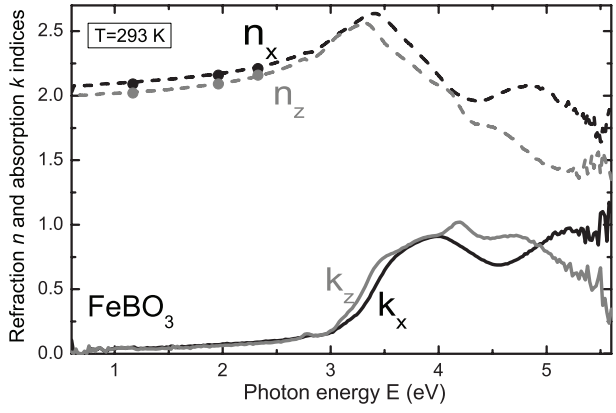

Figure 4.6: Dispersion of the refraction n and absorption k indices for the light polarized perpendicular (black line) and parallel (gray line) to the optical axis z. •'s represent the data from [20].

(Fig. 4.5).

4.2.3 Magneto-optical properties

The components of the dielectric permittivity tensor for $FeBO_3$ arising in the magnetically ordered phase are listed in Table 4.1. Only the components relevant to the experimental geometry shown in Fig. 4.7(a,d) are considered.

In the spectral region 1.5-2 eV, in which the magneto-optical properties are studied, the absorption can be neglected and the antisymmetric part ε^a_{ij} of the dielectric permittivity tensor, describing the Faraday effect, is purely imaginary. $FeBO_3$ is characterized by one of the highest values of Faraday rotation among the iron oxides, with a maximum observed in the green part of the spectra close to the absorption edge [20, 21]. However, when light propagates along the z axis the Faraday rotation is zero (ε^a_{xy}=0) and, therefore, observation of the Faraday effect is possible only for light with a wave vector making a finite angle with the z axis. In this case the rotation of the polarization of light caused by the Faraday effect is strongly modulated by the crystallographic birefringence. The interplay between these two effects leads to drastic changes in the resulting rotation of the polarization plane, depending on the incidence angle between the wave vector and the z axis [20]. In Fig. 4.7(b) the rotation of the polarization plane ϕ_F is shown as a function of the magnetic field applied along the x axis for the photon energy $E = 1.54$ eV and for the angle of incidence of 10°. This angle was chosen to satisfy the condition for the largest measured rotation 0.7° of the

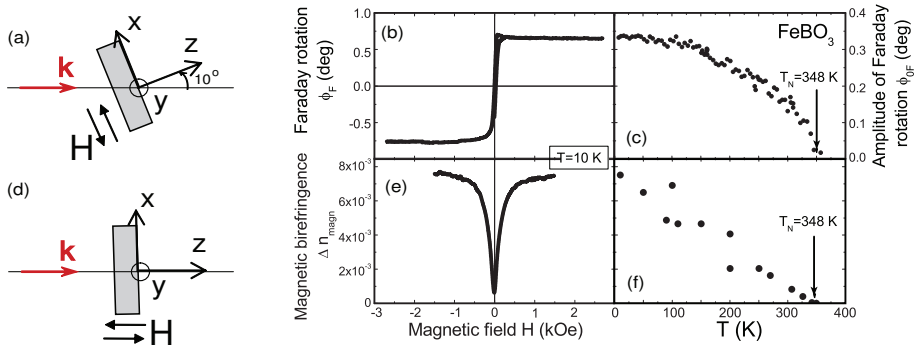

Figure 4.7: The field (b) and temperature (c) dependences of the Faraday rotation ϕ_F measured in geometry (a). The field (e) and temperature (f) dependences of the MLB Δn_{magn} measured in geometry (d).

polarization plane caused by a combination of Faraday rotation and crystallographic birefringence. Taking into account the crystallographic birefringence $\Delta n = 0.08$ we found that for the given angle of incidence such a rotation of the polarization plane corresponds to an intrinsic Faraday rotation of 456 deg/cm, in agreement with results of Ref. [22].

The magnetic linear birefringence (MLB) was measured in the experimental geometry shown in Fig. 4.7(d) using the setup described in Section 2.2.3 (Fig. 2.4(c)). The CW He-Ne laser (E=1.96 eV) was used as the light source. The field dependence of the MLB measured at T=10 K is shown in Fig.4.7(e). The MLB signal decreases with increasing temperature and disappears when approaching the temperature of transition to the paramagnetic phase T_N (Fig.4.7(f)).

4.3 Linear optical properties of $GaFeO_3$

4.3.1 Anisotropy of dielectric permittivity

The contributions of different origin to the dielectric permittivity tensor for $GaFeO_3$, belonging to the orthorhombic point group $m'2'm$ (space group $Pc2_1n$), are listed in Table 4.1. Both crystallographic and magnetic contributions for $GaFeO_3$ were found from Tables presented in [11]. The components of the tensor describing the MLB (magnetic part of ε^s_{ij}) are constructed as $\varepsilon^s_{ij} = \chi^{(\mathrm{i})}_{ijzz} M_z^2$, where $\chi^{(\mathrm{i})}_{ijkl}$ is a fourth rank polar (i)-tensor. Analogously, the components of the ε^a_{ij} are found as $\varepsilon^a_{ij} = \chi^{(\mathrm{i})}_{ijz} M_z$,

Table 4.2: Crystallographic and magnetic contributions to the dielectric permittivity tensor $\hat{\varepsilon}$ for $GaFeO_3$.

ε^s_{ij}	Crystallographic contribution	Contribution caused by M_z	ε^a_{ij}	Contribution caused by M_z
xx	ε_{xx}	$a_1 M_z^2$		
yy	ε_{yy}	$a_2 M_z^2$		
zz	ε_{zz}	$a_3 M_z^2$		
xy	–	–	xy	$K_1 M_z$
xz	–	–	xz	–
yz	–	–	yz	–

where $\chi^{(i)}_{ijk}$ is a third rank axial i-tensor.

4.3.2 Optical spectra

The optical properties below the band gap

The absorption spectra of GaFeO for light polarized along the x and z crystallographic axes measured in the range of 1-2.2 eV are shown in Fig.4.8(a). The spectra were obtained using the measurements in transmission which are restricted to the region of low absorption only. As seen from Fig. 4.8(a), the band at energy 1.52 and the shoulder at 1.98 eV can be distinguished in the absorption spectra. They can be assigned to the localized $d-d$ transitions ${}^6A_1 \rightarrow {}^4T_1$ (1.5 eV) and ${}^6A_1 \rightarrow {}^4T_2$ (2.0 eV) (Fig. 4.2). The intensity of these transitions is noticeably higher than in $FeBO_3$ [17] where the absorption coefficient does not exceed 200 cm^{-1} at these energies. The increase of the intensity of these electric dipole forbidden transitions in $GaFeO_3$ can be understood as follows. This prohibition can be lifted if the symmetry of the Fe^{3+} environment is lowered. In $GaFeO_3$ iron ions are located at two octahedral and one tetrahedral oxygen clusters and are shifted from the centra of these clusters. In $FeBO_3$, in contrast, the Fe^{3+} ions are in a centrosymmetric environment. Therefore, the intensity of the localized d-d transitions is expected to be higher in $GaFeO_3$ than in $FeBO_3$ [17], which is indeed observed in our experiments.

The absorption above 2.2 eV exceeds 1000 cm^{-1} and the optical properties of $GaFeO_3$ in this region can be studied only in reflection. The spectra of the dielectric function $\varepsilon = \varepsilon_1 - i\varepsilon_2$ for light polarized along all three crystallographic axes of $GaFeO_3$ are shown in Fig. 4.9(a). The lowermost transition which can be distinguished in the spectra is situated at the energy E=2.5 eV. This transition can be assigned to the

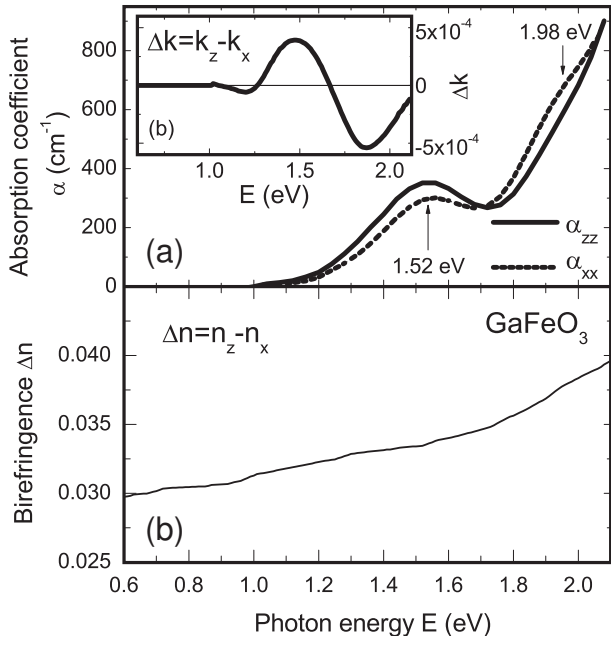

Figure 4.8: (a) Spectral dependencies of the absorption coefficient of $GaFeO_3$ for the light polarized along the x (dashed line) and z (solid line) axes. Inset shows the spectrum of the dichroism $\Delta k_{z-x} = k_z - k_x$. (b) The birefringence $\Delta n_{z-x} = n_z - n_x$

transition ${}^6A_1 \rightarrow {}^4A_1, {}^4E$, which is, again, forbidden in the electric-dipole approximation, but is typically enhanced in iron oxides. The strong enhancement of the intensity of this transition in $GaFeO_3$ can be explained, on the one hand, by the non-centrosymmetric environment of Fe^{3+} ions. On the other hand, the charge-transfer transitions, which were shown to contribute to the intensity of the similar transition in $FeBO_3$ [13], are situated at lower energy in $GaFeO_3$. The lowest identified from the dielectric function spectra transition is situated at 3.3 eV (vs. 3.4 eV in $FeBO_3$). This difference is rather small to explain the large difference in the intensities of the $d-d$ transition in $FeBO_3$ and $GaFeO_3$. However, as will be discussed below, the precise identification of the position of the absorption bands in $GaFeO_3$ is difficult and the charge transfer transitions in $GaFeO_3$ can also be at energies lower than 3.3 eV. Therefore, their effect on the intensity of the ${}^6A_1 \rightarrow {}^4A_1, {}^4E$ can be stronger than in $FeBO_3$.

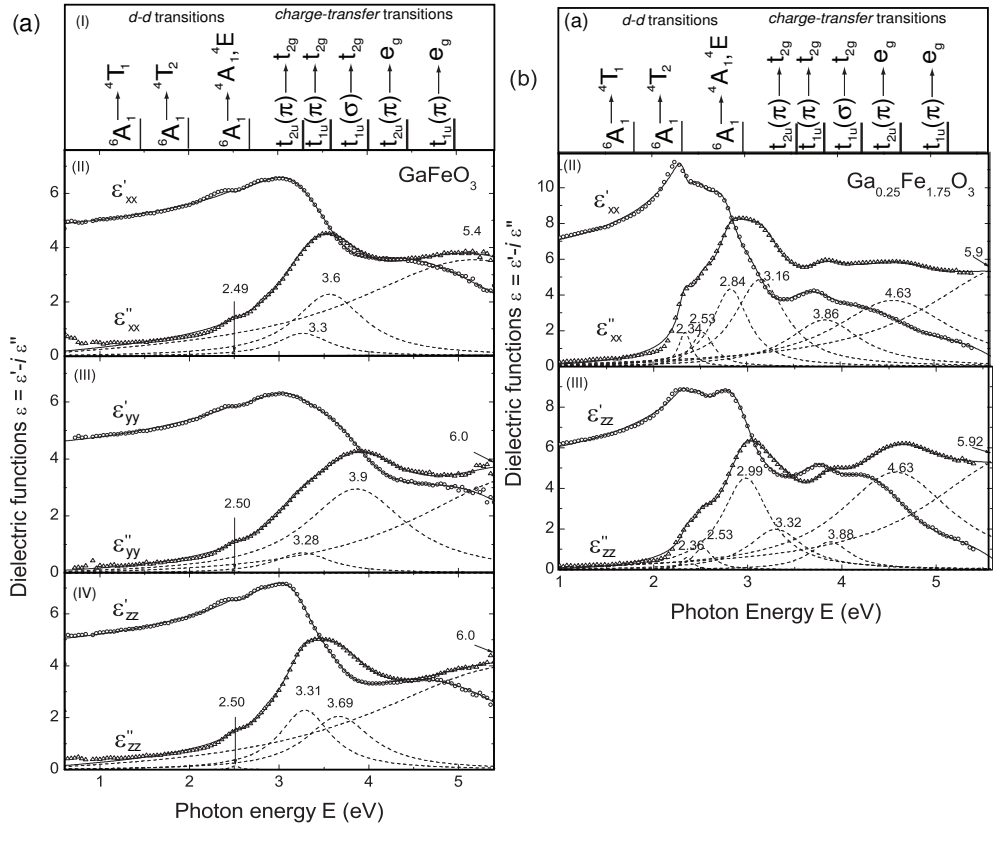

Figure 4.9: (a) Spectral dependencies (symbols) of the dielectric functions ε' and ε'' of $GaFeO_3$ for three principal polarizations and their fit (lines) using Eq. (4.1). (b) Spectral dependencies (symbols) of the dielectric functions ε' and ε'' of $Ga_{0.25}Fe_{1.75}O_3$ for two principal polarizations and their fit (lines) using Eq. 4.1. Upper panels show the scheme of the localized *d-d* and charge-transfer transitions according to [4].

Optical properties above the band gap

The strong absorption above E =3 eV is caused by the CT transitions. In this spectral range the optical spectra of $GaFeO_3$ (Fig. 4.9(a)) do not reveal well-pronounced bands which could be unambiguously assigned to the CT transitions in the FeO_6 cluster, shown in Fig. 4.9(a-I). For comparison the spectra for $Ga_{0.25}Fe_{1.75}O_3$ are presented in Fig. 4.9(b-II,III). In contrast to $GaFeO_3$, the latter possesses a far better resolved structure in the optical spctra. This difference can be explained from the difference in the crystallographic positions occupied by Fe^{3+} ions in these two compounds. Indeed, Fe^{3+} ions in $GaFeO_3$ occupy three nonequivalent positions (two of which have an octahedral symmetry and one - tetrahedral (See Fig. 3.3)) of the ligand surrounding [23]. The energy levels of the iron ions in these positions are, therefore, different. Data shown in Fig. 4.9(a-II,III,IV) are, in principle, composed of superpositions of transitions in different FeO_6 clusters, which leads to the poorly resolved structure of the spectra. In contrast, in $Ga_{0.25}Fe_{1.75}O_3$, possessing a trigonal structure, the Fe^{3+} ions only occupy octahedral (O_h) positions with the same parameters. The optical spectra of this compound, therefore, can be easily decomposed into separate transitions, as shown in Fig. 4.9(b-II,III).

The spectra of $\hat{\varepsilon}$ for $GaFeO_3$ are different for all three axes confirming the fact that the crystal is orthorhombic biaxial (See Table 4.2). The optical anisotropy in the xy and yz planes exceeds the one in the xz plane. The most intense transition for the light polarized along the y axis is at a 0.3 eV higher energy than for the light polarized perpendicular to this axis in the xz plane.

It is interesting to compare the intensity of the transition ${}^6A_1 \rightarrow {}^4A_1, {}^4E$, centered at energy 2.5 eV in $GaFeO_3$ and $Ga_{0.25}Fe_{1.75}O_3$. The orbital-parity prohibition for this transition can be lifted by the distortion of the symmetry of the iron ion environment and by the proximity of the allowed strong optical transitions. On the one hand, the intensity of the ${}^6A \rightarrow {}^4A_1, {}^4E$ transition in $GaFeO_3$ (Fig. 4.9(a)) is noticeably lower than in $Ga_{0.25}Fe_{1.75}O_3$, although the crystallographic positions of the iron ions in the former compound are less symmetric. On the other hand, the first charge transfer transition in $Ga_{0.25}Fe_{1.75}O_3$ is situated at E=2.84 eV, while in $GaFeO_3$ it is found to be close to 3.2 eV. Moreover, the intensity of this transition in $Ga_{0.25}Fe_{1.75}O_3$ is much stronger. Therefore, the enhancement of the intensity of ${}^6A_1 \rightarrow {}^4A_1, {}^4E$ is defined mostly by the vicinity of the allowed charge-transfer transitions. This resembles the situation with the enhancement of the ${}^6A_1 \rightarrow {}^4A_1, {}^4E$ transition in $FeBO_3$ as compared with $GaFe_3(BO_3)_4$ (See Section 4.2).

4.3.3 Linear magneto-optical properties

The uniaxial magneto-crystalline anisotropy of $GaFeO_3$ determines the sensitivity of the magneto-optical measurements to the geometry of the experiment. Fig. 4.10(a) shows the Faraday rotation as a function of the applied magnetic field measured at

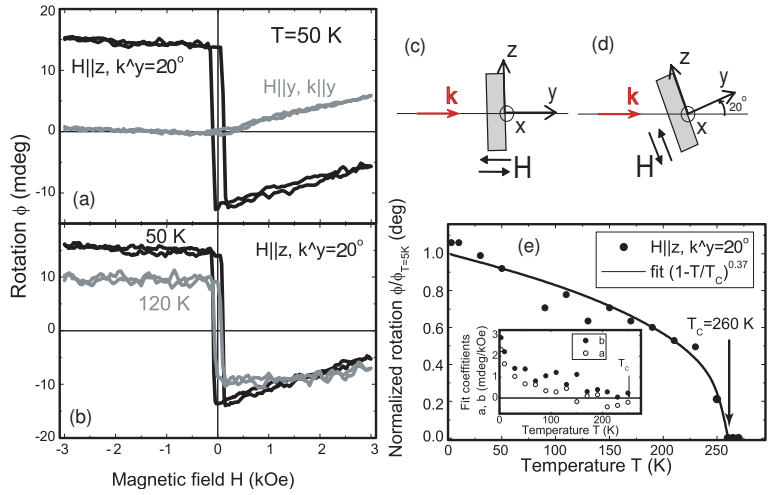

Figure 4.10: (a) Field dependence of the Faraday rotation measured in the experimental geometries shown in (c-d). (b) Field dependence of the Faraday rotation measured in the geometry shown in (d) for two temperatures. (e) Temperature dependence of the normalized Faraday rotation measured in the geometry shown in (d). Inset: Temperature dependence of the fit parameters a and b (Eq. 4.2) obtained from the measurements in the geometry (d).

T=50 K using the experimental setup depicted in Fig. 2.4(a). The measurements were done in two experimental geometries presented in Fig. 4.10(c-d). In the case (c) the conventional Faraday geometry was used, when the magnetic field is applied along the normal to the sample and the light propagates parallel to the field. However, for the sample used this direction is along the y axis which is the hard axis of the magnetization and the off-diagonal element ε^a_{xz} of the dielectric permittivity tensor is zero. Therefore, no Faraday rotation should be observed. In the second experimental geometry (Fig. 4.10(d)) the magnetic field was applied along the sample surface parallel to the easy magnetic axis z. The angle of incidence was chosen to be 20° in order to get the projection of the wavevector $\mathbf{k}$ of the light on the magnetization. The measured rotation of the light polarization in this geometry is defined by the nonzero component ε^a_{xy}. Indeed, a well pronounced hysteresis loop in the Faraday rotation was observed as shown in Fig. 4.10(a-b). The small coercivity (less then 100 Oe) of the curves is in an agreement with the hysteresis loops obtained from SQUID measurements [24]. The amplitude of the Faraday rotation decreases from 20 mdeg at T=5 K to zero at T_C=260 K, which is the Curie temperature for the studied sample.

The dependence of the Faraday rotation on the temperature is described by the Curie law $\phi/\phi_{T=5K} = (1 - T/T_C)^{0.37}$.

It is important to note that the measured value of the rotation is not a "true" Faraday effect. The sample is biaxial (See Table 4.2) and, therefore, the crystallographic birefringence distorts the polarization of light propagating in the sample. As is seen from Fig.4.8(b), the difference in the refraction indices for the light polarized along the x and z axes is Δn=0.035, which corresponds to a total phase difference of (225+2·360) deg for the two orthogonally polarized waves, gained in the sample of thickness 60 μm. Moreover, the magnetic birefringence $\Delta\varepsilon^{\mathrm{mag}} = (a_1 - a_3)M_z^2$ is also present in the xz plane.

From Fig. 4.10(a) one can see that in both experimental geometries there is a contribution to the measured Faraday rotation, which is linear in the applied field, with the slope being different for positive and negative field. The slope of this contribution changes with temperature (Fig. 4.10(b)), possessing the same trend for the signal measured in both geometries. Such a dependence on the applied magnetic field can be approximated by two contributions, which are odd and even functions of the applied field

$$\phi(H) = a \cdot H + b \cdot |H|, \tag{4.2}$$

where a and b are temperature dependent parameters. As it is shown in the Inset in Fig. 4.10(e) both contributions vanish as the temperature approaches the transition point to the paramagnetic state, indicating that they are related to the magneto-optical response. (i) The presence of the linear contribution $a \cdot H$ observed for the magnetic field applied along the hard magnetic axis y can be explained by assuming that the magnetization rotates over a small angle from the easy z axis when the amplitude of the magnetic field increases. The presence of this linear contribution in the measurements with the field along the z axis might indicate that actually the applied field makes a small but finite angle with this axis. (ii) The growth of the M_y component of the magnetization also leads to an additional optical anisotropy in the xz plane ($\varepsilon_{xx} \sim \chi_{xxyy}M_y^2$, $\varepsilon_{zz} \sim \chi_{zzyy}M_y^2$ [11]). The interplay between effects (i) and (ii) can lead to the presence of odd and even in magnetic field contributions to the rotation of the polarization.

4.4 Second harmonic generation in $GaFeO_3$

As is shown in Section 4.3.3 the rotation of the polarization of light in $GaFeO_3$ caused by the Faraday effect is unavoidably modulated by the crystallographic birefringence and is rather small, not exceeding 20 mdeg at low temperature. Therefore this effect might not provide sufficient sensitivity to detect changes in the magnetic state induced by laser pulses, which are typically rather small and do not exceed a couple of percents of the total magnetization of the sample. In this case other magneto-optical

phenomena are required in order to perform the pump-probe experiments. Magnetic second harmonic generation is a good candidate for this [25].

4.4.1 Crystallographic and magnetic nonlinear susceptibilities

The expression for the nonlinear polarization $P_i(2\omega)$ induced in a medium by an electric field of light $E_j(\omega)$ can be written in the form (see Eq. (2.17)):

$$P_i(2\omega) = \left[\chi^{(\mathrm{i})}_{ijk} + \chi^{(\mathrm{c})}_{ijk} e^{\mathrm{i}\delta}\right] E_j(\omega) E_k(\omega), \tag{4.3}$$

where the crystallographic $\chi^{(\mathrm{i})}_{ijk}$ and magnetic $\chi^{(\mathrm{c})}_{ijk}$ susceptibilities are real numbers, δ is a phase difference between magnetic and crystallographic contributions, which approaches $\pi/2$ at the limit far from optical resonances [25].

In the magnetically ordered state $GaFeO_3$ belongs to the magnetic point group $m'2'm$. In our experiment the wave vector of the incident light was making an angle of 20^{o} with the y axis, as shown in Fig. 4.11(b). For this experimental geometry the following non-zero components of the nonlinear susceptibilities are relevant

$$\chi^{(\mathrm{i})} \begin{cases} a = yxx,\ b = yyy,\ c = yzz, \\ d = xxy = xyx,\ e = zzy = zyz \end{cases} \tag{4.4a}$$

$$\chi^{(\mathrm{c})} \begin{cases} A = xxx,\ B = xyy,\ C = xzz, \\ D = yyx = yxy,\ E = zzx = zxz, \end{cases} \tag{4.4b}$$

where abbreviations of the type $yxx = \chi_{yxx}$ etc. were used. It is interesting to note, that none of the components appearing in the tensor responsible for the crystallographic SHG appears in the magnetic part and *vice versa*. Therefore, it is possible to distinguish the contributions of different origin to the SHG signal by using proper combinations of the polarizations of the fundamental and SHG beams.

In the experiments the orientation of the analyzer axis was fixed in one of two positions, (i) parallel to the x axis of the sample and (ii) perpendicular to this axis. The dependence of the SHG signal on the orientation of the polarization plane ξ of the incoming fundamental light was studied for these two cases. The measurements were done in transmission. For the geometry shown in Fig. 4.11(b) the following expressions describing the intensity of the SHG light can be obtained for the cases (i) and (ii), respectively

$$I^{2\omega}_{\parallel x} = |A\cos^2\xi + (B\sin^2\alpha + C\cos^2\alpha)\sin^2\xi + d\sin 2\xi\sin\alpha|^2; \tag{4.5a}$$

$$\begin{aligned} I^{2\omega}_{\perp x} = |[a\cos^2\xi + (b\sin^2\alpha + c\cos^2\alpha)\sin^2\xi + D\sin 2\xi\sin\alpha|\sin\alpha] \\ +[e\sin^2\xi\sin^2 2\alpha + E\sin 2\xi\cos\alpha]\cos\alpha|^2, \end{aligned} \tag{4.5b}$$

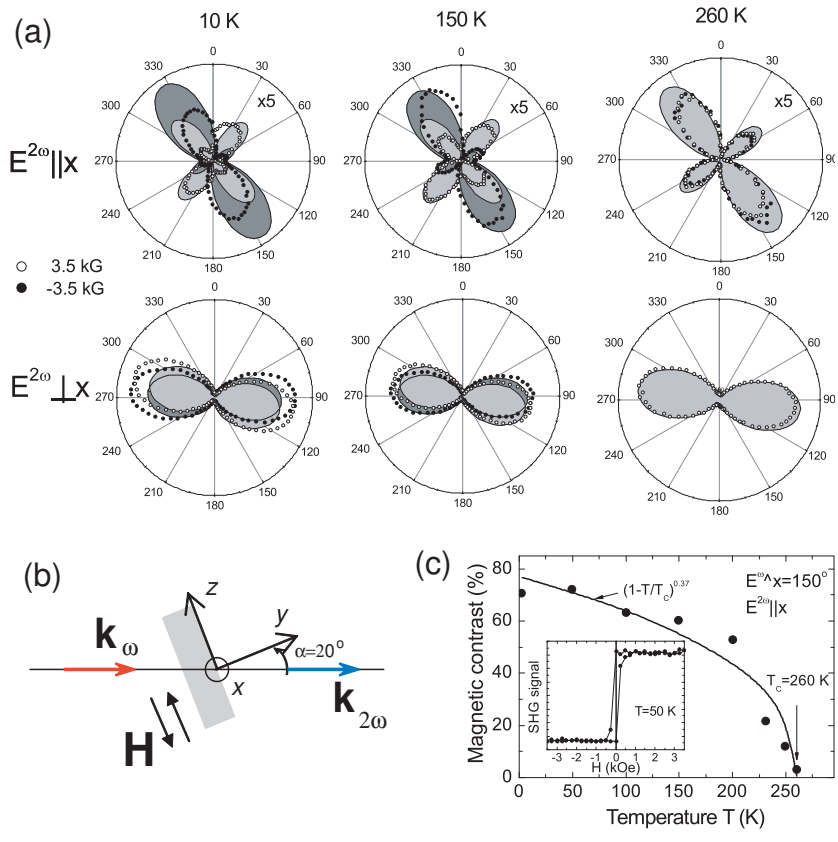

Figure 4.11: (a) The intensity of the SHG light polarized along (upper row) and perpendicular (lower row) to the x axis as a function of the incoming polarization ξ of the fundamental light, measured for the applied magnetic field $\pm 3.5\,\mathrm{kG}$ at several temperatures. $\xi = 0^o$ corresponds to $E^\omega \| x$. The dark and light gray areas represent the results of the fits using Eqs. (4.5) for negative and positive fields, respectively, which correspond to the opposite signs of $\chi^{(c)}$. (b) The relative orientation of the crystallographic axes, applied magnetic field and propagation direction of the fundamental and SHG light. (c) The temperature dependence of the SHG magnetic contrast for E^ω making an angle of 150^o with the x axis and $E^{2\omega} \| x$. Inset shows the SHG hysteresis loop at T=50 K.

where α is the angle of incidence for the fundamental beam. In the particular case of normal incidence (α=0) the equations have a simple form

$$I_{\parallel x}^{2\omega} = |A\cos^2\xi + C\sin^2\xi|^2; \tag{4.6a}$$

$$I_{\perp x}^{2\omega} = |E\sin 2\xi|^2, \tag{4.6b}$$

and no crystallographic contribution to the SHG signal can be observed for both orientations of the analyzer.

4.4.2 Crystallographic and magnetic contributions to SHG

In Fig.4.11(a) the intensity of the SHG light polarized parallel or perpendicular to the x axis as a function of the polarization of the fundamental light is shown for the temperatures 10 K, 150 K and 260 K. The difference between curves measured at positive and negative magnetic field applied along the z axis is clearly seen below the Curie temperature T_C=260 K. In Fig. 4.5(c) the magnetic contrast (2.33) for the fundamental light polarized at ξ =-30^o with respect to the x axis and SHG light polarized along this axis is shown as a function of temperature. The magnetic contrast follows the same type of dependence on the temperature as the linear magneto-optical Faraday effect (Fig. 4.10(b)) and disappearing in the vicinity of the Curie temperature. The maximum SHG magnetic contrast is as high as 80% at low temperatures.

From Fig. 4.11(b) one can see that the largest SHG intensity is observed for the case when both fundamental and SHG light are polarized perpendicularly to the x axis. At the same time the magnetic contrast observed for this configuration is the smallest. This indicates that the dominating contribution to the SHG signal is caused by the $b = yyy$ component of the nonlinear susceptibility, and is related to the spontaneous electric polarization present in $GaFeO_3$ along this axis. It is this axis along which the Fe^{3+} ions are shifted from the centers of the oxygen clusters, and, therefore, the symmetry breaking is most prominent in this direction (See Chapter 3.2). Consequently, the nonlinear susceptibility $b = yyy$ is expected to be dominating. This contribution to the SHG signal was shown to be strongest also for the SHG photon energy 1.55 eV [26]. Note, that due to a rather small angle of incidence ($\alpha = 20^o$) the contribution to the SHG proportional to $b = yyy$ is small ($\sim 0.03b$). However, the absolute value of b is significantly higher than the other components of $\chi^{(i),(c)}$. Thus, the SHG signal for $E^\omega \parallel E^{2\omega} \perp x$ is mainly defined by the b component of $\chi^{(i)}$.

The large value of the $b = yyy$ component also leads to the fact that the observation of the purely magnetic contribution to the SHG signal (Eq. (4.6)) is preferably to be carried out in the geometry with the analyzer axis being parallel to the x axis. From Eqs. (4.5) it follows that the crystallographic susceptibility $b = yyy$ causes the SHG light to be polarized along the y axis. Therefore, even a small nonzero angle of incidence α would lead to the appearance of a strong crystallographic SHG signal in this geometry.

The measurements of the magnetization-induced SHG in $GaFeO_3$ with Curie temperature 205 K were reported in [27] for the spectral range 1-2.5 eV (for the fundamental light). The measurements were done in reflection from the xz surface for the incoming light polarized parallel to the x axis. The maximum magnetic contribution was found to arise from the component $A = xxx$ of the magnetic susceptibility. Our experiments show that the dominating contribution is caused by the $D = yxy = yyx$ component of the susceptibility. The maximum of the crystallographic contribution was attributed in [27] to the component $a = yxx$ of the crystallographic susceptibility. However, our experiments show that the dominating contribution to the SHG is due to the $b = yyy$ component, when the polarizations of both fundamental and SHG light have projections on the y axis, being the direction of the spontaneous electric polarization. This component, however, could not be detected in the measurements in reflection form the xz plane performed in [27]. Additionally, in [27] the magnetic contribution of type $P_y(2\omega) = \chi^{(c)}_{yxx} E_x(\omega)$ was expected to be present in the SHG signal. However, in the experiment they did not observe this contribution and proposed that it is much smaller than the crystallographic one of the same symmetry. We argue that the nonlinear magnetic susceptibility does not have such a component (see Eq.4.3), which is supported by our experimental results and in the agreement with the experimental data [27].

References

[1] A. B. P. Lever, *Inorganic Electronic Spectroscopy* (Elsevier, Amsterdam, 1984).

[2] Y. Tanabe and S. Sugano, J. Phys. Soc. Japan **9**, 753 (1954).

[3] J. S. Griffith, *The Theory of Transition Metal Ions* (Cambridge University Press, Cambridge, 1961).

[4] A. I. Likhtenshteĭn, A. S. Moskvin, and V. A. Gubanov, Sov. Phys.- Solid State **24**, 2049 (1982).

[5] P. A. Usachev, R. V. Pisarev, A. M. Balbashov, A. V. Kimel, A. Kirilyuk, and T. Rasing, Phys. Solid State **47**, 2292 (2005).

[6] A. M. Clogston, J. Appl. Phys. **31**, 198S (1960).

[7] F. J. Kahn, P. S. Pershan, and J. P. Remeika, Phys. Rev. **186**, 891 (1969).

[8] A. K. Zvezdin and V. A. Kotov, *Modern Magnetooptics and Magnetooptical Materials* (IOP Publishing, Bristol, 1997).

[9] G. A. Smolenskiĭ, R. V. Pisarev, and I. G. Siniĭ, Sov. Phys. - Usp. **18**, 410 (1975).

[10] J. Ferré and G. A. Gehring, Rep. Prog. Phys. **47**, 513 (1984).

[11] R. R. Birss, *Symmetry and Magnetism* (North-Holland, Amsterdam, 1966).

[12] E. A. Turov, A. V. Kolchanov, V. V. Men'shenin, I. F. Mirsaev, and V. V. Nikolaev, *Symmetry and physical properties of antiferromagnets (in Russian)* (Fizmatlit, Moscow, 2001).

[13] S. G. Ovchinnikov and V. N. Zabluda, J. Exp. Theor. Phys. **98**, 135 (2004).

[14] I. S. Edel'man, A. V. Malakhovskiĭ, T. I. Vasil'eva, and V. N. Seleznev, Sov. Phys. - Sol. State **14**, 2442 (1972).

[15] V. N. Zabluda, A. V. Malakhovskiĭ, and I. S. Edel'man, Sov. Phys. - Sol. State **27**, 77 (1985).

[16] B. Andlauer, O. F. Schirmer, and J. Schneider, Sol. St. Comm. **13**, 1655 (1973).

[17] A. M. Kalashnikova, V. V. Pavlov, R. V. Pisarev, L. N. Bezmaternykh, M. Bayer, and T. Rasing, JETP Lett. **80**, 293 (2004).

[18] A. G. Gavrilyuk, I. A. Troyan, and S. G. Ovchinnikov, J. Exp. Theor. Phys. **99**, 566 (2004).

[19] A. V. Postnikov, St. Bartkowski, and M. Neumann, Phys. Rev. B **50**, 14849 (1994).

[20] R. Wolfe, A. J. Kurtzig, and R. C. LeCraw, J. Appl. Phys. **41**, 1218 (1970).

[21] A. J. Kurtzig, R. Wolfe, and R. C. LeCraw, Appl. Phys. Lett. **14**, 350 (1969).

[22] W. Jantz, J. R. Sandercock, and W. Wettling, J. Phys. C **9**, 2229 (1976).

[23] S. C. Abrahams, M. J. Reddy, and J. L. Bernstein, J. Chem. Phys. **42**, 3957 (1965).

[24] J.-Y. Kim, T. Y. Koo, and J.-H. Park, Phys. Rev. Lett. **96**, 047206 (2006).

[25] M. Fiebig, V. V. Pavlov, and R. V. Pisarev, J. Opt. Soc. Am. B **22**, 96 (2005).

[26] K. Eguchi, Y. Tanabe, T. Ogawa, M. Tanaka, Y. Kawabe, and E. Hanamura, J. Opt. Soc. Amer. **22**, 128 (2005).

[27] Y. Ogawa, Y. Kaneko, J. P. He, X. Z. Yu, T. Arima, and Y. Tokura, Phys. Rev. Lett. **92**, 047401 (2004).

CHAPTER 5

Phenomenological theory of the excitation of spin precession by short laser pulses[1]

5.1 Introduction

The excitation of coherent spin precession by ultrashort laser pulses is a relatively new field despite of the fact that the interactions of such pulses with condensed matter is a subject of intense study for almost three decades. Moreover, the generation of nonmagnetic excitations, such as coherent phonons, by picosecond and subpicosecond pulses is an intensively studied subject with a thoroughly developed theoretical and phenomenological apparatus for the description of the experimentally observed results [1].

The description of the excitation of coherent spin precession by light up to now has been described using classical Landau-Lifshitz equations and so-called light-induced effective fields (See [2] and references therein). In this Chapter we present another approach, based on the representation of magnons via their normal coordinates. The coupling of light with magnons is described by a Raman tensor. By using this approach, the solution of the problem of the interaction of light with magnetic matter is reduced to the solution of a simple equation of motion for the normal coordinates, which is common for all wave processes, independent on their nature [3, 4]. Indeed, it

[1]Based on: A. M. Kalashnikova, A. V. Kimel, R. V. Pisarev, V. N. Gridnev, A. Kirilyuk, and Th. Rasing, *Phys. Rev. Lett.* **99**, 167205 (2007) and A. M. Kalashnikova, A. V. Kimel, R. V. Pisarev, V. N. Gridnev, P. A. Usachev, A. Kirilyuk, and Th. Rasing, *Phys. Rev. B* **78**, 104301 (2008).

is this approach that is traditionally used for the description of light-induced coherent phonons. The specificity of the problem for the light-magnetic matter interaction is contained in the form of the normal coordinates describing a coherent spin precession. Along with this, we consider the generation of coherent spin precession using the Landau-Lifshitz equation and discuss the consistency of these two methods.

5.2 Coherent spin precession in a multi-sublattice magnetic medium

Before presenting details of our approach and its results, we briefly introduce the basic definitions regarding the equilibrium magnetic structure and spin precession, which are used below.

5.2.1 Equilibrium orientation of the magnetic moments and the effective field

Expression for the magnetic energy

The equilibrium position of the magnetic moment $\mathbf{M}$ of free ion, not coupled to the magnetic moments of other ions, is defined by the minimum of the interaction energy between the magnetic moment and the external field $\mathbf{H}$: $\mathcal{H}_{\mathrm{H}} = -\mathbf{HM} = \min$. Therefore, the magnetic moment is oriented along the applied magnetic field. In a crystal, however, there are strong exchange interactions between the magnetic moments and weaker relativistic interactions defining the magnetic anisotropy. The Hamiltonian describing the energy of the crystal in this case has at least three terms:

$$\mathcal{H} = \mathcal{H}_{\mathrm{E}} + \mathcal{H}_{\mathrm{A}} + \mathcal{H}_{\mathrm{H}} + ..., \tag{5.1}$$

where $\mathcal{H}_{\mathrm{E}}$ and $\mathcal{H}_{\mathrm{A}}$ describe the exchange and magneto-crystalline anisotropy energy, respectively. The equilibrium orientation of the magnetic moments in a crystal, therefore, is defined by the minimum of the energy (5.1).

The explicit form of the exchange energy for the i-th ion with a magnetic moment $\mathbf{M}_i$ is

$$\mathcal{H}_{\mathrm{E}_i} = -\sum_{j(i\neq j)} 2J_{ij}\mathbf{M}_i\mathbf{M}_j, \tag{5.2}$$

where $\mathbf{M}_j$ is the magnetic moment of the neighboring ion. J_{ij} is the exchange integral, defining the splitting energy between the states with parallel and antiparallel orientations of the magnetic moments of the neighboring ions. Therefore, if the sign of J is positive, the state with $\mathbf{M}_i$ being parallel to $\mathbf{M}_j$ is favorable and the crystal possesses ferromagnetic ordering. Otherwise the magnetic moments are antiparallel. In this case the type of magnetic ordering depends on the origin of the magnetic moments $\mathbf{M}_{i,j}$. If they are equal, then the crystal is antiferromagnetic. Otherwise, ferrimagnetism is observed.

The magnetic structure of a ferromagnetically ordered medium is usually described in terms of the magnetization

$$\mathbf{M} = \sum_{i=1..N} \mathbf{M}_i, \tag{5.3}$$

where N is the total number of different magnetic sublattices. Antiferromagnetic structures are described in terms of the ferromagnetic vector (5.3) and the antiferromagnetic vectors

$$\mathbf{L}_i = \mathbf{M}_j - \mathbf{M}_k. \tag{5.4}$$

The total number of antiferromagnetic vectors $\mathbf{L}_i$, required to describe the magnetic properties of the medium, is defined by the number of the different magnetic sublattices comprising the medium. In the discussion below we consider the simple case of a two-sublattice medium, which, however, allows to demonstrate what happens when a multi-sublattice system is subjected to short laser pulses. The remarkable features that then appear cannot be observed in simple ferromagnets. To describe such a multi-sublattice magnetic structure, two vectors $\mathbf{M} = \mathbf{M}_1 + \mathbf{M}_2$ and $\mathbf{L} = \mathbf{M}_1 - \mathbf{M}_2$ are required, with $\mathbf{M}_{1(2)}$ being the magnetic moments of the two sublattices. The exchange term in the expression for the energy (5.1) has the form [5]:

$$\mathcal{H}_E = \frac{A}{2}\mathbf{L}^2 + \frac{B}{2}\mathbf{M}^2, \tag{5.5}$$

with A and B constants.

In antiferromagnets $B > 0$ and, consequently, $\mathbf{M} = 0$ in equilibrium. Such crystals are *compensated* antiferromagnets, i.e. $\mathbf{M}_1$ and $\mathbf{M}_2$ are aligned antiparallel to each other and $|\mathbf{M}_1| = |\mathbf{M}_2|$. However, in a number of magnetic crystals possessing antiferromagnetic ordering an additional Dzyaloshinsky-Moriya term [6, 7] is present in Eq. (5.1):

$$\mathcal{H}_\mathrm{D} = dM_iL_j \, (i \neq j), \tag{5.6}$$

where i, j denote the projections on the crystallographic axes x, y or z. Presence of this term means that a non-zero magnetization directed perpendicular to $\mathbf{L}$ can exist in such a crystal, i.e. the magnetic moments of the sublattices are canted from the fully antiparallel alignment. Such materials are called weak ferromagnets. The weak ferromagnetism arises from the antisymmetric exchange interactions, which are related to the nonequivalent position of the ions from the different sublattices in the crystal [6, 7].

The exchange energy $\mathcal{H}_\mathrm{E}$ is isotropic and depends exclusively on the relative orientation of the magnetic moments of the ions. The Dzyaloshinsky-Moriya interaction leads to the existence of the magnetization in a certain direction with respect to the antiferromagnetic vector. The orientation of the magnetic moments and, consequently, of $\mathbf{M}$ and $\mathbf{L}$ with respect to certain directions in the crystal is the result of the magnetic anisotropy. A particular case of this anisotropy is called magneto-crystalline

anisotropy, which plays a leading role when the deformations, defects and mechanical stresses do not distort the crystallographic lattice significantly. In the simplest case of a ferromagnetic crystal, the energy of the magneto-crystalline anisotropy is

$$\mathcal{H}_{\mathrm{A}} = k_1 \sin^2 \alpha + k_2 \sin^4 \alpha + ..., \tag{5.7}$$

where α is the angle between $\mathbf{M}$ and the magnetization easy-plane. This expression is obtained by the decomposition of the magnetic anisotropy energy into terms of different power in the magnetization projections on the coordinate axes. Because of the energy being invariant with respect to time inversion, only even powers of the projections enter the expression (5.7). The signs of the anisotropy constants k_1 and k_2 define the favorable orientations of the magnetization. The magneto-crystalline anisotropy of the easy-plane type is observed if $k_1 < 0$ and $k_2 = 0$. If $k_1 > 0$ and $k_2 = 0$ the crystal possesses an easy axis of magnetization. For the antiferromagnetic crystal having two sublattices, the energy of the magneto-crystalline anisotropy is

$$\mathcal{H}_{\mathrm{A}} = k_1'(\sin^2 \alpha_1 + k_2 \sin^2 \alpha_2) + ..., \tag{5.8}$$

where $\alpha_{1,2}$ are the angles between the magnetic moments of the sublattices and the antiferromagnetic axis, which can be an easy or hard axis depending on the sign of k_1'. The plane, perpendicular to the magnetic axis is referred to as the basal plane. In terms of ferromagnetic and antiferromagnetic vectors, the magneto-crystalline anisotropy term in Eq. (5.1) can be written as:

$$\mathcal{H}_A = \frac{a}{2} l_z^2 + \frac{b}{2} m_z^2. \tag{5.9}$$

The positive sign of the constants a and b corresponds to the magneto-crystalline anisotropy of the easy-plane type. The z axis is the magnetic hard axis and the xy plane is the magnetic easy-plane.

Effective fields

It is common to describe the magnetization equilibrium orientation in terms of the *effective field* which is found as the derivative of the energy (5.1) with respect to the magnetic moments of the sublattices $\mathbf{M}_i$:

$$\mathbf{H}_i^{\mathrm{eff}} = -\frac{\partial \mathcal{H}}{\partial \mathbf{M}_i}. \tag{5.10}$$

The effective field $\mathbf{H}_i^{\mathrm{eff}}$ describes the resulting action of the surrounding and of an applied magnetic field on the i-th magnetic ion. This effective field can be decomposed into the effective exchange field $\mathbf{H}_{E_i} = -\partial \mathcal{H}_E / \partial \mathbf{M}_i$, the effective Dzyaloshinsky field $\mathbf{H}_{D_i} = -\partial \mathcal{H}_D / \partial \mathbf{M}_i$, the effective anisotropy field $\mathbf{H}_{A_i} = -\partial \mathcal{H}_A / \partial \mathbf{M}_i$ and the

applied magnetic field $\mathbf{H} = -\partial\mathcal{H}_H/\partial\mathbf{M}_i$. Often there are values of these fields which are obtained from various measurements in order to describe the actual magnetic structure of the crystals. The geometrical sum of these fields defines the equilibrium orientation of the magnetic moments in a crystal.

If the magnetic structure is described in terms of the ferromagnetic and antiferromagnetic vectors, it is convenient to introduce the effective fields

$$\mathbf{H}_{\mathbf{M}}^{\text{eff}} = -\frac{\partial\mathcal{H}}{\partial\mathbf{M}}, \; \mathbf{H}_{\mathbf{L}_i}^{\text{eff}} = -\frac{\partial\mathcal{H}}{\partial\mathbf{L}_i}. \tag{5.11}$$

Below, they are referred to as the *effective ferromagnetic and antiferromagnetic fields*, respectively. Note, that these effective fields are written for the case of a two-sublattice medium only. For a medium consisting of more than two magnetic sublattices, the total number of effective fields (5.11) corresponds to the total number of sublattices.

5.2.2 Coherent spin precession

When deviated from its equilibrium position, a magnetic moment starts a precessional motion around this position with an amplitude of precession decaying (Fig. 5.1) if no additional external ac magnetic field compensates this decay. Due to the strong coupling between the magnetic moments of the different ions in a solid, they precess coherently, forming a so-called spin-wave, the k-vector of which depends on the excitation conditions. This coherent precessional motion of the magnetic moments can be treated using different approaches. On the one hand, the precession of the magnetization (of separate sublattices or a whole sample) around an effective magnetic field can be considered. On the other hand, the more general *classical Hamiltonian approach* can be used [3, 4, 8]. This approach yields a tool to describe the waves in a medium independent on the particular origin of these waves. The coherent spin precession in solids is an example of such waves.

Coherent spin precession and the Landau-Lifshitz equation in a multi-sublattice medium

In the discussion below only processes involving no change of the absolute value of the magnetic moment, $\mathbf{M}_0 = const$, are considered. Therefore, the precession can be described by a vector $\mathbf{m}(t)$ as shown in Fig. 5.1:

$$\mathbf{M}(t) = \mathbf{M}_0 + \mathbf{m}(t). \tag{5.12}$$

If we chose the coordinate frame in such a way that the effective field and, consequently, the magnetic moment equilibrium direction is along the z axis, then the precession is described by the time-dependent vector $\mathbf{m}(t) = m_x\mathbf{x} + im_y\mathbf{y}$, where $\mathbf{x}$ and $\mathbf{y}$ are unit vectors. The z component of the magnetic moment is $M_z\mathbf{z} = \mathbf{M}_0$.

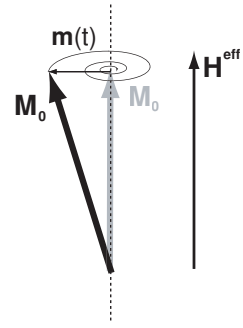

Figure 5.1: Precession of a magnetic moment $\mathbf{M} = \mathbf{M}_0 + \mathbf{m}(t)$ around an effective field $\mathbf{H}^{\text{eff}}$.

The precession of the magnetic moment shown in Fig. 5.1 is described by the Landau-Lifshitz (L-L) equation:

$$\frac{d\mathbf{m}}{dt} = -\gamma \mathbf{m} \times \mathbf{H}^{\text{eff}}, \tag{5.13}$$

if the damping is not of importance. Otherwise, an additional term accounting for the energy dissipation is introduced. In the discussion below the damping of the precession does not play an essential role and, therefore, Eq. (5.13) is used.

If a simple ferromagnetic medium, characterized by only one magnetic sublattice, is considered, Eq. (5.13) can be used directly to describe the precessional dynamics of the magnetization. However, in the case of a multi-sublattice (in particular, a two-sublattice antiferromagnetic) medium, Eq. (5.13) has to be written for each sublattice. It is more convenient to consider instead motions of the ferromagnetic $\mathbf{M}$ and antiferromagnetic $\mathbf{L}$ vectors, which are described by a set of modified L-L equations [5, 9]:

$$\frac{d\mathbf{m}}{dt} = -\gamma \left(\mathbf{m} \times \mathbf{H}_{\mathbf{m}}^{\text{eff}} + \mathbf{l} \times \mathbf{H}_{\mathbf{l}}^{\text{eff}} \right); \tag{5.14a}$$

$$\frac{d\mathbf{l}}{dt} = -\gamma \left(\mathbf{m} \times \mathbf{H}_{\mathbf{l}}^{\text{eff}} + \mathbf{l} \times \mathbf{H}_{\mathbf{m}}^{\text{eff}} \right), \tag{5.14b}$$

where the damping terms were omitted. The dynamical vector $\mathbf{l}(t)$ is introduced as

$$\mathbf{L}(t) = \mathbf{L}_0 + \mathbf{l}(t), \tag{5.15}$$

where $\mathbf{L}_0$ is the equilibrium antiferromagnetic vector. This form of the L-L equations for a multi-sublattice magnetic medium is convenient, because it shows explicitly that, for example, in a compensated antiferromagnet, a deviation of the antiferromagnetic vector from equilibrium leads to the occurrence of a dynamic magnetization $d\mathbf{m}/dt = -\gamma \mathbf{l} \times \mathbf{H}_{\mathbf{L}}^{\text{eff}}$ [10].

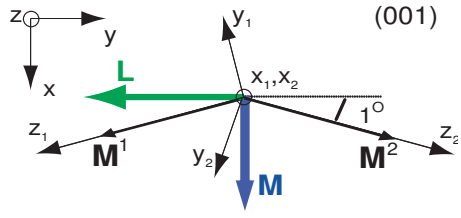

Figure 5.2: The choice of the local coordinate systems $\{x_1, y_1, z_1\}$ and $\{x_2, y_2, z_2\}$ for Eq. (5.16). Note, that the length of $\mathbf{L}$ and the canting of the sublattice magnetizations $\mathbf{M}^{1,2}$ are not to scale.

Coherent spin waves and the classical Hamiltonian formalism

Spin waves can be treated using the classical Hamiltonian formalism, which is one of the general methods for the description of waves of various origin [3, 4]. The Hamiltonian formalism for magnons in a magnetic dielectric was developed in Ref. [8] and the application of this approach to the case of magnons excited by laser pulses was demonstrated by us in [11] and extensively described in Ref. [12] for several examples of magnetically-ordered media. Here we consider in detail the particular case of a two-sublattice antiferromagnet of an easy-plane type, i.e. $FeBO_3$.

The deviation of the magnetization of the k-th sublattice from equilibrium can be considered in a local coordinate system, where the z_k axis is directed along the equilibrium sublattice magnetization, as shown in Fig. 5.2. Then, for the case of a homogenous precession, the canonical variables b_k can be introduced through the linearized Holstein-Primakoff transformation [13]

$$b_k = \frac{M^k_{x_k} + iM^k_{y_k}}{\sqrt{2\gamma_k \mathcal{M}_k}}, \tag{5.16}$$

where $k = 1, 2$ for the two sublattice antiferromagnet and $\mathcal{M}_k$ and γ_k are the magnetization and the gyromagnetic ratio of the k-th sublattice, respectively. $M^k_{x_k(y_k)}$ is the projection of the magnetization of the k-th sublattice on the $x_k(y_k)$ axis of the k-th local coordinate system. The equation of motion for these variables is

$$\mathrm{i}\frac{\partial b_k}{\partial t} = \frac{\partial \mathcal{H}}{\partial b^*_k}; \; -\mathrm{i}\frac{\partial b^*_k}{\partial t} = \frac{\partial \mathcal{H}}{\partial b_k}, \tag{5.17}$$

where $\mathcal{H} = \mathcal{H}_{\text{magnon}} + \mathcal{H}_{\text{int}}$. Hamiltonian $\mathcal{H}_{\text{magnon}}$ describes the coherent magnons and is a quadratic function of the variables $\{b_k, b^*_k\}$. $\mathcal{H}_{\text{int}}$ describes the interaction of magnons with an external stimulus, which is an electric field of light in our case, and is considered in Section 5.3. Now we assume that there is no external stimulus.

The Hamiltonian $\mathcal{H}_{\text{magnon}}$ can be reduced to the diagonal form

$$\mathcal{H}_{\text{magnon}} = \sum_n \Omega_n Q_n Q_n^*, \tag{5.18}$$

by performing the transformation from the canonical variables b_k to normal coordinates Q_n of the n-th spin precession eigenmode. The Q_n in this case are the classical analogs of the quantum mechanical creation and annihilation operators [14] and satisfy the equation of motion

$$\mathrm{i}\frac{dQ_n}{dt} = \frac{\partial \mathcal{H}}{\partial Q_n^*}. \tag{5.19}$$

The transformation is (See Eq. (12) in [12])

$$b_k = \sum_n (u_{kn}^* Q_n - v_{kn} Q_n^*), \tag{5.20}$$

where the coefficients u_{kn}, v_{kn} should satisfy the conditions that guarantee that the transformation (Eq. (5.20)) is canonical and Q_n is a normal coordinate (Eqs. (8-11) in [12]).

For a two sublattice antiferromagnet, possessing an easy-plane magnetic anisotropy (e. g. $FeBO_3$), the transformation $b_k \to Q_n$ holds [15]

$$b_1 + b_2 = \sqrt{\frac{\gamma H_E}{\Omega^{\text{FMR}}}}(Q_{\text{FMR}} - Q_{\text{FMR}}^*) + \frac{1}{2}\sqrt{\frac{\Omega^{\text{FMR}}}{\gamma H_E}}(Q_{\text{FMR}} + Q_{\text{FMR}}^*), \tag{5.21a}$$

$$b_1 - b_2 = \sqrt{\frac{\gamma H_E}{\Omega^{\text{AFMR}}}}(Q_{\text{AFMR}} + Q_{\text{AFMR}}^*) + \frac{1}{2}\sqrt{\frac{\Omega^{\text{AFMR}}}{\gamma H_E}}(Q_{\text{AFMR}} - Q_{\text{FMR}}^*), \tag{5.21b}$$

where $\Omega^{(\text{A})\text{FRM}}$ are the frequencies of the (anti)ferromagnetic modes of spin precession and H_E is the effective exchange field, which values are given in Chapter 3. $Q_{(\text{A})\text{FMR}}$ are the normal coordinates for these modes.

For the FMR mode of spin precession we find that

$$b_1 + b_2 = \frac{1}{\sqrt{2\gamma \mathcal{M}_0}}(m_z + \mathrm{i}l_x), \tag{5.22}$$

where $m_z = M^1_{x_1} + M^2_{x_2}$ and $l_x = M^1_{y_1} - M^2_{y_2}$ and x, z are the axes of the general coordinate system of the sample (Fig. 6.5), $\mathcal{M}_0 = \mathcal{M}_1 = \mathcal{M}_2$ is the sublattice magnetization and γ is the gyromagnetic ratio. Combining Eqs. (5.21a) and (5.22) we get

$$\begin{pmatrix} l_x(t) \\ m_y(t) \\ m_z(t) \end{pmatrix} = 2\mathrm{Re}\left(Q(t) \begin{pmatrix} \mathrm{i}a_x \\ \mathrm{i}b_y \\ b_z \end{pmatrix} \right), \tag{5.23a}$$

$$a_x = \sqrt{2\gamma\mathcal{M}_0}\sqrt{\frac{\gamma H_E}{\Omega^{\mathrm{FMR}}}},\ b_z = \frac{1}{2}\sqrt{2\gamma\mathcal{M}_0}\sqrt{\frac{\Omega^{\mathrm{FMR}}}{\gamma H_E}}, \tag{5.23b}$$

$$b_y/a_x = -M^{(0)}_x/L^{(0)}_y,\ b_z/a_x = \Omega^{\mathrm{FMR}/2\gamma H_E}, \tag{5.23c}$$

$$\begin{aligned} l_x(t) &= \mathrm{i}a_x(Q - Q^*), \\ m_y(t) &= \mathrm{i}b_y(Q - Q^*), \\ m_z(t) &= b_z(Q + Q^*). \end{aligned} \tag{5.23d}$$

where $Q(t)$ describes the coherent magnons in the time domain, while $\{\mathrm{i}a_x, \mathrm{i}b_y, b_z\}$ describe the magnon polarization.

Similarly, for the AFMR mode of spin precession we find

$$b_1 - b_2 = \frac{1}{\sqrt{2\gamma\mathcal{M}_0}}(l_z + \mathrm{i}m_x), \tag{5.24}$$

where $l_z = M^1_{x_1} - M^2_{x_2}$ and $m_x = M^1_{y_1} + M^2_{y_2}$ and x, z are the axes of the general coordinate system of the sample (Fig. 6.5). Therefore, the relations between the normal coordinate for this mode and the deviations of the ferromagnetic and antiferromagnetic vectors are

$$\begin{pmatrix} m_x(t) \\ l_y(t) \\ l_z(t) \end{pmatrix} = 2\mathrm{Re}\left(Q(t) \begin{pmatrix} b_x \\ a_y \\ \mathrm{i}a_z \end{pmatrix} \right), \tag{5.25a}$$

$$b_x = \sqrt{2\gamma\mathcal{M}_0}\sqrt{\frac{\gamma H_E}{\Omega^{AFMR}}},\ a_z = \frac{1}{2}\sqrt{2\gamma\mathcal{M}_0}\sqrt{\frac{\Omega^{\mathrm{AFMR}}}{\gamma H_E}}, \tag{5.25b}$$

$$b_x/a_y = -M^{(0)}_x/L^{(0)}_y,\ a_z/b_x = \Omega^{AFMR}/2\gamma H_E, \tag{5.25c}$$

$$\begin{aligned} m_x(t) &= b_x(Q + Q^*), \\ l_y(t) &= a_y(Q + Q^*), \\ l_z(t) &= \mathrm{i}a_z(Q - Q^*), \end{aligned} \tag{5.25d}$$

The equation of motion for each of these modes of precession in the absence of the external stimuli, such as light (which is considered below) has the form

$$\frac{dQ}{dt} + \mathrm{i}\Omega_0 Q = 0, \tag{5.26}$$

where Q and Ω_0 are the normal coordinate and the frequency of the corresponding mode of coherent spin precession, respectively.

5.3 Interaction of short laser pulses with magnetic media: impulsive stimulated Raman scattering (ISRS)

The excitation of the coherent spin precession by short laser pulses has been demonstrated experimentally by several groups [16, 17, 18, 19, 20]. Several direct and indirect mechanisms were considered to explain the observed effects (see Table 1.1). The light induced change of the shape [16] or magnetocrystalline [19] anisotropy fields and the light-induced spin-reorientation transition [20] are examples of possible indirect mechanisms, as considered in Chapter 1. The direct mechanism was proposed to manifest itself in experiments described in [17, 21], where the precession was induced via a so-called *ultrafast opto-magnetic inverse Faraday effect*, i.e the generation of an effective magnetic field by circularly-polarized light pulses. The microscopic mechanism of this phenomenon was proposed to be a stimulated Raman scattering. No extensive elaboration of this assumption were presented, though. Below we present a phenomenological consideration of the process of light-induced generation of coherent spin precession employing an approach used previously [22], and as well applying the classical Hamiltonian formalism, which was previously successfully used for the description of the light-induced excitation of another type of coherent processes in media - phonons, or lattice vibrations (for a review see [1, 23]).

5.3.1 Spontaneous, stimulated and impulsive stimulated Raman scattering

The possibility to excite coherent processes - phonons and magnons - by light was considered theoretically already in 1960's by Shen and Bloembergen [24, 25]. The microscopic process of this excitation is Raman scattering. Consider a photon with energy $\hbar\omega_i$ lower than the energy of the allowed electronic transition $|g\rangle \rightarrow |e\rangle$ (Fig. 5.3(a)). Then this photon stimulates the transition of an electron into a virtual state, which is a superposition of the ground state $|g\rangle$ and all excited states $|e\rangle$. If selection rules allow, this electron relaxes into one of the sublevels of the ground state, which corresponds to some excitation of the material, such as a phonon (vibrational sublevel) or magnon (sublevel with reversed spin, as shown in Fig. 5.3(a)). The energy of this excited sublevel differs from the energy of the initial state by $\hbar\Omega_0$, where Ω_0 is the

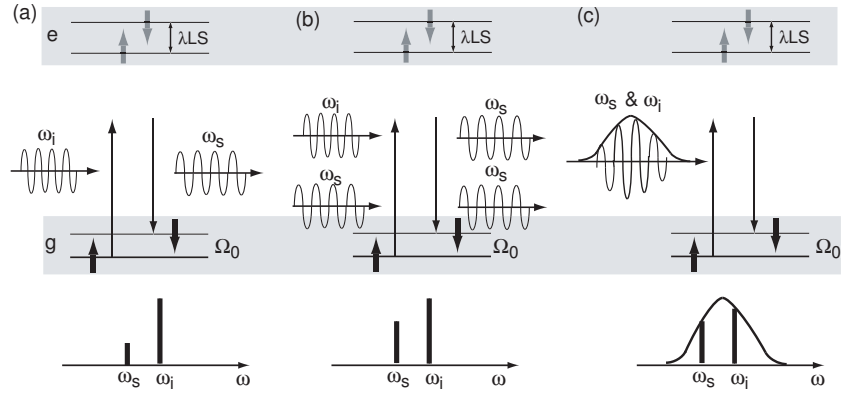

Figure 5.3: Schematic representation of Raman scattering (RS) on magnons. (a) Spontaneous RS photon with frequency ω_i, which is below an absorption gap of a medium, is scattered in photon with frequency $\omega_s = \omega_i - \Omega_0$, where Ω_0 is the frequency of a magnon, created in the process. (b) Stimulated RS for two monochromatic waves with frequencies ω_i and ω_s. (c) Impulsive stimulated Raman scattering, where a short laser pulse contains photons with both frequencies ω_i and ω_s

eigenfrequency of the phonon or magnon. In order to satisfy the energy conservation law, the re-emitted (scattered) photon during this process has an energy and frequency $\hbar\omega_s$ different from those of the initial photon

$$\omega_i = \omega_s \pm \Omega_0, \tag{5.27}$$

where the '+' sign corresponds to the generation of an excitation in the medium. The '-' sign corresponds to the inverse processes where a transition is made to a sublevel of $|g\rangle$ lower than the initial one. The same is valid for the k-vectors of the initial ($\mathbf{k}_i$) and scattered ($\mathbf{k}_s$) photons and the coherent wave excited in the medium ($\mathbf{K}_0$)

$$\mathbf{k}_i = \mathbf{k}_s \pm \mathbf{K}_0. \tag{5.28}$$

The spin of the electron cannot be changed in the process of the optical electric-dipole transition $|g\rangle \rightarrow |e\rangle$. Therefore, to realize the reversal of the spin of the electron in the process of Raman scattering, a spin-orbit interaction ($E_{S-O} = \lambda LS$) in the virtual state is required, as illustrated in Fig. 5.3(a). Then the reversal of the spin can take place while the system is in the virtual excited state. The following relaxation of the electron to the ground state is only possible to a sublevel with the spin reversed with respect to the initial direction.

The process considered above is called *spontaneous* Raman scattering. It is known that the efficiency of this process can be increased if two monochromatic waves with energies $\hbar\omega_i$ and $\hbar\omega_s$ are simultaneously present (Fig. 5.3(b)) [26]. Then the transition of the electron from the virtual excited state to the ground state obtains stimulated character. Such a process of light scattering is referred to as *stimulated* Raman scattering (SRS). SRS can be seen as if light exerts in a medium the driving force, oscillating with the frequency $\Omega_0 = \omega_i - \omega_s$.

The use of a short laser pulse with a spectral width $\Delta\omega$ larger than the frequency Ω_0 leads to new features in the process of Raman scattering. Indeed, if $\Delta\omega >> \Omega_0$, then such a pulse contains both photons ω_i and ω_s involved in the stimulated Raman scattering (Fig. 5.3(c)). However, there is a fundamental difference between the SRS process involving two monochromatic waves and the one employing a single short light pulse. While in the former case the driving force acting on the medium possesses a continuous oscillating character, in the latter case the driving force exists only during the presence of the light pulse, which is much shorter than the period of the material excitation. The latter process is called, therefore, *impulsive stimulated Raman scattering* (ISRS).

In the beginning of the 1980's it was shown experimentally that ISRS leads to efficient excitation of acoustic phonons via picosecond pulses [27, 28, 29, 30]. The development of mode-locked femtosecond lasers has since then resulted in a large number of experimental and theoretical works and a substantial progress in the field of ultrafast light-matter interactions (for reviews see [1, 23, 31, 32]). In view of the current interest in ultrafast spin dynamics, the generation of coherent magnons via impulsive stimulated Raman scattering is an intriguing option. Indeed, second-order ISRS was shown to be the mechanism for the generation of a magnon squeezed state [33]. However, only recently first-order stimulated Raman scattering was suggested as the mechanism for the experimentally observed coherent magnon generation [17]. In this and the following Chapter we unambiguously demonstrate the generation of coherent magnons via first-order ISRS in a two-sublattice antiferromagnetic.

5.3.2 Equation of motion for the normal coordinate of a coherent magnon driven by a light-induced force

In this Section we consider the excitation of coherent spin precession by laser pulses using an approach, where the light is described by a classical electric field E and the coherent excitation in the medium is described by the normal coordinate Q introduced in the previous Section. This way to describe the interaction of laser pulses with a medium has been used widely when the generation of coherent phonons is considered [1, 28, 31]. However, in the case of a magnon, Q describes the precessional motion and is complex, as can be seen from Eqs. (5.23). This is in contrast to the case of phonons, where the normal coordinates describe ion displacements and are therefore

real variables (we consider the excitation of coherent phonons in Chapter 7).

The Hamiltonian equation of motion for a transparent medium described by $\mathcal{H} = \mathcal{H}_{\text{magnon}} + \mathcal{H}_{\text{int}}$ has the form [3, 4, 8]

$$\mathrm{i}\frac{\partial Q}{\partial t} = \frac{\partial \mathcal{H}}{\partial Q^*}, \tag{5.29}$$

that can be easily transformed into the equation

$$\frac{dQ}{dt} + \mathrm{i}\Omega_0 Q = -\mathrm{i}\frac{\partial \mathcal{H}_{\text{int}}}{\partial Q^*}, \tag{5.30}$$

using Eqs. (5.18, 5.26)

When optical absorption is significant, the more general equation holds

$$\frac{dQ}{dt} + \mathrm{i}\Omega_0 Q = -iF(t), \tag{5.31}$$

where the form of the driving force $F(t)$ depends on the type of process leading to the magnon excitation. The solution of this equation of motion is found in the form

$$Q(t) = -\mathrm{i}e^{-\mathrm{i}\Omega_0 t}\int_{-\infty}^{t} dt' F(t') e^{i\Omega_0 t'} \tag{5.32}$$

The initial conditions for which we find the solution are $Q(t \to -\infty) = 0$ and $dQ/dt(t \to -\infty) = 0$. The exact form of the solution (5.32) depends on the time-dependence of the driving force $F(t)$ exerted by the laser pulse. In general, Eq. (5.31) is not restricted to the case of ISRS only.

5.3.3 Optical excitation of coherent magnons in a transparent medium

The interaction of a laser pulse with a transparent magnetic medium is described in general by the Hamiltonian

$$\mathcal{H}_{\text{int}} = -\frac{\delta\varepsilon_{ij}}{16\pi}\mathcal{E}_i(t)\mathcal{E}_j^*(t), \tag{5.33}$$

where $\mathcal{E}_i(t)$ is the time-dependent amplitude of the electric field of light $\mathbf{E} = \mathrm{Re}\mathcal{E}(t)e^{i\omega t}$. The driving force exerted by laser pulses is impulsive in the case of a non-absorbing medium. The equation of motion for magnons (5.30) then has the form

$$\frac{\partial Q}{\partial t} + \mathrm{i}\Omega_0 Q = -\mathrm{i}\frac{I_0}{4nc}\frac{\partial \varepsilon_{ij}}{\partial Q^*} e_i e_j^* \delta(t), \tag{5.34}$$

where I_0 is the integrated pulse intensity, e_i is a component of the light polarization unit vector, n is the refraction index and c is the speed of light. $\partial\varepsilon_{ij}$ is the modulation

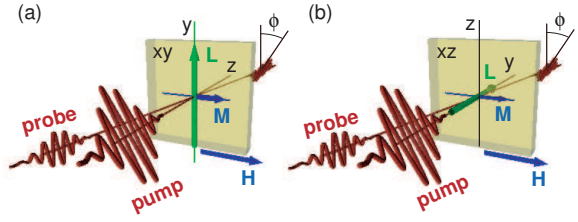

Figure 5.4: Orientation of the sample, external magnetic field and pump and probe beams in the experiments. (a) Pump beam propagates along the z axis perpendicular to the magnetic easy-plane. (b) Pump beam propagates along the y axis parallel to the magnetic easy-plane.

of the dielectric permittivity by the coherent spin precession. The dispersion of $\delta\varepsilon(\omega)$ can be neglected in Eq. (5.34), since the magnon frequency $\Omega_0 = \omega_i - \omega_s \ll \omega_0$ (the central pump frequency) and we consider a medium with low absorption.

The solution (5.32) in the case of an impulsive driving force is

$$Q(t) = -\mathrm{i}F_0 e^{-\mathrm{i}\Omega_0 t} = -F_0\left(\mathrm{i}\cos\Omega_0 t + \sin\Omega_0 t\right), \tag{5.35}$$

where

$$F_0 = \frac{I_0}{4nc}\frac{\partial\varepsilon_{ij}}{\partial Q^*}e_i e_j^*. \tag{5.36}$$

Therefore, the amplitude of the excited spin precession and the polarization of light required for its excitation are defined by the properties of the Raman tensor $\partial\varepsilon_{ij}/\partial Q^*$, which, in turn, are defined by the symmetry of the medium and the properties of the dielectric permittivity tensor ε_{ij}. The components of the tensor ε_{ij} modulated by the ferromagnetic and antiferromagnetic modes of the coherent spin precession for the easy-plane weak ferromagnet $FeBO_3$ are given in Table 5.1.

We consider two directions of the pump pulse propagation, as shown in Fig. 5.4. The pump beam propagates along the optical z axis in the first case and along the y axis in the second one. In both cases the magnetic field $\mathbf{H}$ is applied in the "easy plane"of magnetic anisotropy, along the x axis. As shown below, the excitation of coherent magnons in these two cases is significantly different.

Table 5.1: The modulation of the dielectric permittivity tensor ε_{ij} by FMR and AFMR spin precession. Underlined are the components used in the discussion of the FMR mode excitation via ISRS. The coordinate axes x, y, z are chosen as shown in Fig. 3.2. The magnetic field is assumed to be along the x axis, so that $\mathbf{L}^{(0)} \| y$, $\mathbf{M}^{(0)} \| x$. Singly and doubly underlined are the components which are crucial for the excitation of the FMR mode of spin precession in the considered experiments by pulses propagating along the y and z axes, respectively.

Tensor element	FMR (l_x, m_y, $m_z \neq 0$)	AFMR (m_x, l_y, $l_z \neq 0$)	Mixed contribution
ε^s_{xx}	$b_1 l_x^2 + c_2 m_y l_x - c_3 l_x m_z$	$b_2 L_y l_y + c_1 m_x l_y +$ $b_5 L_y l_z + c_8 M_x l_z$	0
ε^s_{yy}	$b_2 l_x^2 - c_1 m_y l_x + c_3 l_x m_z$	$b_1 L_y l_y - c_2 m_x l_y -$ $b_5 L_y l_z - c_8 M_x l_z$	0
ε^s_{zz}	$b_3 l_x^2 - c_4 m_y l_x$	$b_3 L_y l_y + b_8 l_z^2 +$ $c_4(M_x l_y + m_x L_y)$	0
$\underline{\underline{\varepsilon^s_{xy}}}$	$(b_1 - b_2) l_x L_y + c_3 L_y m_z -$ $\frac{1}{2}(c_1 + c_2)(M_x l_x - m_y L_y)$	0	$b_5 l_x l_z - c_8 m_y l_z$
$\underline{\varepsilon^s_{xz}}$	$2b_4 l_x L_y - c_6 L_y m_z +$ $c_5(m_y L_y - M_x l_x)$	0	$b_6 l_x l_z - c_7 m_y l_z$
ε^s_{yz}	$b_4 l_x^2 + c_5 m_y l_x + c_6 l_x m_z$	$b_6 L_y l_z + c_7 M_x l_z$	0
$\underline{\underline{\varepsilon^a_{xy}}}$	$\underline{\underline{\mathrm{i}K m_z}}$	0	0
$\underline{\varepsilon^a_{xz}}$	$\mathrm{i}K_1 m_y + \underline{\mathrm{i}K_2 l_x}$	0	0
ε^a_{yz}	0	$\mathrm{i}K_1 m_x - \mathrm{i}K_2 l_y$	0

Excitation of magnons by optical pulses with wave a vector perpendicular to the easy-plane of magnetic anisotropy

To describe the interaction of the pump pulses propagating along the z axis with the medium one has to consider the components $\delta\varepsilon^a_{xy}$ and $\delta\varepsilon^s_{xy}$ of the dielectric permittivity tensor. We find the main contributions to $\varepsilon^{a(s)}_{xy}$ caused by the magnons using Table 5.1, Eq.(5.23d) and taking into account that $L^{(0)}_y \gg M^{(0)}_x$, $l_x \gg m_z$:

$$\delta\varepsilon^a_{xy} = -\delta\varepsilon^a_{yx} = \mathrm{i}Km_z = \mathrm{i}Kb_z(Q+Q^*), \tag{5.37a}$$

$$\delta\varepsilon^s_{xy} = \delta\varepsilon^s_{yx} \approx GL^{(0)}_y l_x = \mathrm{i}GL^{(0)}_y a_x(Q-Q^*), \tag{5.37b}$$

where $G = b_1 - b_2$ in the notation used in [11].

In the case of circularly polarized light $\sigma^{\pm}$, the contribution from the antisymmetric part $\delta\varepsilon^a$ of the dielectric permittivity vanishes and the solution of Eq. (5.34) has the following form

$$Q^{\sigma^{\pm}}(t) = \pm\frac{1}{8nc}Kb_zI_0[\sin\Omega_0 t + \mathrm{i}\cos\Omega_0 t], \tag{5.38a}$$

$$m_z^{\sigma^{\pm}}(t) = \pm\frac{1}{4nc}Kb_z^2I_0\sin\Omega_0 t, \tag{5.38b}$$

$$l_x^{\sigma^{\pm}}(t) = \pm\frac{1}{4nc}Kb_za_xI_0\cos\Omega_0 t, \tag{5.38c}$$

where the $\pm$ signs correspond to opposite senses of helicity of the circularly polarized pump pulses. This result is, in general, consistent with that of [17], where a helicity dependent spin precession excitation was observed and stimulated Raman scattering was proposed as a possible microscopic mechanism.

For light linearly polarized at an angle θ with respect to the y axis, the contribution from the symmetric part $\delta\varepsilon^s_{xy}$ vanishes and the solution of Eq. (5.34) has the form

$$Q^{lin}(t) = \frac{1}{8nc}GL^{(0)}_y a_xI_0\sin 2\theta[-\cos\Omega_0 t + \mathrm{i}\sin\Omega_0 t], \tag{5.39a}$$

$$m_z^{lin}(t) = -\frac{1}{4nc}GL^{(0)}_y b_za_xI_0\sin 2\theta\cos\Omega_0 t, \tag{5.39b}$$

$$l_x^{lin}(t) = -\frac{1}{4nc}GL^{(0)}_y a_x^2I_0\sin 2\theta\sin\Omega_0 t, \tag{5.39c}$$

showing that the initial phase and amplitude of the excited coherent magnons can be controlled not only by the helicity of the circularly polarized laser pulses but also by the azimuthal angle θ of the linearly polarized pulses. Note, that the amplitudes of the spin precession excited by circularly and linearly polarized light are defined by the first and second order magneto-optical susceptibilities K and G, respectively. In magnetically ordered solids these susceptibilities can be comparable in magnitude [34, 35].

Excitation of magnons by optical pulses with a wave vector parallel to the antiferromagnetic vector

To describe the interaction of the pump pulses propagating along the y axis with the medium one has to consider the components $\delta\varepsilon^a_{xz}$ and $\delta\varepsilon^s_{xz}$ of the dielectric permittivity tensor. Taking into account the ellipticity of the spin precession, Eqs. (5.23d) and the ratio between L^0_y and M^0_x we obtain

$$\begin{aligned}\delta\varepsilon^a_{xz} &= -\delta\varepsilon^a_{zx} = \mathrm{i}(K_1 m_y + K_2 l_x)\\ &= (K_1 b_y + K_2 a_x)(Q - Q^*),\end{aligned} \tag{5.40a}$$

$$\delta\varepsilon^s_{xz} = \delta\varepsilon^s_{zx} \approx 2b_4 L^{(0)}_y l_x = \mathrm{i}2b_4 L^{(0)}_y a_x (Q - Q^*), \tag{5.40b}$$

Therefore, the magnons excited by linearly and circularly polarized light are described as follows

$$\begin{aligned}Q^{lin}(t) = \frac{1}{4nc} b_4 L^{(0)}_y a_x I_0 \sin 2\theta\\ \times \left[-\cos\Omega_0 t + \mathrm{i}\sin\Omega_0 t\right],\end{aligned} \tag{5.41a}$$

$$Q^{\sigma^\pm}(t) = \mp\frac{1}{8nc}(K_1 b_y + K_2 a_x) I_0 \left[-\cos\Omega_0 t + \mathrm{i}\sin\Omega_0 t\right], \tag{5.41b}$$

$$m^{lin}_z(t) = -\frac{1}{2nc} b_4 L^{(0)}_y a_x b_z I_0 \sin(2\theta)\cos\Omega_0 t, \tag{5.41c}$$

$$l^{lin}_x(t) = -\frac{1}{2nc} b_4 L^{(0)}_y a^2_x I_0 \sin(2\theta)\sin\Omega_0 t, \tag{5.41d}$$

$$m^{\sigma^\pm}_z(t) = \pm\frac{1}{4nc}(K_1 b_y + K_2 a_x) b_z I_0 \cos\Omega_0 t, \tag{5.41e}$$

$$l^{\sigma^\pm}_x(t) = \pm\frac{1}{4nc}(K_1 b_y + K_2 a_x) a_x I_0 \sin\Omega_0 t. \tag{5.41f}$$

5.3.4 Role of the light polarization and angular momentum in ISRS

As shown above, the phenomenological theory of ISRS predicts that the excitation of coherent magnons can be realized by both circularly and linearly polarized pulses, with an efficiency defined by the properties of the medium in question. The role of the polarization in the process of the interaction of light with a magnetic medium has been questioned during the last decade. Indeed, the manipulation of magnetization by light, i.g. demagnetization, spin precession excitation or even switching, requires the transfer of angular momentum to or from the spin system. Therefore, circularly polarized laser pulses were considered as a possible source of the required angular momentum. The assumed transfer of angular momentum from photons to spins, in

turn, rose the question about the feasibility of the all-optical control of the magnetization. Indeed, the estimation in [36] showed that the number of photons involved in typical magneto-optical experiments is by far not enough to supply the angular momentum required for a significant direct perturbation of the spin system. Later, experiments showed that, despite this prediction, circularly polarized pulses can fully reverse the magnetization in metallic films [37]. Therefore, the role of photons as a source of angular momentum remained a puzzle.

From the considered model of the ISRS it follows that even linearly polarized pulses, carrying no angular momentum, can excite a coherent spin precession. In the next Chapter we show that this can indeed be observed experimentally. This suggests that the photons do not serve as a source of angular momentum themselves but rather mediate this transfer between spins and other degrees of freedom in the medium. Indeed, the stimulated character of the process implies that the polarization (as well as the frequency and the propagation direction) of the scattered photon is preset by the polarization (frequency and direction) of the photon contained in the initial light pulse. A change of angular momentum of the light would imply a change of the outgoing polarization, which is not the case in the ISRS.

5.3.5 Optical excitation of coherent magnons in an absorbing medium

Although the interaction of light pulses with a transparent medium are the scope of this and the following Chapter, we consider here briefly the opposite situation, where the absorption can not be neglected, in order to show the principle difference between these two cases. If the absorption in the medium is considerable one can not use the Hamiltonian $\mathcal{H}_{\text{int}}$ (5.33) [26] and express the driving force exerted by a laser pulse as a delta-function. Instead, in analogy with the case of coherent phonon excitation [1, 38], the driving force can have a non-impulsive character. The experimental evidence of such type of processes can be found in [19, 21] where 100 fs laser pulses were reported to induce a quasi-stationary change of the magneto-crystalline anisotropy. Such a process can be considered as a *displacive* excitation of coherent magnons (DECM). The latter would correspond to a non-Raman process of magnon excitation. Moreover, for the case of light-induced coherent phonon excitation it was shown theoretically and experimentally that in an absorbing medium a combination of resonant Raman scattering and non-Raman (displacive) processes has to be considered [39].

Absorption (e.g., by impurity centers [19]) is involved in the displacive process and the driving force is described by a Heaviside *step*-function. Eq. (5.31) gets the form

$$\frac{\partial Q}{\partial t} + i\Omega_0 Q = \begin{cases} -\mathrm{i}F_0, & t > 0 \\ 0, & t < 0 \end{cases}, \tag{5.42}$$

where F_0 can in general be complex $F_0 = F_0' + iF_0''$. The solution (Eq. (5.32)) of the

equation of motion becomes

$$Q(t) = F_0' \frac{\cos\Omega_0 t - \mathrm{i}\sin\Omega_0 t - 1}{\Omega_0} + \mathrm{i}F_0'' \frac{\cos\Omega_0 t - \mathrm{i}\sin\Omega_0 t - 1}{\Omega_0}. \tag{5.43}$$

If, for example, $\Re F_0 = 0$, $\Im F_0 \neq 0$, then

$$Q(t) = \mathrm{i}F_0 \frac{e^{-\mathrm{i}\Omega_0 t} - 1}{\Omega_0}; \tag{5.44a}$$

$$m_z(t) = 2F_0 b_z \frac{\sin\Omega_0 t}{\Omega_0}; \tag{5.44b}$$

$$l_x(t) = 2F_0 a_x \frac{[1 - \cos\Omega_0 t]}{\Omega_0}. \tag{5.44c}$$

Note, that the spin precession excited via ISRS or DECM is characterized by a radically different time behavior. Namely, for the case of ISRS (Eqs. (5.38c,5.39b) and (5.41c,5.41e)) only terms with a *cosine*-like time dependence appear, indicating that right after the excitation by the light pulse, the spins are out of their equilibrium positions. This is never the case for DECM (Eqs. (5.44)). Moreover, in the case of ISRS the spins precess around their original equilibrium directions, as depicted by the *sine*- and *cosine*-like time dependence of $l_x(t)$ and $m_z(t)$ (Eq. (5.39c). In contrast, the DECM mechanism leads to a spin precession around a "new"equilibrium direction generated by the light pulse. A $(1 - \cos\Omega_0 t)$ dependence is therefore expected for $l_x(t)$. This allows one to distinguish between these two mechanisms in the experiment.

5.4 Interactions of short laser pulses with matter: opto-magnetism

The excitation of coherent spin precession by short laser pulses has been described previously using an approach, in which light acts on the spins as an effective light-induced magnetic field pulse [22]. For example, in [17] circularly polarized light pulses were suggested to act on the rare-earth orthoferrite $DyFeO_3$ as an effective magnetic field $\mathbf{H}^{\mathrm{eff}} = K\,[\mathbf{E} \times \mathbf{E}^*]$, which, strictly speaking, was defined for a cubic paramagnetic medium [40]. The resulting spin precession was described by the Landau-Lifshitz (L-L) equation [41]. In this Section we use a similar, but extended, approach, based on light-induced effective fields together with the L-L equation. We reveal some important features that were omitted from the considerations before [17, 19, 21, 42], i.e. the peculiarities of the approach when applied to a multi-sublattice medium. The necessity of this development was already noticed in [43]. We note that the procedure presented in this Section is an alternative to the approach developed above in this Chapter.

5.4.1 Effective fields in a multi-sublattice magnetic medium

To describe the impulsive action of light on the spin system, we introduce the light-induced effective fields

$$\mathbf{H}_i^{\text{eff}} = -\frac{\partial \mathcal{H}_{\text{i,int}}}{\partial \mathbf{M}_i}, \tag{5.45}$$

where $\mathbf{M}_i$ is the sublattice magnetization and $\mathcal{H}_{\text{i,int}}$ is the Hamiltonian describing the interaction of light with the i-th sublattice. For the case of a one-sublattice ferromagnetic medium, the further description of the light-matter interaction is trivial because one ferromagnetic vector $\mathbf{M}$ is sufficient to describe the collective response of the magnetic system to the light action. For the case of multi-sublattice magnetic medium the response of each sublattice should be considered. Alternatively, such a medium can be described by a ferromagnetic vector $\mathbf{M}$ and several antiferromagnetic vectors $\mathbf{L}_j$, where $j = 1, .., n-1$ and n is the number of magnetic sublattices. Particularly, $FeBO_3$ has two magnetic sublattices with magnetizations $\mathbf{M}_1$ and $\mathbf{M}_2$. The interaction of light with each sublattice can be described by the effective field $\mathbf{H}_1^{\text{eff}} = -\partial \mathcal{H}_{1,\text{int}}/\partial \mathbf{M}_1$ and $\mathbf{H}_2^{\text{eff}} = -\partial \mathcal{H}_{2,\text{int}}/\partial \mathbf{M}_2$. Making a transition from the sublattice magnetizations to the ferromagnetic $\mathbf{M} = \mathbf{M}_1 + \mathbf{M}_2$ and antiferromagnetic $\mathbf{L} = \mathbf{M}_1 - \mathbf{M}_2$ vectors, one obtains two effective fields

$$\mathbf{H}^{\text{eff}} = -\frac{\partial \mathcal{H}_{\text{int}}}{\partial \mathbf{M}}; \tag{5.46a}$$

$$\mathbf{h}^{\text{eff}} = -\frac{\partial \mathcal{H}_{\text{int}}}{\partial \mathbf{L}}, \tag{5.46b}$$

which can also be understood as $\mathbf{H}^{\text{eff}} = \mathbf{H}_1^{\text{eff}} + \mathbf{H}_2^{\text{eff}}$ and $\mathbf{h}^{\text{eff}} = \mathbf{H}_1^{\text{eff}} - \mathbf{H}_2^{\text{eff}}$. The latter field accounts for the non-equivalent response of the Fe^{3+} ions at different crystallographic positions to the action of light. Below we show that it is this field $\mathbf{h}^{\text{eff}}$ that induces the spin precession in a weak ferromagnet. Note that, in general, for a medium with n magnetic sublattices there are $n-1$ fields $\mathbf{h}_j^{\text{eff}} = -\partial \mathcal{H}_{\text{int}}/\partial \mathbf{L}_j$.

5.4.2 Excitation of the spin precession in two-sublattice weak ferromagnet

To describe the optical excitation of coherent spin precession we insert the effective fields (5.46) into the Landau-Lifshitz equations for a multi-sublattice medium (5.14) and take into account the impulsive character of these fields.

We again consider two possible experimental geometries shown in Fig. 5.4. For the pump pulses propagating along the z axis, the Hamiltonian $\mathcal{H}_{\text{int}}$ can be found from Eqs.(5.33) and Table 5.1

$$\mathcal{H}_{\text{int}}^{\sigma^{\pm}} = \frac{1}{16\pi}\varepsilon_{xy}^{a}\mathcal{E}_x(t)\mathcal{E}_y^*(t) = \pm\frac{I_0}{8nc}Km_z\delta(t), \tag{5.47}$$

where $\mathcal{E}_{x(y)}(t)$ are the time-dependent $x(y)$ components of the electric field of light. Therefore there is only a "ferromagnetic"effective field induced by such a pulse

$$\mathbf{H}^{\text{eff},\sigma^\pm} = -\frac{\partial \mathcal{H}_{\text{int}}^{\sigma^\pm}}{\partial \mathbf{m}} = \mp \frac{I_0}{8nc} K\delta(t)\hat{z}; \tag{5.48a}$$

$$\mathbf{h}^{\text{eff},\sigma^\pm} = -\frac{\partial \mathcal{H}_{\text{int}}^{\sigma^\pm}}{\partial \mathbf{l}} = 0, \tag{5.48b}$$

Taking into account the equilibrium orientation of the ferro- and antiferromagnetic vectors ($\mathbf{M}\|x$,$\mathbf{L}\|y$) we find that the torque, created by the light-induced effective field $\mathbf{H}^{\text{eff},\sigma^\pm}$ is

$$\frac{d\mathbf{m}}{dt} = -\gamma \mathbf{M} \times \mathbf{H}^{\text{eff},\sigma^\pm} =$$
$$-\gamma (M_x \cdot H_z^{\text{eff},\sigma^\pm})\hat{y} = \pm\gamma \frac{I_0}{8nc} K M_x^{(0)} \delta(t)\hat{y}; \tag{5.49a}$$

$$\frac{d\mathbf{l}}{dt} = -\gamma \mathbf{L} \times \mathbf{H}^{\text{eff},\sigma^\pm} =$$
$$-\gamma (L_y \cdot H_z^{\text{eff},\sigma^\pm})\hat{x} = \pm\gamma \frac{I_0}{8nc} K L_y^{(0)} \delta(t)\hat{x}. \tag{5.49b}$$

Therefore, circularly polarized pulses propagating along the z axis create a torque that moves the spins in the xy plane. When the pulse is gone (after 150 fs), the spins are out of their equilibrium orientation set by the effective fields $\mathbf{H}_E+\mathbf{H}_D+\mathbf{H}_A+\mathbf{H}_{A'}+\mathbf{H}_{\text{ext}}$. Therefore, the spins start to precess around their "*old*" orientations defined by the effective fields. This model is in full agreement with the results obtained above, where circularly polarized light is shown to excite *cosine*-like oscillations of $l_x(t)$ (5.38c) and *sine*-like oscillations of $m_z(t)$ [Eq. (5.38b)].

Interaction of linearly polarized pulses propagating along the z axis is described by the Hamiltonian (See Table 5.1)

$$\mathcal{H}_{\text{int}}^{\text{lin}} = \frac{I_0\delta(t)}{4nc}[(b_2 L_y^{(0)2} + c_1 M_x^{(0)} L_y^{(0)})\cos^2\theta +$$
$$(b_1 L_y^{(0)2} - c_2 M_x^{(0)} L_y^{(0)})\sin^2\theta +$$
$$\frac{1}{2}((b_1 - b_2) l_x L_y^{(0)} - \frac{1}{2}(c_1 + c_2)(M_x^{(0)} l_x - m_y L_y^{(0)}) + c_3 L_y^{(0)} m_z)\sin 2\theta +$$
$$(b_5 L_y^{(0)} + c_8 M_x^{(0)}) l_z \cos 2\theta]. \tag{5.50}$$

The light-induced effective fields in this case are

$$\mathbf{H}^{\text{eff,lin}} = -\frac{\partial \mathcal{H}_{\text{int}}^{\text{lin}}}{\partial \mathbf{M}} = -\frac{I_0\delta(t)}{4nc} \begin{bmatrix} (c_1\cos^2\theta - c_2\sin^2\theta) L_y^{(0)}\hat{x} \\ -\frac{1}{4}(c_1 + c_2) L_y^{(0)} \sin 2\theta \hat{y} \\ \frac{1}{2} c_3 \sin 2\theta L_y^{(0)} \hat{z} \end{bmatrix} \tag{5.51a}$$

$$\mathbf{h}^{\text{eff,lin}} = -\frac{\partial \mathcal{H}_{\text{int}}^{\text{lin}}}{\partial \mathbf{L}} =$$

$$\frac{I_0\delta(t)}{4nc}\begin{bmatrix} \frac{1}{2}((b_1-b_2)L_y^{(0)} - \frac{1}{2}(c_1+c_2)M_x^{(0)})\sin 2\theta\hat{x} \\ ((b_2\cos^2\theta + b_1\sin^2\theta)L_y^{(0)} + (c_1\cos^2\theta - c_2\sin^2\theta)M_x^{(0)})\hat{y} \\ (b_5 L_y^{(0)} + c_8 M_x^{(0)})\cos 2\theta\hat{z} \end{bmatrix} \tag{5.51b}$$

Only the components H_z, H_y, h_x of these fields can lead to an excitation of the FMR mode of spin precession. Therefore, the torques, exerted by the linearly polarized pulse propagating along the z axis is

$$\frac{d\mathbf{m}}{dt} = -\gamma[\mathbf{M}\times\mathbf{H}^{\text{eff,lin}} + \mathbf{L}\times\mathbf{h}^{\text{eff,lin}}] = -\gamma[(M_x^{(0)}\cdot H_z^{\text{eff,lin}})\hat{y} +$$
$$(M_x^{(0)}\cdot H_y^{\text{eff,lin}} + L_y^{(0)}\cdot h_x^{\text{eff,lin}})\hat{z}] \cong \gamma\frac{I_0\delta(t)}{8nc}(b_1-b_2)L^{(0)2}\sin 2\theta\hat{z}, \tag{5.52}$$

where we took into account that $M_x \ll L_y$. There is also the torque

$$\frac{d\mathbf{l}}{dt} = -\gamma(L_y^{(0)}\cdot H_z^{\text{eff,lin}})\hat{x} = \gamma\frac{I_0\delta(t)}{8nc}c_3 L^{(0)2}\sin 2\theta\hat{x}. \tag{5.53}$$

Therefore, the linearly polarized pulses propagating along the z axis can excite a spin precession because of the light induced effective field $\mathbf{h}^{\text{eff,lin}}\|x$. In contrast to a circularly polarized pulse, the effective field $h_x^{\text{eff,lin}}$ induced by a linearly polarized light pulse [Eq. (5.51b)] exerts a torque [Eq. (5.52)] that pushes the spins out of the xy plane. Therefore, the spin motion after the end of the pump pulse is described by $l_x(t) \sim \sin\Omega_0 t$ and $m_z(t) \sim \cos\Omega_0 t$ (compare with Eqs. (5.39b,5.39c)

For the case of pump pulses propagating along the y axis the same procedure can be followed and gives the following results for circularly polarized pulses

$$\mathbf{h}^{\text{eff},\sigma^{\pm}} = \mp\frac{I_0}{8nc}K_2\delta(t)\hat{x}; \tag{5.54a}$$

$$\frac{dm_z^{\sigma^{\pm}}}{dt} = \pm\gamma\frac{I_0}{8nc}K_2 L_y^{(0)2}\delta(t). \tag{5.54b}$$

Thus, the effect of a circularly polarized pulse propagating along the y axis resembles that of a linearly-polarized one propagating along the z axis [Eq. (5.52)]. Namely, the effective field induced by the former and latter pulses is h_x^{eff} and the spins move out of the xy plane during the pulse.

5.4.3 Inverse magneto-optical effects

A separate remark is required concerning the term inverse Faraday effect used in [17, 21, 42]. Following the same logic the effective fields induced by linearly polarized

light can be referred to as a manifestation of an *ultrafast* inverse Cotton-Mouton, or inverse Voigt, effect. However, in the original papers on these phenomena [40, 44, 45, 46] the inverse Faraday effect was introduced to describe the magnetization induced in a paramagnetic medium by circularly polarized 30 ns pulses. There are several different mechanisms leading to this latter phenomenon, such as an optical Stark effect and a mixing different amounts of excited states into the ground state [26]. In contrast, in [17] the term *ultrafast* inverse Faraday effect was introduced for the effective magnetic field induced by circularly polarized ultrashort laser pulses that lead to the excitation of spin precession. As we have shown here and in the next Chapter, the microscopic mechanism of this effect is ISRS, in which the optical electric fields mix the ground state with excited states and create Raman coherence between the magnetic sublevels of the ground state. One should therefore be careful and keep in mind the drastic difference between the experiments with nanosecond and subpicosecond laser pulses. If the duration of the pulse is comparable to the time required for the repopulation of the different magnetic sublevels of the ground state ($\sim$ ns), such a long excitation leads to a laser-induced magnetization not observed in the experiments with subpicosecond pulses.

In the next Chapter we present the experimental results on the light-induced coherent spin precession in the easy-plane weak ferromagnet $FeBO_3$ and discuss the agreement between the theory developed here and the experimental data. We show that there are specific features in the process, which should be taken into account when dealing with a multi-sublattice medium.

References

[1] R. Merlin, Solid State Comm. **102**, 207 (1997).

[2] A. V. Kimel, A. Kirilyuk, F. Hansteen, R. V. Pisarev, and T. Rasing, J. Phys.: Cond. Matter **19**, 043201 (2007).

[3] V. E. Zakharov and E. A. Kuznetsov, *Soviet Scientific Reviews, Section C Mathematical Physics Reviews* (OPA, Amsterdam, 1984).

[4] V. E. Zakharov and E. A. Kuznetsov, Phys. Usp. **40**, 1087 (1997).

[5] E. A. Turov, *Physical Proparties of Magnetically Ordered Crystals* (Academic Press, London, 1965).

[6] I. Dzyaloshinsky, J. Phys. Chem. Solids **4**, 241 (1958).

[7] T. Moriya, Phys. Rev. **120**, 91 (1960).

[8] V. S. L'vov, *Nonlinear Spin Waves (in Russian)* (Nauka, Moscow, 1987).

[9] A. S. Borovik-Romanov and N. M. Kreines, Phys. Rep. **81**, 351 (1982).

[10] A. F. Andreev and V. I. Marchenko, Sov. Phys. Usp. **23**, 21 (1980).

[11] A. M. Kalalshnikova, A. V. Kimel, R. V. Pisarev, V. N. Gridnev, A. Kirilyuk, and T. Rasing, Phys. Rev. Lett. **99**, 167205 (2007).

[12] V. N. Gridnev, Phys. Rev. B **77**, 094426 (2008).

[13] T. Holstein and H. Primakoff, Phys. Rev. **58**, 1098 (1940).

[14] A. I. Akhiezer, V. G. Bar'yakhtar, and S. V. Peletminskii, *Spin Waves* (North-Holland, Amsterdam, 1968).

[15] V. S. Lutovinov and V. L. Safonov, Sov. Phys. Solid State **22**, 1541 (1980).

[16] M. van Kampen, C. Jozsa, J. T. Kohlhepp, P. LeClair, L. Lagae, W. J. M. de Jonge, and B. Koopmans, Phys. Rev. Lett. **88**, 227201 (2002).

[17] A. V. Kimel, A. Kirilyuk, P. A. Usachev, R. V. Pisarev, A. M. Balbashov, and T. Rasing, Nature (London) **435**, 655 (2005).

[18] G. Ju, A. Vertikov, A. V. Nurmikko, C. Canady, G. Xiao, R. F. C. Farrow, , and A. Cebollada, Phys. Rev. B **57**, R700 (1998).

[19] A. K. F. Hansteen, A. V. Kimel and T. Rasing, Phys. Rev. Lett. **95**, 047402 (2005).

[20] A. V. Kimel, A. Kirilyuk, A. Tsvetkov, R. V. Pisarev, and T. Rasing, Nature (London) **429**, 850 (2004).

[21] F. Hansteen, A. Kimel, A. Kirilyuk, and T. Rasing, Phys. Rev. B **73**, 014421 (2006).

[22] A. V. Kimel, A. Kirilyuk, F. Hansteen, R. V. Pisarev, and T. Rasing, J. Phys.: Condens. Matter **19**, 043201 (2007).

[23] T. Dekorsy, G. C. Cho, and H. Kurz, *Light scattering in solids* (Springer, Berlin, 2006), vol. VIII.

[24] Y. R. Shen and N. Bloembergen, Phys. Rev. **137**, A1787 (1965).

[25] Y. R. Shen and N. Bloembergen, Phys. Rev. **143**, 372 (1966).

[26] Y. R. Shen, *Principles of Nonlinear Optics* (J. Wiley & Sons, New York, 1984).

[27] K. A. Nelson, R. J. D. Miller, D. R. Lutz, and M. D. Fayer, J. Appl. Phys. **53**, 1144 (1981).

[28] Y.-X. Yan, E. B. Gamble, Jr., and K. A. Nelson, J. Chem. Phys. **83**, 5391 (1985).

[29] Y.-X. Yan and K. A. Nelson, J. Chem. Phys. **87**, 6240 (1994).

[30] Y.-X. Yan and K. A. Nelson, J. Chem. Phys. **87**, 6257 (1994).

[31] L. Dhar, J. A. Rogers, and K. A. Nelson, Chem. Rev. **94**, 157 (1994).

[32] J.-C. Diels and W. Rudolph, *Ultrashort Laser Pulse Phenomena* (Academic Press, Amsterdam, 2006), 2nd ed.

[33] J. Zhao, A. V. Bragas, D. J. Lockwood, and R. Merlin, Phys. Rev. Lett. **93**, 107203 (2004).

[34] G. A. Smolenskiĭ, R. V. Pisarev, and I. G. Siniĭ, Sov. Phys. - Usp. **18**, 410 (1975).

[35] J. Ferré and G. A. Gehring, Rep. Prog. Phys. **47**, 513 (1980).

[36] B. Koopmans, M. van Kampen, J. T. Kohlhepp, and W. J. de Jonge, Phys. Rev. Lett. **85**, 844 (2000).

[37] C. D. Stanciu, F. Hansteen, A. Kimel, A. Tsukamoto, A. Itoh, A. Kirilyuk, , and T. Rasing, Phys. Rev. Lett. **99**, 047601 (2007).

[38] H. J. Zeiger, J. Vidal, T. K. Cheng, E. P. Ippen, G. Dresselhaus, and M. S. Dresselhaus, Phys. Rev. B **45**, 786 (1992).

[39] J. F. W. G. A. Garrett, T. F. Albrecht and R. Merlin, Phys. Rev. Lett. **77**, 3661 (1996).

[40] P. S. Pershan, J. P. van der Ziel, and L. D. Malmstrom, Phys. Rev. B **143**, 574 (1965).

[41] L. Landau and E. Lifshitz, Phys. Z. Sowjetunion **8**, 153 (1935).

[42] C. A. Perroni and A. Liebsch, Phys. Rev. B **74**, 134430 (2006).

[43] S. R. Woodford, A. Bringer, and S. Blügel, J. Appl. Phys. **101**, 053912 (2007).

[44] L. P. Pitaevskii, Sov. Phys. - JETP **12**, 1008 (1961).

[45] J. P. van der Ziel, P. S. Pershan, and L. D. Malmstrom, Phys. Rev. Lett. **15**, 190 (1965).

[46] P. S. Pershan, Phys. Rev. **130**, 919 (1963).

CHAPTER 6

Impulsive excitation of coherent magnons in $FeBO_3$[1]

6.1 Introduction

The phenomenological theory of coherent magnon generation via ISRS, considered in the previous Chapter, predicts that the process has to occur for both linearly and circularly polarized pump pulses. However, the experimental data on coherent spin precession excitation by light [1, 2] reported so far, were obtained with circularly polarized pulses. The earlier reported excitation of coherent spin precession by linearly polarized light [2, 3] was related to photo-induced anisotropy, which is an indirect process that manifests itself differently than ISRS, as discussed in Chapter 5.3.5. Below we present results of a comprehensive experimental study of light-induced spin precession in the two sublattice ferromagnet $FeBO_3$, which specific magnetic and magneto-optical properties allowed us to reveal important features of the process.

6.2 Experimental

The optically excited spin precession in $FeBO_3$, was studied by means of a magneto-optical pump-probe technique, described in Chapter 2. The amplified laser pulses with a duration τ=150 fs, central photon energy E_0=1.54 eV, power P=800 μJ/pulse

[1] Based on: A. M. Kalashnikova, A. V. Kimel, R. V. Pisarev, V. N. Gridnev, A. Kirilyuk, and Th. Rasing, *Phys. Rev. Lett.* **99**, 167205 (2007) and A. M. Kalashnikova, A. V. Kimel, R. V. Pisarev, V. N. Gridnev, P. A. Usachev, A. Kirilyuk, and Th. Rasing, *Phys. Rev. B* **78**, 104301 (2008).

and a repetition frequency of γ=1 kHz from a Ti:sapphire laser, were split into a pump beam and a less intense probe beam. The probe pulses could be delayed with respect to the pump ones by a time delay Δt=0-3 ns. The polarization of the pump pulses was linear or circular, being controlled by half- and quarter-wave plates. The probe pulses were linearly polarized. The pump beam was focused onto a spot of about 100 μm in diameter on the sample. The probe beam was focused onto a somewhat smaller spot within the pump spot. The angle of incidence for the probe beam was 10^{o}, while the pump beam was at normal incidence. Two experimental geometries were used: the magnetic field was always applied along the x axis, while the pump pulses were propagating along either the z or the y axis (Fig. 5.4).

The spin precession induced by the pump pulses leads to a perturbation of the dielectric permittivity tensor (see Table 5.1) which, in turn, leads to a change in the polarization of the probe beam via the Faraday effect or magnetic linear birefringence. By measuring the rotation of the probe polarization as a function of the time delay between pump and probe pulses, we can monitor the pump-induced spin precession in the time domain. Note that in a typical optical pump-probe experiment in transmission, only spin-waves with very small wave-vectors $k < 10^{-2}\mathrm{cm}^{-1}$ are excited and detected, because the excitation spot is large. Therefore we consider only spin-waves with $k = 0$, i.e. homogeneous spin precession.

6.3 Detection of the light-induced FMR mode of spin precession

The rotation of the probe polarization as a function of time delay between pump (propagating along the z axis) and probe pulses is shown in Fig. 6.1(a) for different values of the applied magnetic field. Clear magnetic field-dependent oscillations are observed in these data. In Fig. 6.1(c) the dependence of the oscillation frequency on the magnetic field is plotted. This dependence is in good agreement with the behavior of the FMR mode (Fig. 3.2(b)), which is described by Eq. (3.3a). Similarly, the dependence of the frequency of the oscillations on temperature (Fig. 6.1(d)) is consistent with the temperature behavior that one would expect for the FMR mode [4, 5]. Our experimental data thus clearly show that the 150 fs laser pulses propagating along the z axis excite the FMR mode of coherent spin precession in $FeBO_3$.

The FMR mode supposes, as described in Section 3.1.3, oscillations of the l_x, m_y and m_z components of $\mathbf{l}(\mathrm{t})$ and $\mathbf{m}(\mathrm{t})$. There are various magneto-optical effects that can serve as a probe of such a precession. That is, in the experimental geometry shown in Fig. 6.1(b), the spin precession may lead to a transient rotation of the probe polarization via both the Faraday effect and the magnetic linear birefringence (MLB). For instance, $m_z(t)$ can be detected using the Faraday effect with the probe polarization rotation $\phi(t)$ equal to

$$\phi_F(t) = \omega_0 d \frac{\delta\varepsilon^a_{xy}(t)}{n} = \omega_0 d \frac{K m_z(t)}{n}, \tag{6.1}$$

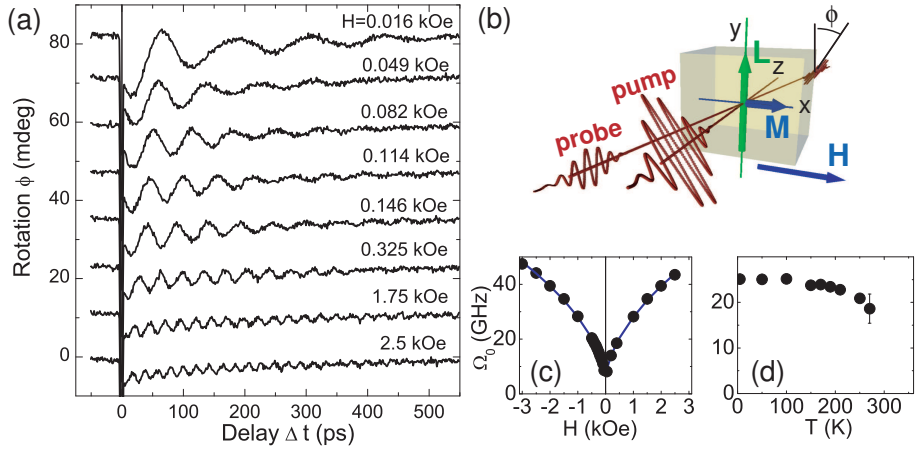

Figure 6.1: Excitation and detection of the ferromagnetic mode of spin precession by linearly polarized pump pulses measured in the experimental geometry shown in (b). (a) Pump-induced rotation of the probe polarization ϕ as a function of time delay between linearly polarized pump and probe pulses for different values of the applied magnetic field. (c) The frequency Ω_0 of the observed oscillations as a function of the applied field strength H (symbols) and its fit using Eq. (3.3a) (solid line). (d) The frequency Ω_0 of the oscillations as a function of temperature T. The results were obtained for a pump intensity of $10\,\mathrm{mJ/cm^2}$. Pump pulses were linearly polarized with azimuthal angle $\theta = 45^\mathrm{o}$. Results in (b,c) were obtained at a temperature T=10 K.

where ω_0 is the pulse central frequency, d is the sample thickness and n is the refractive index. In turn, $l_x(t)$ oscillations cause MLB, which also leads to a rotation of the probe polarization:

$$\phi_{MLB}(t) = \omega_0 d \frac{\delta\varepsilon^s_{xy}(t)}{n} \approx \omega_0 d \frac{G L_y^{(0)} l_x(t)\cos(2\xi)}{n}, \tag{6.2}$$

where $G = b_1 - b_2$ is the magneto-optical coefficient (See Table 5.1) and ξ is the incoming polarization of the probe pulse. A straightforward way to distinguish these two contributions to the rotation of the probe polarization is to study their dependence on ξ. In the case of the Faraday effect, the incoming polarization does not affect the measured signal $\phi(t)$. In contrast, in the case of MLB the signal should possess a dependence on ξ with a 180° period. In order to distinguish between the Faraday effect and MLB, we have performed measurements in the experimental geometry shown in Fig. 6.2(b). The probe beam was propagating along the z-axis and, thus, the effect of the crystallographic birefringence on the measured signal was minimized.

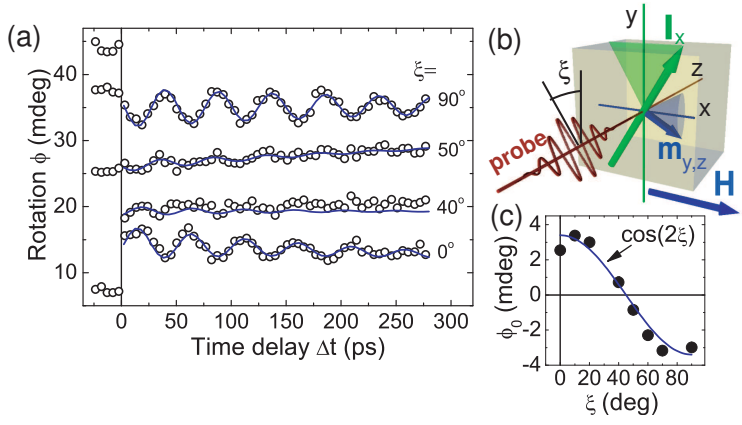

Figure 6.2: (a) The pump-induced probe polarization rotation $\phi(t)$ as a function of the time delay between pump and probe pulses measured for different initial probe polarization ξ for the experimental geometry shown in (b). Solid lines represent the fit using $\phi(\Delta t) = \phi_0 \sin(\Omega_0 \Delta t)$, $\Delta t > 0$. (c) Dependence of the amplitude of the oscillations ϕ_0 on the initial probe polarization ξ. The results were obtained for a temperature T=10 K, pump intensity of 10 mJ/cm^2 and applied magnetic field H=1.75 kOe. Pump pulses were linearly polarized with azimuthal angle $\theta = 45^\circ$ (pump pulse is not shown in (b) for the sake of simplicity).

In Fig. 6.2(a) the rotation of the probe polarization is shown as a function of the time delay between pump and probe pulses for various orientations of the incoming probe polarization ξ. A clear 180° dependence of the signal on ξ is observed (Fig. 6.2(a,c)). This indicates that the measured signal originates from the transient MLB (Eq. (6.2)) and reveals an in-plane motion of the antiferromagnetic vector $\mathbf{L}$. The fact that MLB dominates over the Faraday effect is caused by the strong ellipticity of the FMR mode of spin precession: since the magneto-optical constants K and G are comparable for the photon energy E=1.54 eV, the ratio between the transient Faraday effect and MLB is mainly defined by the ratio of the dynamic components of magnetic vectors m_z/l_x and is expected to be as small as 0.01 (See Eq. (3.5)).

6.4 Excitation of coherent magnons by polarized pump pulses

Fig.6.3(a) shows the spin precession excited by linearly polarized pump pulses incident along the z-axis for various azimuthal orientations of the pump polarization θ, as shown in Fig.6.3(b). The spin precession amplitude clearly depends on θ (Fig. 6.3(c)).

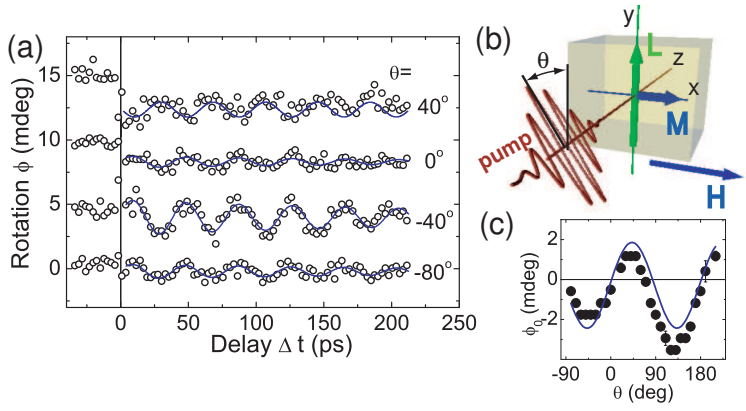

Figure 6.3: (a) The oscillations of the probe polarization as a function of the time delay between linearly polarized pump and probe pulses for different orientations of the pump polarization. The pump pulses propagate along the z axis shown in (b). The probe pulse is not shown in (b) for sake of simplicity. (c) The amplitude of the oscillations as a function of the pump polarization azimuthal angle (symbols) and its fit using Eq. (6.3) (line). The results were obtained at T=10 K, H=1.75 kOe and I=10 mJ/cm^2.

The effect of circularly polarized pulses appeared to be dependent on the mutual orientation of pump propagation direction and antiferromagnetic vector $L_y^{(0)}$. As can be seen from Fig. 6.4(a), circularly polarized pump pulses propagating along the z axis do excite spin precession, but changing their helicity affects neither amplitude nor the phase of the oscillations ($\phi^{\sigma^+} - \phi^{\sigma^-} = 0$). In contrast, the spin precession excited by circularly polarized pump pulses propagating along the y axis changes phase by 180° when the pump helicity of the light is reversed (Fig. 6.4(b)). Previously, the excitation of coherent spin precession by circularly polarized 100 fs pulses was demonstrated in [1, 2, 6] The circularly polarized pulses were shown to act on the spins as effective magnetic field pulses with a direction depending on the helicity. The phase of the excited precession, therefore, was controlled by the helicity of the pump pulses. The strength of this light-induced effective magnetic field was shown to be linearly dependent on the pump intensity, which was consistent with the proposed explanation in terms of the so-called ultrafast inverse Faraday effect (IFE). The IFE is determined by the same magneto-optical susceptibility that also accounts for the Faraday effect and is expected to be allowed in media of any symmetry. Therefore, the absence of this effect in the results shown in Fig. 6.4(a) is, at first glance, puzzling considering the fact that the Faraday effect in $FeBO_3$ is one of the strongest among

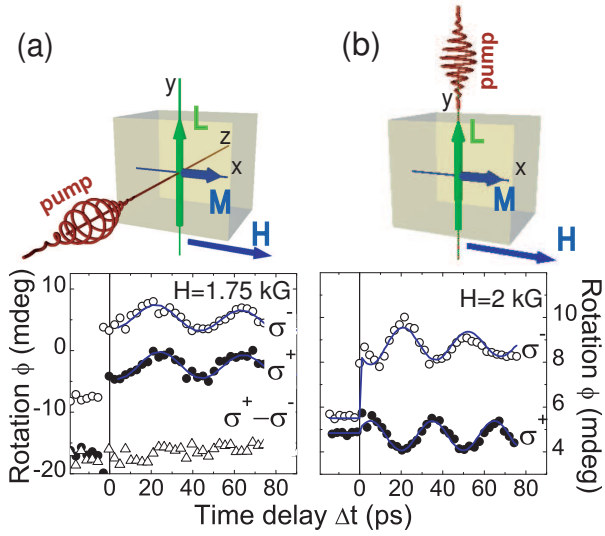

Figure 6.4: Spin precession excited by circularly polarized pump pulses propagating along (a) the z axis and along (b) the y axis. $\sigma^+ - \sigma^-$ is the difference between the spin precession amplitude excited by right- and left-handed circularly polarized pump pulses. In both cases the magnetic field is applied along the x axis and the probe is at 10^o from the pump propagation direction. The results are obtained at T=10 K and I=10 mJ/cm^2.

the iron oxides [7]. We note, that the incompleteness of such an interpretation was pointed out in [8].

Below we show that this observation, together with the observed polarization dependence of the excitation, can both be explained by taking into account the strongly elliptical character of the spin precession modes in $FeBO_3$. We note, that, as one can see in Figs. 6.1(b) and 6.3(a), there is an offset of the oscillations from the zero-line that decays on long time scales. This shift is of a non-magnetic origin because it does not depend on the applied magnetic field. From Figs. 6.1(b) and 6.3(a) one can see, moreover, that this shift is present even for polarizations of pump and probe beams that show no spin precession oscillations. We attribute this shift to optically-induced birefringence and, hence, omit it from the discussion of the experimental results.

Table 6.1: Phenomenological expressions for light-induced coherent spin precession in $FeBO_3$ obtained from the model of ISRS and light-induced effective fields.

Experimental geometry	ISRS	Opto-magnetism
$\mathbf{k}^{\text{pump}} \parallel z$ Linear polarization	$m_z(t) = -\frac{1}{4nc} \times \text{GL}^{(0)} b_z a_x I_0 \sin 2\theta \cos \Omega_0 t$ $l_x(t) = -\frac{1}{4nc} \times \text{GL}^{(0)} a_x^2 I_0 \sin 2\theta \sin \Omega_0 t$	$dm_z^0/dt =$ $\gamma \frac{I_0 \delta(t)}{8nc} G L_y^{(0)2} \sin 2\theta$
$\mathbf{k}^{\text{pump}} \parallel z$ Circular polarization	$m_z(t) = \pm\frac{1}{4nc} K b_z^2 I_0 \sin \Omega_0 t$ $l_x(t) = \pm\frac{1}{4nc} K a_x b_z I_0 \cos \Omega_0 t$	$dl_x^0/dt =$ $\pm\gamma \frac{I_0 \delta(t)}{8nc} K L_y^{(0)}$
$\mathbf{k}^{\text{pump}} \parallel y$ Circular polarization	$m_z(t) =$ $\pm\frac{1}{4nc}(K_1 b_y + K_2 a_x) b_z I_0 \cos \Omega_0 t$ $l_x(t) =$ $\pm\frac{1}{4nc}(K_1 b_y + K_2 a_x) a_x I_0 \sin \Omega_0 t$	$dm_z^0/dt =$ $\pm\frac{I_0 \delta(t)}{8nc} K_2 L_y^{(0)2}$

6.5 ISRS as the mechanism of coherent magnon excitation

The predictions of the phenomenological theory considered in the previous Chapter are summarized in Table 6.1 in order to make the following analysis of the experimental results more convenient.

To reveal the excitation mechanism of coherent magnons in $FeBO_3$ we consider first the excitation of spin precession by linearly polarized pump pulses propagating along the z axis (Fig. 6.1(b)). Combining Eq. (6.2) and Eq.(5.39c) (See also Table 6.1) for the transient rotation of the probe polarization caused by magnons excited via ISRS we obtain

$$\phi^{lin}(t) = A \frac{I_0}{4nc} G L_y^{(0)2} a_x^2 \sin 2\theta \sin \Omega_0 t, \tag{6.3}$$

where $A = \omega_0 d/n$, θ is the azimuthal angle of the pump polarization, Ω_0 is the FMR frequency, $G = b_1 - b_2$ is the magneto-optical coefficient (See Table 5.1), I_0 is the integrated pump pulse intensity, ω_0 is the pump pulse central frequency and n is the

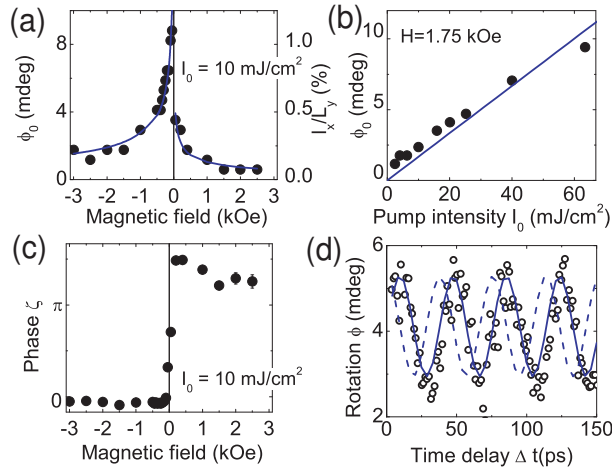

Figure 6.5: Experimental dependencies of the oscillations amplitude ϕ_0 (dots) on (a) the magnetic field H and (b) pump intensity I_0. Solid lines in (a,b) represent the dependencies described by Eq.(6.3). (c) Initial phase ζ of the pump-induced oscillations as a function of the magnetic field H when described by $\phi(\Delta t) = \phi_0 \sin(\Omega_0 \Delta t + \zeta)$. A typical experimental curve $\phi(\Delta t)$ is shown (dots) in (d). For reference, the curves $\phi(\Delta t) = \phi_0 \sin(\Omega_0 \Delta t + 0)$ (solid line) and $\phi(\Delta t) = \phi_0 \sin(\Omega_0 \Delta t + \pi/2)$ (dashed line) are shown. The experimental results shown in (a-d) are obtained for the pump polarization $\theta = 45°$ and temperature T=10 K.

refraction index at ω_0.

Comparison of Eq. (6.3) with the experimental results shows good agreement. In particular, the experimentally obtained dependence of the oscillation amplitude on the applied magnetic field H (Fig. 6.5(a)) is described by $\phi^{lin}(H) \sim a_x^2 \sim 1/\Omega_0 \sim 1/\sqrt{H}$, following Eq. (6.3). The pump-induced oscillations of the probe polarization should, according to Eq. (6.3), possess a *sine*-like behavior in the time domain, which is, indeed, observed in the experiment (Fig. 6.5(b,d)) for the magnetically saturated sample. The theoretically predicted dependence of the oscillation amplitude on the polarization of the pump pulses $\phi^{lin}(\theta) \sim \sin 2\theta$ shows good agreement with our experimental data (Fig. 6.3(c)).

In the case of circularly polarized pump pulses, the transient rotation of the probe polarization excited by pulses propagating along the z and the y axes, respectively, can be expressed as:

$$\phi^{\sigma^{\pm}\|z}(t) = \pm AGL_y^{(0)} a_x \left[\frac{I_0}{4nc} K b_z \cos \Omega_0 t \right] \sim b_z a_x \tag{6.4a}$$

$$\phi^{\sigma^{\pm}\|y}(t) = \pm AK_2 \left[\frac{I_0}{4nc}(K_1 b_y + K_2 a_x) a_x \sin \Omega_0 t \right] \sim a_x^2 \qquad (6.4b)$$

Now, keeping in mind that the FMR precession possesses strong ellipticity, i.e. $b_z << a_x$, we obtain that $\phi^{\sigma^{\pm}\|z} << \phi^{\sigma^{\pm}\|y} \simeq \phi^{lin\|z}$. Our experimental data (Fig. 6.4) show that, indeed, circularly polarized laser pulses effectively excite a helicity-dependent spin precession only when propagating along the y axis. It is worth to note that these results are in perfect agreement with the observation of spontaneous Raman scattering in $FeBO_3$ reported in [5]. There it was shown that, because of spin precession ellipticity, the scattering of light propagating along the z axis is defined mainly by the second-order magneto-optical constant (i.e. by G in Eg. (6.3)), while the scattering of light propagating along the y axis is defined by a first order magneto-optical constant (i.e. by K_1 and K_2 in Eg. (6.4b)). Similar effect of spin precession ellipticity on the Raman scattering intensity was reported in [9] for orthoferrites.

Here we would like to comment on the distinction between our results and those reported in [2, 3]. There the experimental observation of coherent spin precession excited by linearly polarized laser pulses in ferrimagnetic garnet films was reported. A quasi-stationary photo-induced change in magnetic anisotropy was proposed to be the mechanism of the excitation. Such a process can be qualified as a non-Raman process, as discussed in Section 5.3.5 (Eq. (5.44)). For the case of $FeBO_3$ the oscillations of $l_x(t)$ and, consequently, $\phi(t)$ excited via such a process should obey a (1-cos $\Omega_0 t$)-like dependence on the time delay between pump and probe pulses.[1] In our experiment $\phi(t) \sim l_x(t) \sim \sin \Omega_0 t$ (see Figs. 6.1(a),6.3(a) and 6.5(b)). Besides, the dependence of the amplitude of the excited precession on the pump pulse intensity (Fig. 6.5(d)) in our experiment is different from the one observed in [3]. The photo-induced change in magneto-crystalline anisotropy was suggested to be related to the absorption by impurity centers. As their concentration is limited, the dependence of the excited spin precession amplitude on the pump intensity indeed showed saturation. However, no saturation of the spin precession amplitude on the pump intensity was observed in our experiments within the experimentally studied range of 0-60 mJ/cm^2 (Fig. 6.5(c)).

Thus, the experimentally observed excitation of coherent magnons in $FeBO_3$ can be unambiguously described in terms of impulsive stimulated Raman scattering. The efficiency of the excitation by the pump pulses with certain polarization is defined by the ellipticity of the magnon mode. It is therefore interesting and important to demonstrate that the same results can be obtained using the light-induced effective fields obtained in Chapter 5. To this the following Section is devoted.

[1] Such a kind of dependence was indeed observed for the M_z component of the magnetization in the ferrimagnetic garnet film[2]

6.6 Light-induced effective fields and the role of the spin precession ellipticity

The expressions for the light-induced effective field and torques exerted by these fields were obtained in Chapter 5.4. As was discussed there, the considerations based on these light-induced fields and on the ISRS predict the same response of the spin system to the action of the laser pulses (See also Table 6.1).

Here we clarify the role of the spin precession ellipticity and show that the extended consideration of the light-induced fields allows to take into account these features of the process. In order to do so we present simulations of the interaction of the spin system with the pump pulses propagating along the z axis (Fig. 6.6), which is based on the light-induced effective fields obtained in Section 5.4.2. First, we consider the case of linearly polarized pump pulses. During the pulse the light-induced torque dm_z/dt (See Table 6.1) pushes the spins out of the xy plane (Fig. 6.6(a)). This results in a finite value of the dynamic component of the magnetization $m_z(\Delta t = 0)$ right after the pulse. The torque dm_z/dt and, consequently, $m_z(\Delta t = 0)$ are defined by the magneto-optical constant G, light intensity I_0 and polarization θ. When the light pulse is gone, the precessional motion of the spins towards their equilibrium position starts and after a quarter of the spin precession period the deviation of the spins is characterized by the value $l_x(\Delta t = \pi/2\Omega_0) = l_x^{\max}$ (Fig. 6.6(b)). This value defines the amplitude of the signal $\phi(t)$ measured in the experiment (See Eq. (6.2)). Because of the strong ellipticity of the spin precession (Eq. (3.5)) this deviation is two orders of magnitude larger than the initial one: $l_x^{\max} = (2\gamma H_E/\Omega_0)m_z(\Delta t = 0) = (2\gamma H_E/\Omega_0)GI_0L_y^2$.

For the circularly polarized pulses the situation is opposite. The torque dl_x/dt created by the pump pulse (Table 6.1) rotates the spins in the xy plane, leading to a finite value $l_x(\Delta t = 0) \sim KI_0L_y$ right after the pulse (Fig. 6.6(c)). However, this deviation is along the direction in which the elliptical spin precession possesses the maximal amplitude. Therefore, the amplitude of the measured signal is defined by $l_x^{\max} = l_x(\Delta t = 0)$ and is much weaker than the amplitude of the precession excited by the linearly polarized pump pulses: $l_x^{\sigma,\max}/l_x^{\mathrm{lin},\max} = (\Omega_0/2\gamma H_E)K/GL_y \sim 0.01$. This explains the fact that a helicity-dependent spin precession was not observed in the experiments with the pump pulses propagating along the z axis (Fig. 6.4(a)).

In contrast, circularly polarized pump pulses propagating along the y axis create a torque dm_z/dt (Table 6.1) and the situation resembles the one considered above for the linearly polarized pulses, propagating along the z axis (See Table 6.1). Therefore, the amplitude of the helicity-dependent spin precession excited by circularly polarized pump pulses propagating along the y axis (Fig. 6.4(b)) is comparable with the amplitude of the spin precession excited by the linearly polarized ones propagating along the z axis. Note, that this strong effect of the circularly polarized light originates from the effective field h_x^{eff}, directed perpendicular to the propagation direction of light, rather than from the field H_y^{eff} along the propagation direction. This is opposite to

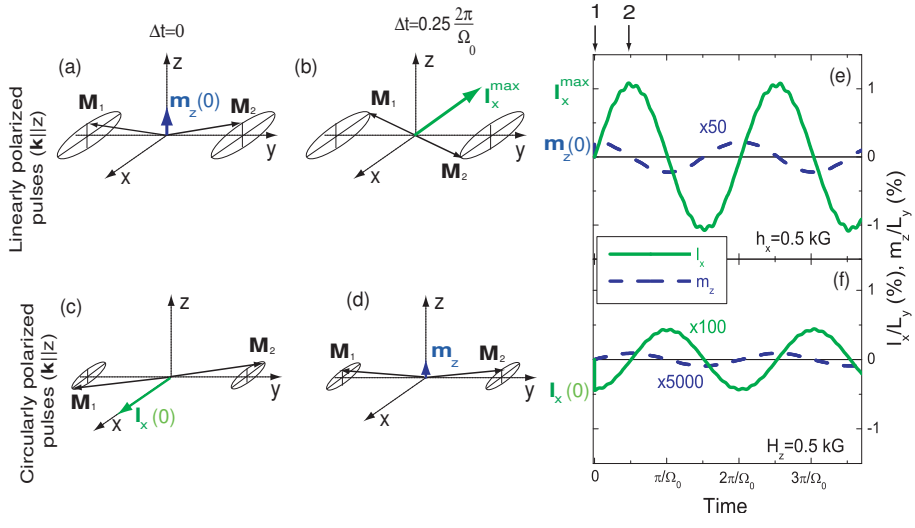

Figure 6.6: Schematic representation of the FMR precession excited by linearly (a,b) and circularly (c,d) polarized pulses propagating alone the z axis. m_z and l_x are dynamic components of the ferromagnetic and antiferromagnetic vectors. For the sake of simplicity, the ratio m_z/l_x is taken to be only 0.5, the weak ferromagnetism is neglected and the purely antiferromagnetic alignment is depicted. (e,f) Time dependence of l_x (gray solid lines) and m_z (black dashed lines) as obtained from the simulations. In simulations the 150 fs effective field pulse induced by linearly (h_x^{eff} (5.51b)) or circularly (H_z^{eff} (5.48a)) polarized light was inserted in the L-L equations (3.2). The light-induced effective field value was taken as 1 kG for both linearly and circularly polarized pulses, the applied magnetic field value was 1 kG, the exchange, Dzyaloshinsky and anisotropy fields values were taken from [10]. During the pulse ($\Delta t = 0$) the effective field induced by (a) linearly or (c) circularly polarized pulses creates the torque dm_z/dt (dl_x/dt) that pushes the spins out of (within) the xy plane. This corresponds to point 1 on the graphs (e,f). After the pump pulse $\mathbf{M}$ and $\mathbf{L}$ start to precess around their "old" equilibrium positions. Point 2 on the graphs (e,f) corresponds to the positions of these vectors after one quarter of the FMR period (b,d). The maximal deviation $l_x^{\max}$ of $\mathbf{L}$ defines the amplitude of the transient probe polarization measured in the experiments. The weak hight-frequency oscillations visible on graphs (e,f) originate from the AFMR mode.

what one would expect at first glance relying on the simplified model [1], applicable only for isotropic ferromagnetic materials. Therefore, our extended model, accounting for the two magnetic sublattices, fully addresses the comments in [8], where the simplified approach [1] was questioned.

Finally, we would like to note that the approaches based on the equation of motion for the magnon normal coordinates and on the L-L equations are equivalent for the treatment of the experimental results presented in this Chapter. However, the latter approach will be more convenient for the description of large deviations or even switching [11] of spins caused by strong laser pulses, when the equation of motion [Eq. (5.29)] becomes highly nonlinear.

References

[1] A. V. Kimel, A. Kirilyuk, P. A. Usachev, R. V. Pisarev, A. M. Balbashov, and T. Rasing, Nature (London) **435**, 655 (2005).

[2] F. Hansteen, A. Kimel, A. Kirilyuk, and T. Rasing, Phys. Rev. B **73**, 014421 (2006).

[3] A. K. F. Hansteen, A. V. Kimel and T. Rasing, Phys. Rev. Lett. **95**, 047402 (2005).

[4] *Landoldt-Börnstein, Group III Condensed Matter*, vol. 27H (Springer-Verlag GmbH, Berlin, 1993).

[5] W. Jantz, J. R. Sandercock, and W. Wettling, J. Phys. C **9**, 2229 (1976).

[6] C. D. Stanciu, F. Hansteen, A. V. Kimel, A. Tsukamoto, A. Itoh, A. Kirilyuk, and T. Rasing, Phys. Rev. Lett. **98**, 207401 (2007).

[7] A. J. Kurtzig, R. Wolfe, R. C. LeCraw, and J. W. Nielsen, Appl. Phys. Lett. **14**, 350 (1969).

[8] S. R. Woodford, A. Bringer, and S. Blügel, J. Appl. Phys. **101**, 053912 (2007).

[9] R. M. White, R. J. Nemanich, and C. Herring, Phys. Rev. B **25**, 1822 (1982).

[10] J. Schober, IEEE Trans. Mag. **12**, 401 (1976).

[11] C. D. Stanciu, F. Hansteen, A. Kimel, A. Tsukamoto, A. Itoh, A. Kirilyuk, , and T. Rasing, Phys. Rev. Lett. **99**, 047601 (2007).

CHAPTER 7

Impulsive excitation of coherent phonons in $FeBO_3$[1]

7.1 Introduction

The spectrum of various magnetic and non-magnetic coherent excitations in iron borate is broad. For instance, $FeBO_3$ possesses two modes of spin precession. One of them, having a lower frequency, was successfully observed in our experiments, as discussed in the previous Chapter. From the nature of the impulsive stimulated Raman scattering, which was shown to lead to the generation of coherent magnons, it follows that the highest frequency of coherent excitation that can be generated by laser pulses is limited by the pulse duration. To study excitations in a broader spectral range, shorter laser pulses should be used. Therefore, we performed pump-probe experiments using light pulses with a duration of 40 fs instead of 150 fs. In the case of Fourier-transform limited pulses, this change of pulse duration directly converts into an increased band width and, consequently, provides access to higher frequency excitations.

7.2 Light-induced generation of coherent phonons in $FeBO_3$

In Fig. 7.1(a) the transient rotation of the probe polarization, as induced by 40 fs linearly polarized laser pulses, is shown on both long (up to 15 ps) and short (up

[1]Based on: A. M. Kalashnikova, A. V. Kimel, R. V. Pisarev, V. N. Gridnev, P. A. Usachev, A. Kirilyuk, and Th. Rasing, *Phys. Rev. B* **78**, 104301 (2008).

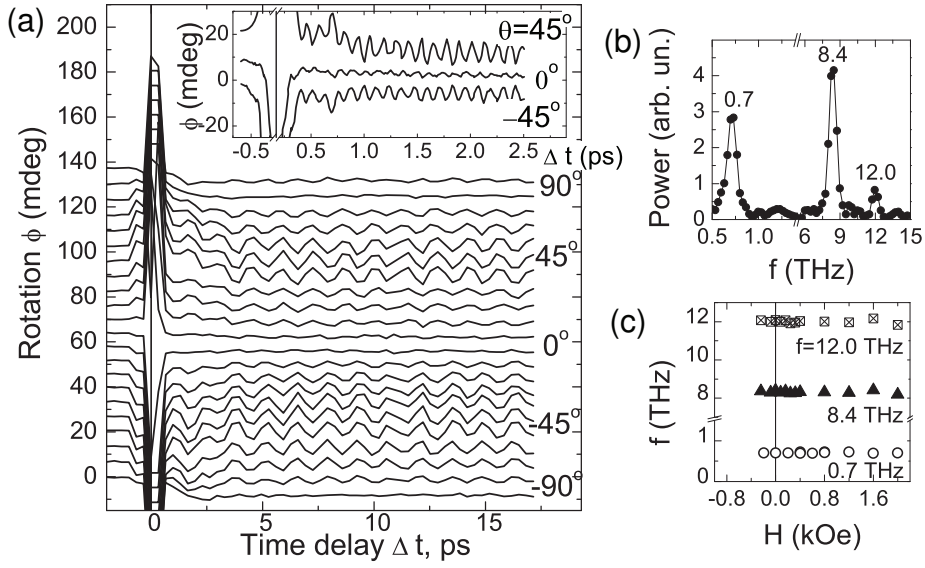

Figure 7.1: (a) Transient rotation of the probe polarization as a function of the time delay between pump and probe pulses for different linear polarizations θ of the pump pulse. Inset: the signal on a shorter time scale 0-2.5 ps. (b) Fourier spectrum of the signal measured at pump polarization $\theta = 45^o$. (c) Dependence of the oscillation frequency on the applied magnetic field (symbols). The results are obtained at T=10 K and I=10 mJ/cm^2.

to 2.5 ps) time scales. Three modes with frequencies f =0.7, 8.4 and 12.0 THz are observed (Fig. 7.1(b)). These frequencies are independent of the applied magnetic field (Fig. 7.1(c)).

The 0.7 THz frequency is approximately twice that of the antiferromagnetic resonance at room temperature [1]. However, in contrast to the behavior of the AFMR mode in $FeBO_3$ [1], this frequency does not show any noticeable dependence on temperature (Fig. 7.3(c)). Therefore, we can conclude that the experimentally observed oscillations are not related to the antiferromagnetic mode of spin precession. This also follows from the conclusions of Section 6.6 that it is the ellipticity of the FMR mode which allows us to observe its excitation. The AFMR mode is characterized by an ellipticity (Eq. (3.6)) that is one order of magnitude smaller than the one of the FMR mode [1, 2]. We note, that in spontaneous Brillouin scattering experiments [3] the intensity of the Stokes lines related to the AFMR was two orders of magnitude lower that those of the FMR.

The frequency of 0.7 THz does not coincide with any of the earlier observed five Raman-active phonon modes (A_{1g} and $4E_g$) [4, 5, 6, 7] nor with the eight infrared-active modes [4, 8]. The *ab initio* calculated spectrum of all possible phonon modes in $FeBO_3$ [9] does not contain any mode close to 0.7 THz. We note that the amplitude of the observed 0.7 THz oscillation shows the strong temperature dependence, which is discussed below.

The 8.4 and 12.0 THz excitations can be attributed to the doubly degenerated Raman-active E_g optical phonon modes with frequencies 8.37 and 12.03 THz [5, 6, 7], respectively (Fig. 7.2). Two infrared-active E_u modes [4, 8] are close in frequency (8.03 and 12.1 THz) as well. However, in our experiments we measure a signal proportional to the finite modulation of the dielectric permittivity by phonons. The latter defines the Raman tensor and, therefore, only Raman-active modes can be detected.

7.3 Generation of the coherent optical phonons in $FeBO_3$ via ISRS

First, we discuss the excitation of the two coherent phonon modes with frequencies 8.4 and 12.0 THz. Several mechanisms of coherent phonon generation by subpicosecond laser pulses were studied experimentally and theoretically, such as ISRS, resonant stimulated Raman scattering and displacive excitation of coherent phonons [12, 13, 14]. The two latter mechanisms rely on real optical transitions [15, 16], and, therefore, are believed not to be effective in our experiment, where the central photon energy of the laser pulse E_0=1.54 eV is almost twice as low as the fundamental absorption edge. The absorption coefficient for E=1.54 eV is 80 cm^{-1}. For the case of ISRS, the excitation of coherent phonons by laser pulses can be described in terms of the equation of motion for the normal coordinate Q of the corresponding phonon mode

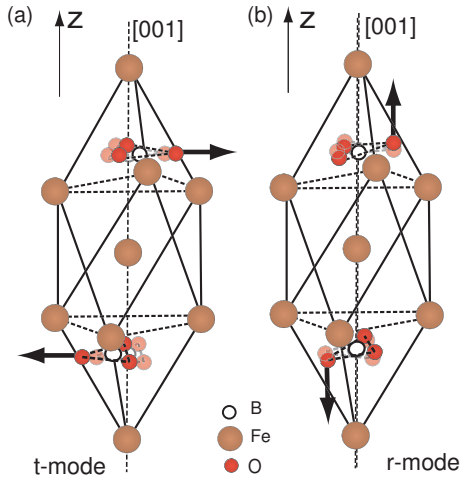

Figure 7.2: Schematic representations of the two doubly degenerate optical phonon modes E_g [4, 10, 11]. Abbreviations t and r stand for translational and rotational modes, respectively.

Table 7.1: Raman and dielectric permittivity tensor components and normal coordinates for two external doubly degenerate modes E_g. $x(y)_i$ and denotes the shift of the i-th ion complex along the $x(y)$ axis (Fig. 7.2). $l_{x(y)i}$ denotes the rotation of this complex with the angular momentum l along the $x(y)$ axis [10].

Ω_k	Type	Normal coordinate Q_k	$\mathcal{R}_{ij}$	$\delta\varepsilon_{ij}$
8.4 THz	trans.	$Q^{t(x)} = x_1 - x_2$ $Q^{t(y)} = y_1 - y_2$	$xx = -yy =$ r_1 $xy = yx =$ r_2	$xx = -yy =$ $\mathrm{r}_1 Q^{t(x)}$ $xy = yx =$ $\mathrm{r}_2 Q^{t(y)}$
12.0 THz	rot.	$Q^{r(x)} = l_{x1} + l_{x2}$ $Q^{r(y)} = l_{y1} + l_{y2}$	$xx = -yy =$ r_3 $xy = yx =$ r_4	$xx = -yy =$ $\mathrm{r}_3 Q^{r(x)}$ $xy = yx =$ $\mathrm{r}_4 Q^{r(y)}$

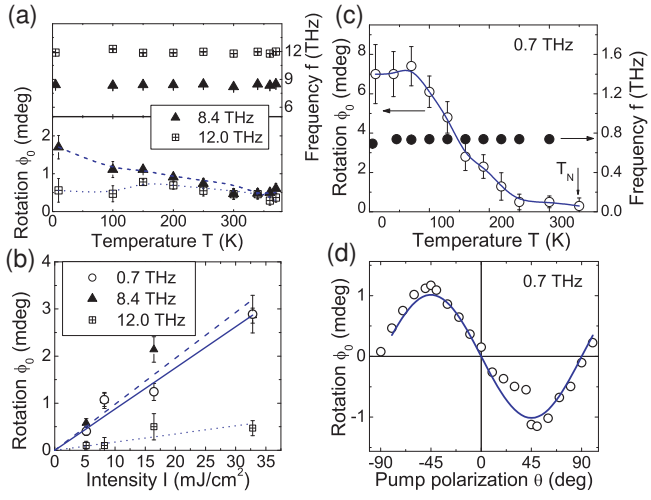

Figure 7.3: (a) Temperature dependence of the frequency f and amplitude ϕ_0 of the excited coherent phonon modes 8.4 and 12.0 THz. (b) Dependence of the amplitude of the observed phonon modes and the 0.7 THz oscillations on the pump intensity I. (c) Temperature dependence of the frequency f and amplitude ϕ_0 of the 0.7 THz oscillations (d) Dependence of the amplitude ϕ_0 of the 0.7 THz oscillations on pump polarization θ.

with an impulsive driving force [17]. This approach allows one to write the equation of motion for each mode separately [4, 18]. Different from the magnon case considered above, for the phonons the normal coordinates Q represent ion displacements and, hence, obey the harmonic-oscillator equation [13]

$$\frac{d^2Q}{dt^2} + \Omega^2 Q = F(t) = \frac{1}{2}\mathcal{R}_{ij}\mathcal{E}_i(t)\mathcal{E}_j^*(t), \tag{7.1}$$

where $\mathcal{R}_{ij} = \partial\varepsilon_{ij}/\partial Q$ is the Raman tensor for crystals of symmetry $R\bar{3}c$ [4] (See Table 7.1). Ω is the frequency of the corresponding phonon mode. The normal coordinates Q for each mode observed in the experiment are listed in Table 7.1. Note, that, in contrast to the case of magnons, the normal coordinates of coherent phonons are real.

In our experiment the pump induced rotation of the probe polarization was measured. From the symmetry properties of the dielectric permittivity tensor (Table 7.1) it follows that only modes described by the normal coordinates $Q^{t(y)}$ and $Q^{r(y)}$ (shown in Fig. 7.2) can contribute to the rotation of the probe polarization (defined by off-diagonal components $\delta\varepsilon_{xy} = \delta\varepsilon_{yx}$) of the dielectric permittivity tensor.

The general solution of Eq. (7.1) and its main properties were extensively discussed in literature (for reviews see [12, 13]). The solution for the case of a linearly polarized pump pulse has the form

$$Q(t) \sim \mathcal{R}_{xy} I_0 \sin(2\theta) \sin \Omega t, \tag{7.2}$$

where I_0 is the integrated intensity of the pump pulse and θ is the azimuthal angle of the pump polarization. The transient rotation of the probe polarization is

$$\phi(t) \sim \mathcal{R}_{xy}^2 I_0 \sin(2\theta) \sin \Omega t, \tag{7.3}$$

where $\mathcal{R}_{xy} = r_2$ (for the t-mode $\Omega = 8.4\,\mathrm{THz}$) and $\mathcal{R}_{xy} = r_4$ (for the r-mode $\Omega = 12.0\,\mathrm{THz}$) are the components of the Raman tensor (Table 7.1). This theoretical dependence of the transient probe polarization rotation on the pump polarization azimuthal angle θ (Inset Fig.7.1(a)) is in good agreement with our experimental data. The amplitude of the rotation ϕ_0 (Fig. 7.3(b)) follows a linear intensity dependence according to Eq.(7.3).

The temperature dependence of the frequency and, particularly, amplitude of the excited coherent phonons (Fig. 7.3(a)) has to be discussed in more detail. Raman scattering from phonons in $FeBO_3$ was reported by several groups [5, 6, 7, 19]. In our experiment the frequency of both observed phonon modes are independent of temperature within the whole studied temperature range of 10-370 K. This is in good agreement with the results of previous works where no [5, 6, 7] or very weak ($\leq$1%) [19] shifts of the frequency with temperature were observed in the range of 10-400 K.

The change of the intensity of the Raman scattering as a function of temperature appeared to be a more intricate issue. In [5, 6] a significant drop (by approximately a factor of 2) of the intensity of the Stokes line of the 12.0 THz phonon in $FeBO_3$ was reported. A similar, but somewhat weaker, temperature dependence was also observed for the 8.4 THz mode. This observation was considered as an indication of the influence of magnetic ordering on the phonon Raman scattering. Results published later [7] reproduced the experimental observation of [5], but the influence of magnetic order on the phonon spectra was disproved. On the other hand, in several other materials, predominantly semiconducting spinels, a magnetic-order dependent Raman scattering from phonons was observed [20]. Several mechanisms responsible for this effect were proposed [7, 21, 22]. In our experiment we did observe a change of the amplitude ϕ_0 of the 8.4 THz mode with temperature, while the amplitude of the 12.0 THz mode is temperature-independent within the fitting error (Fig. 7.3(a)). However, no peculiarities in the temperature dependencies of both modes was observed in the vicinity of the Neel temperature, where the magnetic order experiences drastic changes. Therefore, we conclude that the variations of ϕ_0 with temperature are not related to changes in magnetic ordering.

7.4 Magnetic-order-assisted impulsive generation of the nonmagnetic coherent excitations in $FeBO_3$

The origin of the 0.7 THz oscillations ought to be discussed separately. Neither Brillouin nor Raman scattering spectra [3, 6, 7, 19] nor infra-red absorption spectra [8] have shown any mode with this frequency. We note that there are 27 possible optical phonon modes in $FeBO_3$, nearly half of which have been observed experimentally. Therefore, the pump-probe method used here might reveal additional features in the energy spectrum of $FeBO_3$ which were not accessible via conventional optical studies.

As can be seen from Fig. 7.3(c), the frequency of the 0.7 THz mode does not change in the whole range of temperatures from 10 K up to 300 K where this mode is detected, following the behavior of the coherent phonon modes at 8.4 and 12.0 THz (Fig. 7.3). This suggests that this mode is not an excitation of the spin system.

The amplitude of the 0.7 THz mode, in contrast to its frequency and in contrast to the amplitude of the two observed phonon modes, decreases by an order of magnitude in the temperature range of 10-300 K. Above 300 K the fitting error $\Delta\phi_0$ becomes larger than the signal amplitude ϕ_0 itself. Therefore, a confident determination of the frequency above 300 K was not possible. Such a strong dependence of the amplitude on temperature and its vanishing in the vicinity of the Néel temperature $T_N = 348\,\mathrm{K}$ indicates a possible relation between the observed excitation and the magnetic order.

If the observed mode itself is of non-magnetic origin (as was concluded above), its coupling with the magnetic order in an optical pump-probe experiment can be described by introducing the dielectric tensor components $\delta\varepsilon_{ij}(Q)$, which are functions of both the magnetic order parameter $\mathbf{L}$ and the parameter Q, describing the medium excitation

$$\begin{aligned}\delta\varepsilon_{ij}(Q) = \delta\varepsilon_{ij}^{(0)}(Q) + \\ \delta K1_{ijk}(Q)M_k + \delta K2_{ijk}(Q)L_k + \\ \delta b_{ijkl}(Q)L_kL_l + \delta c_{ijkl}(Q)M_kL_l...,\end{aligned} \tag{7.4}$$

where $\delta\varepsilon_{ij}^{(0)}(Q)$ is defined for the paramagnetic point group $\bar{3}m$ and describes the magnetic-order independent modulations of the dielectric tensor by the excitation Q. If $\delta\varepsilon_{ij}^{(0)}(Q)$=0, this excitation cannot be detected in the paramagnetic phase by means of an optical measurement. $\delta K1_{ijk}(Q)$, $\delta K2_{ijk}(Q)$, $\delta b_{ijkl}(Q)$ and $\delta c_{ijkl}(Q)$ are modulations of the magneto-optical susceptibilities of different order due to the coherent phonons or some other non-magnetic coherent medium excitation. Therefore, the latter terms in Eq.(7.4) describe the contributions to the modulations of the dielectric permittivity, which depend on the magnetic ordering ($\mathbf{M}$ and $\mathbf{L}$) that can thus be detected in the magnetically-ordered phase only. This can explain the decrease of the signal when the temperature is approaching the Neel temperature. On the other

hand, the Raman tensor, describing light scattering from the coherent excitation Q is

$$\mathcal{R}_{ij} = \frac{\delta\varepsilon_{ij}}{\partial Q} = \mathcal{R}_{ij}^{(0)} + \frac{\delta K1_{ijk}}{\partial Q} M_k + \frac{K2_{ijk}}{\partial Q} L_k + \frac{\delta b_{ijkl}}{\partial Q} L_k L_l + \frac{\delta c_{ijkl}}{\partial Q} M_k L_l + ..., \tag{7.5}$$

If $\mathcal{R}_{ij}^{(0)} = 0$, this coherent excitation is Raman-inactive and, thus, its generation via ISRS cannot occur. However, if at least one of the coefficients $\delta K1_{ijk}(Q)$, $\delta K2_{ijk}(Q)$, $\delta b_{ijkl}(Q)$ or $\delta c_{ijkl}(Q)$ is nonzero, this excitation can become Raman-active in the magnetically-ordered phase. Note, that the amplitude of the signal drops with temperature much faster that the magnetization (Fig. 7.3(c)). This might indicate that both excitation and detection of the 0.7 THz mode depend on the presence of the magnetic order. For a more detailed explanation of this excitation further thorough studies are required. We note, that the excitation of this mode is sensitive not only to the presence of magnetic ordering, but also to the polarization of the pump (Fig. 7.3(d)). Therefore, its observation in the experiments on the spontaneous Raman scattering requires both magnetic ordering and a proper choice of the incoming and scattered beam polarizations. This might explain why the mode with such a frequency was not, to the best of our knowledge, detected in the reported experiments on the spontaneous Raman scattering.

References

[1] *Landoldt-Börnstein, Group III Condensed Matter*, vol. 27H (Springer-Verlag GmbH, Berlin, 1993).

[2] J. Schober, IEEE Trans. Mag. **12**, 401 (1976).

[3] W. D. W. W. Wettling and C. E. Patton, J. Appl. Phys. **53**, 8163 (1971).

[4] K. Nakamoto, *Infrared and Raman Spectra of Inorganic and Coordination Compounds* (J. Wiley & Sons, New York, 1986).

[5] I. W. Shepherd, J. Appl. Phys. **42**, 1482 (1971).

[6] I. W. Shepherd, Phys. Rev. B **5**, 4524 (1972).

[7] A. E. Meixner, R. E. Dietz, and D. L. Rousseau, Phys. Rev. B **7**, 3134 (1973).

[8] K. Wakamura, T. Okuda, and T. Tsushima, Opt. Comm. **23**, 249 (1977).

[9] K. Parlinski, J. Łaźewski, P. T. Jochym, A. Chumakov, R. Rüffer, and G. Kresse, Europhys. Lett. **56**, 275 (2001).

[10] S. Bhagavantam and T. Venkatarayudu, *Theory of Groups and its Applications to Physical Properties* (Academic Press, New York, 1969).

[11] I. Nakagawa and J. L. Walter, J. Chem. Phys. **51**, 1389 (1969).

[12] T. Dekorsy, G. C. Cho, and H. Kurz, *Light scattering in solids* (Springer, Berlin, 2006), vol. 8.

[13] R. Merlin, Solid State Comm. **102**, 207 (1997).

[14] L. Dhar, J. A. Rogers, and K. A. Nelson, Chem. Rev. **94**, 157 (1994).

[15] J. F. W. G. A. Garrett, T. F. Albrecht and R. Merlin, Phys. Rev. Lett. **77**, 3661 (1996).

[16] H. J. Zeiger, J. Vidal, T. K. Cheng, E. P. Ippen, G. Dresselhaus, and M. S. Dresselhaus, Phys. Rev. B **45**, 786 (1992).

[17] Y.-X. Yan, E. B. Gamble, Jr., and K. A. Nelson, J. Chem. Phys. **83**, 5391 (1985).

[18] W. Hayes and R. Loudon, *Scattering of Light by Crystals* (John Wiley & Sons, New York, 1978).

[19] N. Koshizuka, T. Ocuda, and U. Udagawa, J. Phys. Soc. Japan **37**, 354 (1974).

[20] E. F. Steigmeier and G. Harbeke, Phys. Kondens. Mater. **12**, 1 (1970).

[21] N. Suzuki and H. Kamimura, Solid State Comm. **11**, 1603 (1972).

[22] N. Suzuki and H. Kamimura, J. Phys. Soc. Japan **35**, 985 (1973).

CHAPTER 8

Dynamics of the photo-induced birefringence in $GaFeO_3$

8.1 Introduction

One of the main requirements for the high efficiency of a *direct* excitation mechanism of light-induced spin precession is a high magneto-optical susceptibility of the medium. Otherwise, the coupling of the electric field of light to the magnons is weak and the mechanism described in the previous Chapters is inefficient. Therefore, in media with a weak linear magneto-optical susceptibility other, *indirect* mechanisms to couple the electric field of light to magnetic excitations of the medium are required. In view of this, so-called magneto-electrics [1, 2, 3] might be interesting candidates. These materials are a particular and most popular case of the whole class of so-called multiferroic materials [4], as discussed in Chapter 1. Manifestations of magneto-electric properties in the optical response of condensed matter have been reported by several groups [5, 6, 7, 8].

The pyroelectric ferrimagnetic gallium ferrite $GaFeO_3$ traditionally has attracted a lot of interest of researchers working with multiferroic materials. Historically, it was the first material with a bulk magnetic moment in which the linear magnetoelectric effect was observed [9]. Moreover, the nature of the magnetoelectric effect in $GaFeO_3$ is of interest itself. In [10] the toroidal moment, the fourth form of the ferroic ordering [4], has been proposed as a cause of a nonsymmetric magnetoelectric effect in $GaFeO_3$. The optical magnetoelectric effect in a single crystal [5] and its enhancement in a patterned structure [11] of $GaFeO_3$ have been reported recently.

In this Chapter the results of pump-probe experiments performed with $GaFeO_3$

are presented. Our main goal was an observation of light-induced spin dynamics and revealing the possible role of the magneto-electric interactions in the process of excitation of the spin system by light. We used two different techniques for measuring the light-induced changes. In both cases optical pump pulses were used to create the excitation in the medium. In order to monitor the dynamics of the light-induced changes the rotation of the probe polarization, i.e. a linear optical response, and the nonlinear optical effect of second harmonic generation (SHG) have been studied as a function of the time delay between pump and probe pulses. SHG is known as a powerful alternative to linear optics, when the latter is not capable to reveal the magnetic properties of a medium. Light-induced dynamics experiments in which the SHG signal was used as a probe tool have been reported in [12, 13, 14, 15, 16, 17, 18]. In $GaFeO_3$ linear magneto-optical susceptibility is rather weak, as discussed in Chapter 4, and, therefore, the use of SHG as a probe could provide a possibility to monitor the spin dynamics excited by light.

8.2 Experimental results

Experimental results discussed in this Section were obtained for a sample, which was a plane-parallel plate cut from the $GaFeO_3$ single crystal. The normal was along the crystallographic y axis, the thickness was $62\,\mu m$. Such a choice of sample orientation is based mostly on the properties of the SHG in $GaFeO_3$, discussed in Section 4. Namely, such an orientation allows to separate experimentally crystallographic and magnetic contributions to the SHG signal.

8.2.1 Dynamics of linear birefringence

The experimental geometry used in these experiments is shown in Fig. 8.1. The probe beam was at normal incidence (parallel to the crystallographic y axis), while the angle of incidence for the pump beam was $\sim 10^{o}$. In this geometry no static Faraday rotation for the probe beam is observed because there is no projection of $\mathbf{k}^{\mathrm{probe}}$ on the magnetization, which is along the z-axis (See the discussion of the linear magneto-optical properties of $GaFeO_3$ in Chapter 4). The pump-induced changes in the rotation of the probe polarization were measured and can reflect the light-induced material excitations of both magnetic and non-magnetic origin. A complex analysis of the dependence of the observed signal on the applied magnetic field, polarization of the pump pulses, temperature etc. is required in order to reveal the origin of the observed effects.

In Fig. 8.2(a) the rotation of the probe polarization as a function of the delay time between pump and probe pulses is shown for different orientations θ of the linear polarization of the pump beam. Clearly, the pump-induced changes of the probe polarization rotation are sensitive to the azimuthal angle of the pump pulse

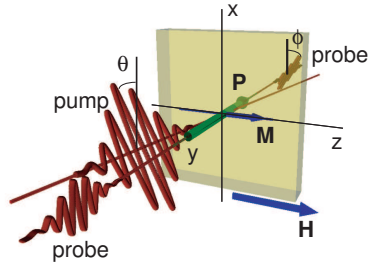

Figure 8.1: The mutual orientation of the crystallographic axes x, y and z and the wavevectors for pump and probe beams for the linear optical pump-probe experiment. ϕ is the measured angle of rotation of the probe polarization. The pump pulses were polarized either linearly with the azimuthal angle θ (as shown) or circularly ($\sigma^{\pm}$). Probe pulses were propagating along the y axis of the crystal. Angle of incidence of the pump beam was 10°. The magnetic field **H** was applied along the z axis of the crystal.

polarization. Moreover, one can distinguish two exponentially decaying processes

$$\phi(\Delta t) = a_1 + A_1 e^{-\Delta t/t_1} + A_2 e^{-\Delta t/t_2}, \tag{8.1}$$

as shown in Fig. 8.3(a,b). One process can be referred to as a "*fast*" and is described by the dependence $A_1 e^{-\Delta t/t_1}$, where $t_1 = 125 \pm 16$ ps. The second - "*slow*" - contribution $A_2 e^{-\Delta t/t_2}$ decays with the characteristic time $t_2 = 2350 \pm 800$ ps. The dependencies of these two contributions on the pump polarization are different, as shown in Fig. 8.3(c). The amplitude A_1 of the "fast" contribution possesses maxima of opposite sign at the polarization $\theta = \pm 45°$ and is zero when the pump is polarized along the x or z axis. The dependence is, therefore, described by the function

$$A_1(\theta) = A_1^0 \sin 2\theta, \tag{8.2}$$

as shown in Fig. 8.3(c). The amplitude A_2 of the "slow" component is insensitive to the pump polarization within the experimental and fit errors.

The changes of the probe polarization induced by the circularly polarized pump pulses are shown in Fig. 8.2(b). Again, two contributions - polarization-dependent

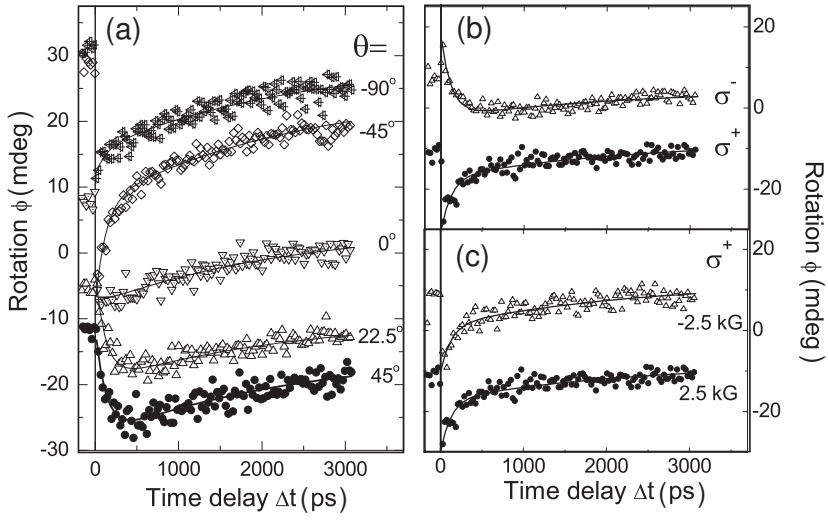

Figure 8.2: Transient probe polarization rotation ϕ as a function of the time delay Δt measured at $T = 10\,\mathrm{K}$ induced (a) the linearly polarized pump pulses with various azimuthal angles θ, (b) by circularly polarized pump pulses with opposite helicities and (c) by circularly polarized pump pulses σ^+ with a magnetic field $\pm 2.5\,\mathrm{kG}$ applied along the z axis, as shown in fig. 8.1(a). Solid lines represent fits using Eq. (8.1)

"fast" and polarization-independent "slow" can be distinguished, with characteristic times corresponding to those for the signal induced by the linearly polarized pulses.

The amplitudes and the decay times of the transient probe polarization rotation ϕ induced by both linearly and circularly polarized pulses, are independent on the external magnetic field applied along the z axis, as shown in Fig. 8.1(a). As an example, the probe polarization rotation ϕ induced by the circularly polarized pulses as a function of the time delay Δt is shown in Fig. 8.2(c) for the applied magnetic field H=+2.5 and -2.5 kG.

The increase of temperature leads to drastic changes in the observed signal. The rotation of the probe polarization as a function of the time delay measured at T=292 K is shown in Fig. 8.4, for several azimuthal angles θ of the linear pump polarization. In contrast to the signal at T=10 K, the dependence $\phi(\Delta t)$ at room temperature can be described by one exponential function $A_2 e^{-\Delta t/t_2}$, with a decay time $t_2 = 550 \pm 15\,\mathrm{ps}$, which is significantly lower than the one at low temperature (see Fig. 8.3(d)). The amplitude A_2 is again independent of the pump polarization. At intermediate temperatures ($T = 200\,\mathrm{K}$) both "fast" polarization-dependent and "slow" polarization-independent components are observed, with decay times reduced with respect to the

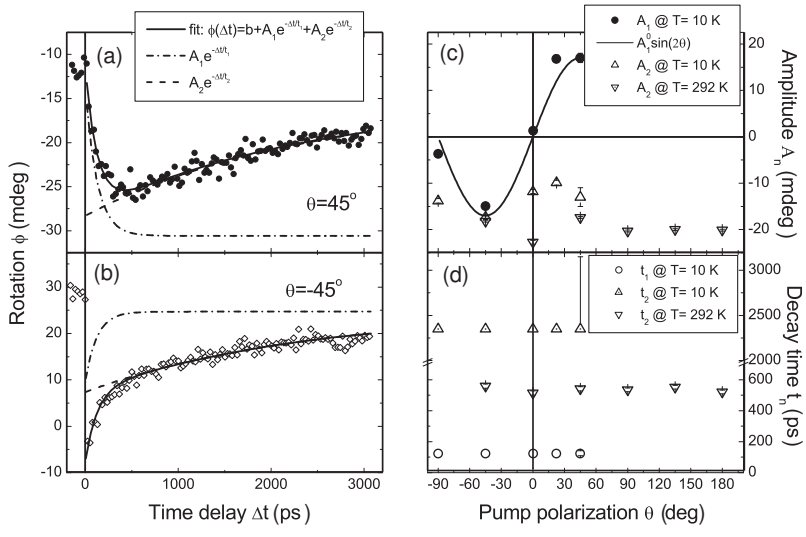

Figure 8.3: Light-induced changes of the probe polarization rotation ϕ measured at $T = 10\,\mathrm{K}$ for the pump polarization (a) $\theta = 45^{\mathrm{o}}$ and (b) $\theta = -45^{\mathrm{o}}$ and its fit using Eq. (8.1). The characteristics of the dynamics of the optical birefringence signal obtained form the fit as a function of pump polarization θ for the temperatures T=10 and 292 K: (c) Amplitudes of the exponential decay A_1 and A_2. Solid line represents the fit of the dependence $A_1(\theta)$ using Eq. (8.2). (d) Decay times t_1 and t_2.

ones at the low temperature: $t_1 = 80 \pm 8\,\mathrm{ps}$ and $t_2 = 1800 \pm 800\,\mathrm{ps}$. We note that the considerable fitting error for the decay time t_2 originates from the fact that this time is comparable with the complete time delay range available in our experiment (0-3960 ps)

8.2.2 Dynamics of the second harmonic generation

The non-linear polarization $\mathbf{P}^{2\omega}$ induced in a SHG process is described by

$$P_i^{2\omega} = (\chi_{ijk}^{(i)} + \chi_{ijk}^{(c)}) E_j E_k^*, \tag{8.3}$$

where $\mathbf{E}$ in the electric field at the fundamental frequency (the electric field of the probe pulses in our experiments). $\hat{\chi}^{(i)}$ is a polar i-tensor, which describes the crystallographic contribution to the SHG signal and $\hat{\chi}^{(c)}$ is a polar c-tensor, describing the

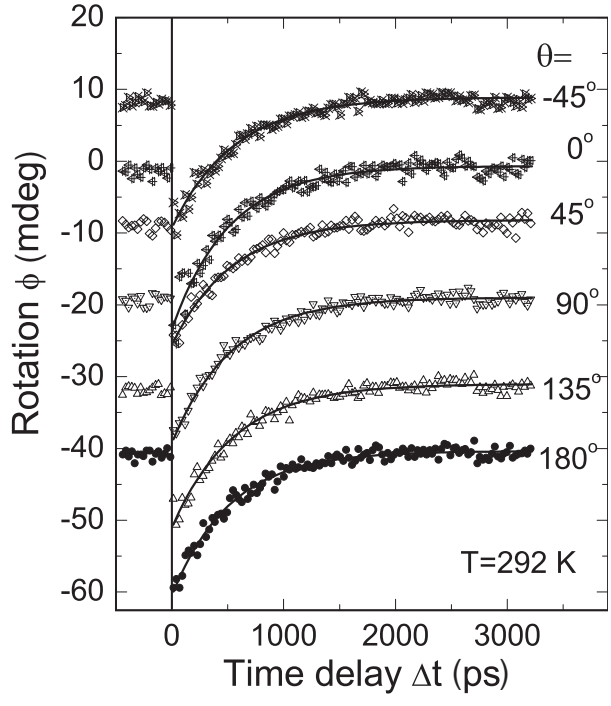

Figure 8.4: Light-induced changes of the probe polarization rotation ϕ measured at $T = 292\,\mathrm{K}$ at different orientations θ of the linear pump polarization, as shown in Fig. 8.1. Solid lines represent a fit using Eq. (8.1).

magnetic-order induced contribution (See Chapter 2.1.3). Therefore, using different mutual orientations of the polarizations of probe pulses, SHG light and the crystallographic axes we can probe the dynamics of the SHG signal, proportional to various components of the tensors $\hat{\chi}^{(i)}$ and $\hat{\chi}^{(c)}$, as discussed in the Chapter 4

In Fig.8.5(b) the time dependence of the transient SHG response is shown as measured in the geometry with $\mathbf{E}^{\mathrm{probe}} \parallel \mathbf{E}^{\mathrm{SHG}} \perp \hat{x}$ and the $\mathbf{k}^{\mathrm{probe}}$ making a finite angle with the y axis (Fig. 8.5(a)). The static measurements (see Chapter 4.4.2) showed that the main contribution to the SHG signal in this geometry is determined by the component $\chi^{(i)}_{yyy} = b$ of the crystallographic nonlinear susceptibility, caused by the spontaneous electric polarization along the y axis. A strong change of the SHG signal ($\sim$10%) is observed after the pump pulse with consequent decay, which can be fitted

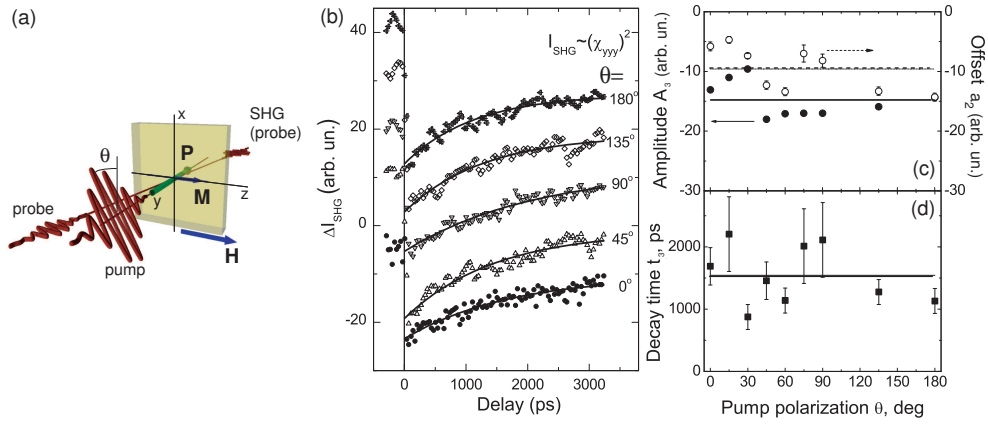

Figure 8.5: (b) Light-induced changes of the SHG component $\Delta I_{\mathrm{SHG}} \sim \chi^2_{yyy}$ measured at $T = 10\,\mathrm{K}$ for different orientations of linear pump polarization in the experimental geometry (a). Solid lines: fit of the experimental dependencies using eq. (8.4). The characteristics of the dynamics of the SHG signal obtained from the fit as a function of pump polarization θ: (c) amplitude of the exponential decay A_3 and offset a_2, (d) Decay time t_3.

by the single exponential function

$$I^{\mathrm{SHG}}(\Delta t) = a_2 + A_3 e^{-\Delta t/t_3}, \tag{8.4}$$

where the decay time $t_3 = 1550 \pm 160\,\mathrm{ps}$. The amplitude A_3 does not depend on the pump pulse polarization, as shown in Fig. 8.5(c).

The character of the time behavior of the light-induced changes ΔI^{SHG} does not evolve with temperature, as shown in Fig. 8.6(a). The amplitude A_3 slightly decreases ($\sim$20%) when the temperature is changed from 10 to 292 K (Fig. 8.6(b)). The decay time t_3 drops by $\sim$80% in the same temperature range (Fig. 8.6(c)).

Fig. 8.7(b) shows the results obtained for the SHG light polarized parallel to the x axis, as shown in (Fig. 8.7(a)). The probe beam was making a finite angle $\alpha = 10^{\mathrm{o}}$ with the y axis. In this case we investigated several orientations of the incoming probe polarization. The SHG signal is defined by the component $\chi^{(c)}_{xxx} = A$, i.e. is magnetic-order induced, when $\mathbf{E}^{\mathrm{probe}} \parallel \hat{x}$. If the electric field of the probe pulses makes a finite angle with the x axis, than the SHG signal is defined by both magnetic ($\sim \chi^{(c)}_{xxx}$, $\chi^{(c)}_{xyy}$, $\chi^{(c)}_{xzz}$) and crystallographic ($\sim \chi^{(i)}_{xxy}$) contributions. Static measurements showed that the major contribution to the static SHG signal in this geometry arises from the component $\chi^{(c)}_{xyy}$, i.e. for the incoming probe polarization perpendicular to

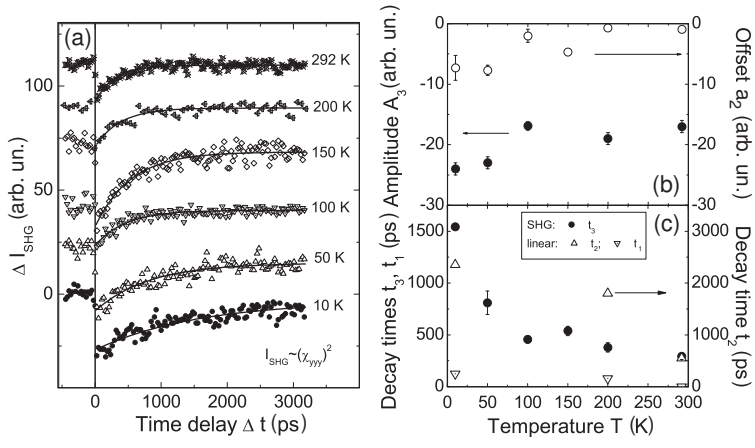

Figure 8.6: (a) Light-induced changes of the SHG component $\Delta I_{\rm SHG} \sim \chi^2_{yyy}$ measured at different temperatures. The characteristics of the dynamics of the SHG signal $\Delta I_{\rm SHG}(\Delta t) = a_2 + A_3 e^{-\Delta t/t_3}$ vs temperature T: (b) Amplitude of the exponential decay A_3 and offset a_2. (c) Decay time t_3. Decay times $t_{1,2}$ for the linear signal (Figs. 8.2(a) and 8.4) are also shown.

the x axis. As can be seen from Fig.8.7(b), the time behavior of the light-induced changes of the SHG signal for probe polarization $\xi = 0^{\rm o}$ and $\xi = 45^{\rm o}$ are very much similar and can again be described by Eq. (8.4), with the decay time $t_3 = 1012 \pm 150$ ps.

8.3 Discussion

Three distinct light-induced processes in the transient linear and nonlinear optical response are observed in our experiments. Their different time constants and the different sensitivity to the polarization of the pump pulses indicate that the intense pump pulses generate several excitations in the media. In this Section we discuss the possible origins of the observed dynamics and whether the multiferroic nature of $GaFeO_3$ manifests itself in the observed effects. We note that the response of $GaFeO_3$ to the pump pulses is drastically different from the one observed for $FeBO_3$. This can be understood from the fact that the linear magneto-optical properties of $GaFeO_3$ do not satisfy one of the main conditions for the direct effects of light on spins, i.e. a strong magneto-optical susceptibility. Moreover, as we discuss below, we did not observe any reliable manifestation of light-induced spin dynamics in $GaFeO_3$. Instead, several processes, related to light-induced change of the linear and nonlinear *optical*

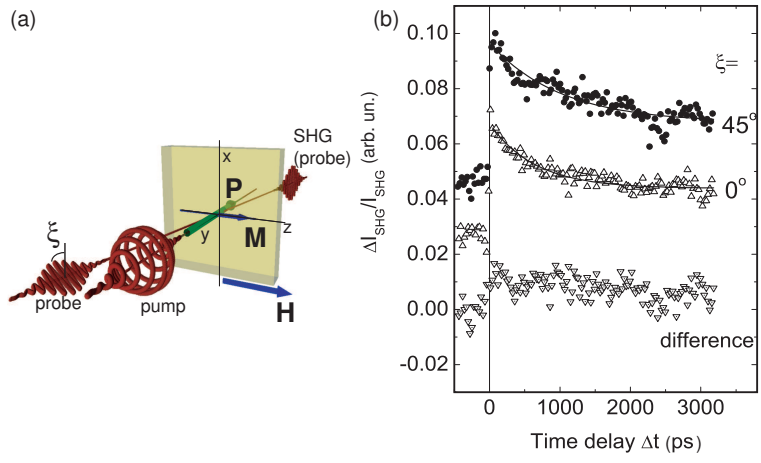

Figure 8.7: (b) Light-induced changes of the SHG component $I_{\mathrm{SHG}} \sim \chi^2_{xij}$, $i,j = x,y,z$ measured for the different orientations of the probe polarization ξ, as shown in (a). Also shown is the difference between signals measured at $\xi = 45^{\mathrm{o}}$ and $\xi = 0^{\mathrm{o}}$ ($\bigtriangledown$). Solid lines: fit, using Eq. (8.4). Temperature T=10 K.

properties of $GaFeO_3$ have been observed.

8.3.1 Light-induced optical birefringence

First we discuss the transient rotation of the probe polarization $\phi(t)$, which is sensitive to the polarization of the pump pulse θ (Eq. 8.2) and is observed at low temperatures (See Figs. 8.2 and 8.3). The rotation of the light (probe) polarization are described by the dielectric permittivity tensor $\hat{\varepsilon}$, which components, in general, can be perturbed in the presence of intense optical pump pulses. This perturbation $\delta\hat{\varepsilon}$ can lead to the transient changes in the rotation of the probe polarization. Thus, if we consider the experimental geometry, the eigenstates of the polarization for the probe beam, propagating along the y axis, can be found as a solution of the system of equations

$$\begin{cases} D_i = (\varepsilon_{ij} + \delta\varepsilon_{ij})E_j \\ D_i = n^2 E_i, \end{cases} \tag{8.5}$$

where the components of the tensor ε_{ij} are given in Table 4.2. The solution of these equations gives two refraction indices

$$n_1^2 = \varepsilon_{xx} + \delta\varepsilon_{xx} + \frac{\delta\varepsilon_{xz}^2}{\Delta\varepsilon_d + \delta\varepsilon_d}; \tag{8.6a}$$

$$n_2^2 = \varepsilon_{zz} + \delta\varepsilon_{zz} - \frac{\delta\varepsilon_{xz}^2}{\Delta\varepsilon_d + \delta\varepsilon_d}, \tag{8.6b}$$

where $\Delta\varepsilon_d = \varepsilon_{xx} - \varepsilon_{zz}$ is the crystallographic birefringence in the plane xz. ε_{ij} and $\delta\varepsilon_{ij}$ are the components of the dielectric permittivity tensor and their changes induced by the intense laser pulses.

The polarization state of these two eigenwaves is defined by the values of the light-induced modulation of the dielectric permittivity. In the absence of the pump pulse ($\delta\varepsilon_{ij} = 0$) they are two waves linearly polarized along the x and z axes. If $\delta\varepsilon_{ij} \neq 0$ these eigenwaves are, in general, two elliptically polarized waves with an ellipticity factor and azimuthal angle[1] dependent on the values of $\hat{\varepsilon}$ and $\delta\hat{\varepsilon}$. In particular, when absorption is neglected, the eigenwaves are two linearly polarized orthogonal waves which polarization plane makes an angle

$$\varsigma = \arctan \frac{\delta\varepsilon_{xz}}{\Delta\varepsilon_d + \delta\varepsilon_d} \tag{8.7}$$

with the x and z axes, respectively (See Fig. 8.8(a)).

In our experiments the probe beam was initially polarized along the x axis. Therefore, in the absence of a pump-induced birefringence (Eqs. 8.11), the probe polarization, being a polarization eigenstate of the medium, is not changed while propagating through the sample. Moreover, from Eqs.(8.7, 8.6) it follows that the light-induced modulation of the diagonal components of the dielectric permittivity tensor $\delta\varepsilon_{xx(zz)}$ alone do not lead to a change of the polarization state for the eigenmodes. Therefore, light-induced modulations $\delta\varepsilon_{xx}$ and $\delta\varepsilon_{zz}$ should not affect the state of the probe polarization. In contrast, the pump-induced modulation $\delta\varepsilon_{xz} = \delta\varepsilon_{zx}$ leads to a change of the polarization state for the eigenmodes and, consequently, can affect the polarization of the probe beam, initially polarized along the x axis. The rotation of the probe polarization in this case can be approximately written as

$$\tan\phi \approx \frac{\sqrt{2}\tan\varsigma}{2}\sqrt{1 - \cos\frac{2\pi}{\lambda}\Delta n d}, \tag{8.8}$$

where λ is the wavelength of the probe beam, $\Delta n = n_1 - n_2$ and d is the thickness of the sample measured along the y axis.

The light-induced change of the probe polarization is sensitive to the linear polarization of the pump pulse, as shown in Figs. 8.2 and 8.3. Therefore, the mechanism of light-induced modulation of the dielectric permittivity $\delta\varepsilon_{ij}$ should be polarization-sensitive. The light-induced optical birefringence is one of the most likely candidates.

For a case of the low absorbtion the influence of the intense laser pulses on the optical properties of a medium can be expressed via a polar i-tensor $\hat{\chi}$ of rank 4

$$\delta\varepsilon_{ij} = \chi_{ijkl} E_k E_l, \tag{8.9}$$

[1]The azimuthal angle in this case is the angle between the crystallographic x axis and the major axis of the polarization ellipse.

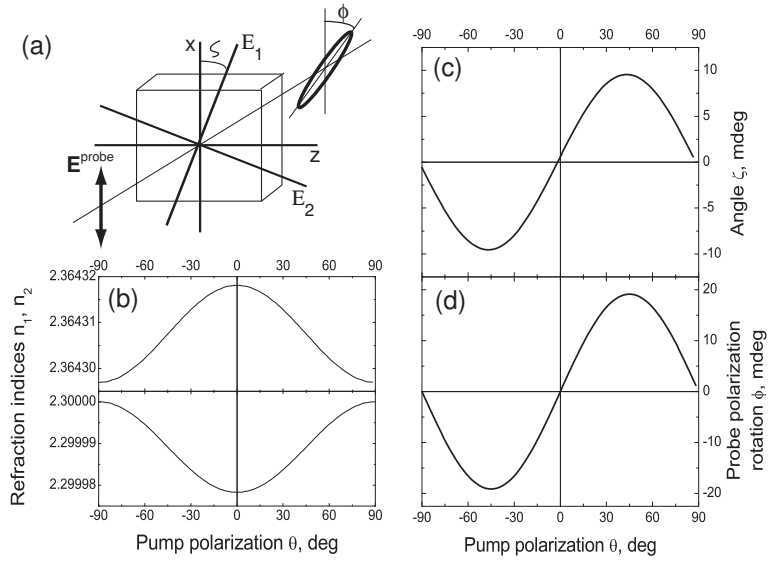

Figure 8.8: (a) Schematic representation of the effect of light-induced birefringence on the probe polarization $\mathbf{E}^{\text{probe}}$. E_1 and E_2 denote the polarization planes for the eigenwaves. (b-d) Results of simulations (see text): dependence of (b) the refraction indices n_1, n_2 (8.6) and (c) the azimuthal angle ς (8.7) for the eigenwaves on the pump polarization θ. (d) Resulting rotation of the probe polarization ϕ as a function of the pump polarization θ. Parameters used in the simulations: ε_{xx}=5.29, ε_{zz}=5.59 (See 4.9(a)), $\delta\varepsilon_{xz} = -5 \cdot 10^{-5} \sin 2\theta$, $\delta\varepsilon_d = -10^{-4} \cos 2\theta$.

where $\delta\varepsilon_{ij}$ is the light-induced change of the components of the dielectric permittivity tensor and $E_{k(l)}$ are components of the electric field of the pump pulse. The tensor χ_{ijkl} has nonzero components in any medium. For the point group of $GaFeO_3$ ($m'2'm$) they are [19]

$$\begin{aligned} xxxx = zzxx + xzzx + zxzx = zzzz = a^l; \\ yyyy = b^l; \\ xxzz = zzxx = c_1^l;\ xzxz = zxzx = c_2^l;\ xzzx = zxxz = c_3^l; \\ xxyy = zzyy = d_1^l;\ xyxy = zyzy = d_2^l;\ xyyx = zyyz = d_3^l; \\ yyxx = yyzz = e_1^l;\ yxyx = yzyz = e_2^l;\ yxxy = yzzy = e_3^l. \end{aligned} \tag{8.10}$$

Considering the experimental geometry used in the measurements and, for the sake of simplicity, neglecting the small angle between the pump pulse propagation direction

and the y axis, we get the following modulation of the dielectric permittivity by the pump pulses:

$$\delta\varepsilon_{xx} = c_1^l I_0 + (c_2^l + c_3^l) I_0 \cos^2\theta; \tag{8.11a}$$

$$\delta\varepsilon_{zz} = c_1^l I_0 + (c_2^l + c_3^l) I_0 \sin^2\theta; \tag{8.11b}$$

$$\delta\varepsilon_d = \delta\varepsilon_{xx} - \delta\varepsilon_{zz} = (c_2^l + c_3^l) I_0 \cos 2\theta; \tag{8.11c}$$

$$\delta\varepsilon_{xz} = \delta\varepsilon_{zx} = \frac{1}{2}(c_2^l + c_3^l) I_0 \sin 2\theta, \tag{8.11d}$$

We performed simulations in order to estimate the value of the light-induced modulation of the dielectric permittivity $\delta\varepsilon_{xz}$ which would lead to a rotation of the probe polarization comparable with the one observed in the experiment. The values of the crystallographic birefringence (ε_{xx} and ε_{zz}) were obtained from the ellipsometric measurements discussed in Chapter 4. The results of the simulations are presented in Fig. 8.8(b-d). A weak change of the off-diagonal component of the dielectric permittivity tensor ($\delta\varepsilon_{xz}/\varepsilon_{xx} \approx 10^{-5}$) leads to a rotation of the probe polarization of about 20 mdeg, which is in agreement with our experimental results (Figs. 8.2(a)). The dependence of the effect on the pump polarization is also in good agreement with the one observed in the experiments (Figs. 8.3(c)).

In a condensed medium, the two main mechanisms of light-induced birefringence are electronic and electrostrictive ones [20]. However, in the case of short (below 1 ns) optical pulses, the contribution of the electrostrictive mechanism to the light-induced birefringence becomes very small as compared to the case of longer pulses [20]. Therefore, the electronic mechanism is expected to play a major role. The electronic contribution to the light-induced birefringence can be observed in both transparent and absorptive media. In a case of a transparent medium the typical response time for the electronic contribution to the light-induced birefringence is of the order of femtoseconds. The effect would be coherent and observed while the pump pulse is present. From our experimental data (Figs. 8.3(a,b,d)) it is follows that the pump-induced effect is observed during a rather long time (t_1=125 ps at T=10 K) after the pump pulse is gone, indicating that the "driving force" causing the birefringence $\delta\hat{\varepsilon}$, deposited in the system by the pulse, decays much slower that the typical time of optical coherence.

This is a direct indication of the fact that absorption plays a significant role in the process. In this case the electronic mechanism involves a population redistribution at the involved energy levels. In our experiments the pulse central photon energy 1.54 eV, although being well below the absorption edge, corresponds to the localized $d-d$ transitions ${}^6A_1 \rightarrow {}^4T_1$ in the Fe^{3+}, which are significantly enhanced due to the strong asymmetry of the crystallographic positions occupied by the iron ions and the admixing of the broad intense charge-transfer transitions above 3 eV (Fig. 4.9(a)). Therefore, this enhanced absorption of the pump pulse might lead to changes of the optical properties of the compound persistent after the end of the pump

pulse. Moreover, the transition ${}^6A_1 \rightarrow {}^4T_1$ possesses some anisotropy in the absorption coefficient $\alpha_{xx} \neq \alpha_{zz}$, as can be seen from the absorption spectra for $GaFeO_3$ (Fig. 4.8(b)). Therefore, a sensitivity of the effect to the polarization of the pump pulse with respect to the crystallographic axes x and z is also expected.

8.3.2 Light-induced dynamics of the SHG signal

The dynamics of the SHG signal polarized along the x axis (Fig. 8.7) might reveal light-induced changes of the magnetization. Indeed, as was shown in Chapter 4.4, the SHG signal in this geometry is defined by several components of the non-linear susceptibility, some of which are of magnetic origin:

$$I^{2\omega}_{\parallel x} = |A\cos^2\xi + (0.04B + 0.96C)\sin^2\xi + 0.17d\sin 2\xi|^2 I^{\omega}_{\text{probe}}; \tag{8.12}$$

where ξ is the polarization angle for the probe beam. The angle of incidence for the probe beam $\alpha = 10^{\text{o}}$ is taken to obtain the numerical coefficients. The nonlinear susceptibilities are (See Eq. 4.4)

$$\chi^{(i)}: \quad d = xxy = xyx, \tag{8.13a}$$

$$\chi^{(c)}: \quad A = xxx,\ B = xyy,\ C = xzz. \tag{8.13b}$$

Thus, the SHG signal for the probe polarization angle $\xi = 0^{\text{o}}$ is defined only by the magnetic contribution to the nonlinear susceptibility

$$I^{2\omega}_{\parallel x}(\xi = 0^o) = |A|^2 I^{\omega}_{\text{probe}}. \tag{8.14}$$

Therefore, the dynamics of the SHG signal measured in this geometry reveals the dynamics of the magnetic contribution to the nonlinear susceptibility

$$\frac{\Delta I^{2\omega}_{\parallel x}}{I^{2\omega}_{\parallel x}}(\xi = 0^o) = \left(1 + \frac{\Delta A}{A}\right)^2 - 1 \approx 2\frac{\Delta A}{A}. \tag{8.15}$$

Here and below we assume the light-induced changes of the nonlinear susceptibility to be small.

For the probe polarization angle $\xi = 45^{\text{o}}$, dynamics of both magnetic and crystallographic components of the nonlinear susceptibility can contribute to the observed signal

$$I^{2\omega}_{\parallel x}(\xi = 45^o) = |0.5A + 0.02B + 0.48C + 0.17d|^2 I^{\omega}_{\text{probe}} = |\chi^{m;45^{\text{o}}} + \chi^{cr;45^{\text{o}}}|^2 I^{\omega}_{\text{probe}}, \tag{8.16}$$

where $\chi^{m;45^o} = 0.5A + 0.02B + 0.48C$ and $\chi^{cr;45^o} = 0.17d$. The light-induced change of the SHG signal is then

$$\frac{\Delta I^{2\omega}_{\parallel x}}{I^{2\omega}_{\parallel x}}(\xi = 45^o) = 2\frac{\Delta\chi^{m;45^o} + \Delta\chi^{cr;45^o}}{\chi^{m;45^o} + \chi^{cr;45^o}} + \left(\frac{\Delta\chi^{m;45^o} + \Delta\chi^{cr;45^o}}{\chi^{m;45^o} + \chi^{cr;45^o}}\right)^2 \approx 2\frac{\Delta\chi^{m;45^o} + \Delta\chi^{cr;45^o}}{\chi^{m;45^o} + \chi^{cr;45^o}}. \quad (8.17)$$

From the analysis of the static SHG signal we can conclude that, for the given polarizations ($\xi = 45^o$, $\mathbf{E}^{2\omega} \parallel \hat{x}$), the crystallographic ($\chi^{cr;45^o}$) and magnetic ($\chi^{m;45^o}$) contributions are comparable, resulting in a high magnetic contrast, as shown in Fig. 4.11(a).

The intensity of the SHG signal polarized perpendicularly to the x axis is described by (See Eq. 4.5(b))

$$I^{2\omega}_{\perp x} = |0.17[a\cos^2\xi + (0.03b + 0.97c)\sin^2\xi + 0.17D\sin 2\xi] + 0.98[0.12e\sin^2\xi + 0.98E\sin 2\xi]|^2, \quad (8.18)$$

where the angle of incidence $\alpha = 10^o$ for the probe beam is taken to obtain the numerical coefficients. The nonlinear susceptibilities are (See Eq.4.4)

$$\chi^{(i)}: \ a = yxx,\ b = yyy,\ c = yzz,\ e = zzy = zyz \quad (8.19a)$$

$$\chi^{(c)}: \ D = yyx = yxy,\ E = zzx = zxz \quad (8.19b)$$

For the geometry used in our experiments ($\xi = 90^o$) the intensity of the SHG signal is

$$I^{2\omega}_{\perp x} = |0.0051b + 0.016c + 0.12e|^2, \quad (8.20)$$

i.e. only the crystallographic contribution to the signal is observed. Consequently, the dynamics of the SHG signal measured in this geometry reveals solely the dynamics of the crystallographic contributions to the susceptibility:

$$\frac{\Delta I^{2\omega}_{\perp x}}{I^{2\omega}_{\parallel x}}(\xi = 90^o) \approx 2\frac{\Delta\chi^{cr;90^o}}{\chi^{cr;90^o}}, \quad (8.21)$$

where $\chi^{cr;90^o} = 0.0051b + 0.016c + 0.12e$.

The Eqs. (8.15, 8.17, 8.21) show that a modulation of the magnetic part of the nonlinear susceptibility due to light-induced changes of the magnetic order would be manifested in the transient SHG signal, shown in Fig. 8.7(b), while the data in Fig. 8.5(b) reveal only the non-magnetic light-induced dynamics. Thus, comparison of the results presented in Figs. 8.5(b) and 8.7(b) allows to draw several conclusions.

First, from Fig. 8.7(b) it follows that, a difference between the transient SHG intensities at $\xi = 0^o$ and $\xi = 45^o$ is below the signal-to-noise ratio in the experiment. Signals measured for these two probe polarizations demonstrate the same behavior, described by Eq. 8.4, with a decay time $t_3 = 1012 \pm 150$ ps. Therefore, the pump-induced changes of the magnetic susceptibility $\Delta\chi_{xxx} = \Delta A$ (Fig.8.7(b)) cannot be directly attributed to light-induced magnetization dynamics.

Second, from Eq. (8.17) it follows that for $\xi = 45^o$ the transient SHG signal might reveal dynamics of both non-magnetic and magnetic contributions to the nonlinear susceptibility. However, only one process described by Eq. (8.4) is observed, leading to the conclusion that the light-induced dynamics of the magnetic and crystallographic contributions to $\hat{\chi}$ are of the same origin.

Third, the light-induced changes of the magnetic susceptibility $\hat{\chi}^m$ dominate in signals observed for the light polarized parallel to the x axis. However, the dynamics of the purely crystallographic contribution to the SHG signal (Fig. 8.5(b)) is again described by Eq. 8.4, with a decay time $t_3 = 1550 \pm 150$ ps, which is quite close to the time obtained for the dynamics of the magnetic contribution (Fig. 8.7(b)). Therefore, we conclude that the transient SHG signal, observed in all three experimental geometries discussed here is of the same origin and not related to light-induced changes of the magnetic order.

The light-induced dynamics of the SHG response measured in all experimental geometries appeared to be insensitive to the polarization of the pump pulses (Fig. 8.5(a)). In the light-induced dynamics of the linear optical signal we can also distinguish a contribution, which is insensitive to the polarization of the pump pulses (Fig.8.3(a,b)). The decay times t_3 and t_2, characterizing these processes, are decreasing with increasing temperature and have a ratio close to 1:2 within the experimental error (Fig. 8.6(c)). These two processes, therefore, might be related to each other.

Indeed, the central photon energy for the pump pulse coincides with the localized $d - d$ transition ${}^6A_1 \rightarrow {}^4T_1$, enhanced by the proximity of the broad intense charge-transfer transitions. Therefore, the dynamics, observed in the linear optical response might be related to the change of population of the ${}^4T_1$ level of the Fe^{3+} ions. The second harmonic generation, in turn, can also utilize this level as an intermediate state and one of the lowest CT excited state above 3 eV as a final state. Therefore, the light-induced changes in the transient SHG response, observed in our experiments, might be related to the light-induced changes in the population of the ${}^4T_1$ level. In this case the decay time t_3 for the transient SHG signal is related to the relaxation of the population of this level and should be twice as short as the one observed in the linear optical experiments, which is close to the results obtained in our experiments. However, systematic measurements of light-induced dynamics as a function of the pump and probe photon energies are required in order to verify this conclusion. The spectral dependence of the static SHG signal in $GaFeO_3$ for the fundamental photon energy in the range close to 1.54 eV has been reported in [21]. However, only the

signal proportional to the magnetic contribution of the nonlinear susceptibility $\sim A = \chi_{xxx}$ has been investigated. In [22] a study of the crystallographic SHG response for the SHG photon energy in the same range is reported. In both cases a resonant enhancement of the SHG signal in the region close to the ${}^6A_1 \rightarrow {}^4T_1$ transition has been observed.

In conclusion, optical pump-probe experiments did not reveal any reliable indication of light-induced magnetization dynamics in the multiferroic $GaFeO_3$. Instead, a light-induced optical birefringence has been observed with a life-time of 125 ps at low temperature. We proposed a correlation between light-induced dynamics of the linear and nonlinear optical response which is related to the light-induced changes of the intensity of the localized $d-d$ transition in Fe^{3+} ions. It is important to note that, although we did observe light-induced dynamics of the SHG signal in the geometry where there is only a magnetic contribution to the SHG response, we cannot ascribe this dynamics to the magnetization. This indicates that the interpretation of the observations of light-induced dynamics in the SHG response of magnetic media requires a careful analysis.

References

[1] G. A. Smolenskii and I. E. Chupis, Sov. Phys. - Usp. **25**, 475 (1982).

[2] M. Fiebig, J. Phys. D: Appl. Phys **38**, R123 (2005).

[3] W. Eerrenstein, N. D. Mathur, and J. F. Scott, Nature (London) **442**, 759 (2006).

[4] N. A. Spaldin and M. Fiebig, Science **309**, 391 (2005).

[5] J. H. Jung, M. Matsubara, T. Arima, J. P. He, Y. Kaneko, and Y. Tokura, Phys. Rev. Lett. **93**, 037403 (2004).

[6] B. B. van Aken, J.-P. Rivera, H. Schmidt, and M. Fiebig, Nature (London) **449**, 702 (2007).

[7] B. B. Krichevtsov, V. V. Pavlov, R. V. Pisarev, and V. N. Gridnev, Phys. Rev. Lett. **76**, 4628 (1996).

[8] G. L. J. A. Rikken, C. Strohm, and P. Wyder, Phys. Rev. Lett. **89**, 133005 (2002).

[9] J. T. Rado, Phys. Rev. Lett. **13**, 335 (1964).

[10] Yu. F. Popov, A. M. Kadomtseva, G. P. Vorob'ev, V. A. Timofeeva, D. M. Ustinin, A. K. Zvezdin, and M. M. Tegeranchi, Sov. Phys. - JETP **87**, 146 (1987).

[11] N. Kida, Y. Kaneko, J. P. He, M. Matsubara, H. Sato, T. Arima, H. Akoh, and Y. Tokura, Phys. Rev. Lett. **96**, 167202 (2006).

[12] T. Gerrits, H. A. M. van den Berg, J. Hohlfeld, L. Bär, and Th Rasing, Nature (London) **418**, 509 (2002).

[13] T. Gerrits, M. L. Schneider, A. B. Kos, and T. J. Silva, Phys. Rev. B **73**, 094454 (2006).

[14] T. Gerrits, T. J. Silva, J. P. Nibargera, and T. Rasing, J. Appl. Phys. **96**, 6023 (2004).

[15] H. Regensburger, R. Vollmer, and J. Kirschner, Phys. Rev. B **61**, 14716 (2000).

[16] A. Melnikov, I. Radu, U. Bovensiepen, O. Krupin, K. Starke, E. Matthias, and M. Wolf, Phys. Rev. Lett. **91**, 227403 (2003).

[17] T. Gerrits, T. J. Silva, and T. Rasing, Rev. Sci. Instrum. **77**, 034704 (2006).

[18] T. Satoh, N. P. Duong, and M. Fiebig, Phys. Rev. B **74**, 012404 (2006).

[19] R. R. Birss, Rep. Prog. Phys. **26**, 307 (1963).

[20] Y. R. Shen, *Principles of Nonlinear Optics* (J. Wiley & Sons, New York, 1984).

[21] Y. Ogawa, Y. Kaneko, J. P. He, X. Z. Yu, T. Arima, and Y. Tokura, Phys. Rev. Lett **92**, 047404 (2004).

[22] K. Eguchi, Y. Tanabe, T. Ogawa, M. Tanaka, Y. Kawabe, and E. Hanamura, J. Opt. Soc. Amer. B **22**, 128 (2005).

Summary

The interaction of ultrashort intense laser pulses with condensed matter has emerged as a subject which combines exciting fundamental physics with important potential applications. During the last two decades many novel, sometimes controversial, effects were observed in magnetic solids subjected to the action of laser pulses with duration below 1 ps=10^{-12} s. These observations provide new, more comprehensive insight into the fundamental properties of matter and light-matter interactions. Moreover, the excitation by sub-picosecond laser pulses brings a medium to a strongly nonequilibrium state and, therefore, opens new pathways for modification and control of material parameters by light on a timescale comparable with the duration of the pulse.

The interest in the effects of subpicosecond laser pulses on magnetically-ordered media grew rapidly after the pioneering observation of the destruction of magnetic order in a metallic film within the first picosecond after excitation by a 60 fs laser pulse. The subsequent experimental and theoretical efforts of many research groups resulted in the discovery of a large number of light-induced ultrafast processes in magnetic media. Along with an interesting physical picture of these processes, the reported observations of *laser-induced ultrafast magnetization dynamics* fuel the discussion on the feasibility of magnetization manipulation by laser pulses. Several important issues should be addressed before it would be possible to claim that the interactions of subpicosecond laser pulses with a magnetic medium are understood. One of these issues is the question about possible paths of angular momentum transfer, which necessarily accompanies the excitation of magnetization dynamics.

The main part of this thesis is devoted to so-called *ultrafast opto-magnetic effects* in a magnetic multi-sublattice medium. An important and unique characteristic of these effects is that their existence and efficiency are determined by the polarization

of the laser pulses and, thus, they are the first to be considered as candidates for the control of spins by light. Moreover, such effects provide an opportunity to clarify the role of photon angular momentum in the excitation of ultrafast spin dynamics.

Our experimental observations of coherent spin precession in iron borate $FeBO_3$ excited by 100 fs laser pulses appeared to contradict previously proposed scenarios. The major novelty consisted in *the generation of coherent spin precession by linearly-polarized laser pulses* and the domination of this effect over the effect of circularly-polarized ones. Earlier, circular polarization was thought to be crucial for the excitation because of the angular momentum carried by circularly polarized photons.

We developed a phenomenological theory to describe the excitation process of coherent spin precession by polarized short laser pulses via *impulsive stimulated Raman scattering* (ISRS), which is a special case of Raman scattering, emerging if the spectral width of the exciting laser pulse exceeds the eigenfrequency of coherent spin precession in the medium (a 100 fs laser pulse at 800 nm corresponds to a spectral width of 45 meV, while spin precession frequencies are typically of the order of a few meV). We also considered the excitation of coherent spin precession using an approach, where the action of the laser pulses and the excited spin precession are described by effective fields and the Lanadau-Lifshitz equation, respectively. Although this approach was used earlier in a certain form to analyze various light-induced processes, we showed that a more intricate situation occurs when a multi-sublattice medium is concerned. In particular, *in a magnetically-ordered medium both circularly and linearly polarized laser pulses can act on spins as pulses of an effective magnetic field.*

This combined theoretical and experimental study allowed us to show unambiguously that ISRS is indeed the microscopical mechanism of the excitation of coherent spin precession in our experiments and in some earlier reported experiments on ultrafast opto-magnetic effects. This mechanism is not restricted to the case of circularly-polarized laser pulses. This observation allowed us to argue that *angular momentum transfer between photons and spins is not required* for the excitation of spin dynamics. It is this transfer which was often considered as an obstacle on the way towards an all-optical magnetization reversal. And indeed, the feasibility of all-optical magnetization reversal was demonstrated recently.

Moreover, we have shown that the efficiency of the spin precession excitation is defined by the magnetic anisotropy of a medium, namely the ellipticity of the spin precession, and not only by its magneto-optical properties, as was thought earlier. Because of this, *the mutual orientation of magnetic moments and laser pulse propagation direction is crucial for the excitation process in a magnetically-ordered medium.* Thus, in a multi-sublattice magnetic medium, a proper choice of this mutual orientation can lead to a significant enhancement or suppression of the excited coherent spin precession. This demonstrates that complex but well defined magnetic structures, such as antiferromagnets and weak ferromagnets are interesting and promising objects for further studies of ultrafast light-induced magnetization dynamics.

Samenvatting

De wisselwerking van ultrakorte laserpulsen met gecondenseerde materie heeft zich ontwikkeld tot een onderwerp waarin spannend fundamenteel onderzoek wordt gecombineerd met belangrijke mogelijke toepassingen. In de laatste twintig jaar zijn er veel nieuwe, soms controversiele, effecten waargenomen in vaste stoffen die waren blootgesteld aan de invloed van laserpulsen die korter waren dan 1ps. Deze waarnemingen hebben geleid tot nieuw en meer volledig inzicht in de fundamentele eigenschappen van materie en in de wisselwerking van licht met materie. Bovendien wordt een medium door de excitatie van sub-picoseconde laserpulsen in een sterk niet-evenwichtstoestand gebracht, waardoor nieuwe mogelijkheden voor de verandering en controle van materiaal parameters door middel van licht worden geboden op een tijdschaal van de pulsduur.

De belangstelling voor de gevolgen van de interactie van subpicoseconde laserpulsen met magnetisch geordende materie groeide explosief na de baanbrekende ontdekking dat de magnetisatie in een metaalfilm binnen een picoseconde verdween na excitatie door een laserpuls van 60fs (femtoseconde). De daarop volgende experimentele en theoretische inspanningen van vele onderzoeksgroepen leidde tot de ontdekking van een groot aantal, door *licht geinduceerde, supersnelle processen in magnetische materialen*. Naast nieuw fysisch inzicht leidde deze waarnemingen tot discussies over de mogelijkheden om met laserpulsen de magnetisatie te kunnen manipuleren. Er moeten echter nog een aantal belangrijke zaken worden opgelost alvorens men kan beweren dat de interactie van subpicoseconde laserpulsen met materie is begrepen. Onder andere wat zijn de mogelijke kanalen voor de, met magnetisatie verandering gepaard gaande, overdracht van draaiimpuls?

Het grootste deel van dit proefschrift is gewijd aan *supersnelle* zogenaamde *opto-*

magnetische effecten in een welbekend en goed gekarakteriseerd materiaal met verschillende magnetische subroosters. Een belangrijke en unieke eigenschap van deze effecten is dat hun optreden en efficientie bepaald worden door de polarisatie van de laser pulsen, waardoor ze bij uitstek geschikt zijn voor de controle van magnetisme met licht. Bovendien geven ze de mogelijkheid om de rol van het draaimoment van fotonen bij de excitatie van magnetisatie dynamica te verhelderen. Onze experimentele waarnemingen betreffende de coherente precessie van de magnetische momenten in $FeBO_3$, geexciteerd door 100 fs laserpulsen, blijken het merendeel van de voorgestelde scenario's te weerspreken. De belangrijkste nieuwe ontdekking is *de generatie van coherente precessie van de magnetische momenten door lineair gepolariseerde laserpulsen*, en het feit dat deze laatste een sterker effect veroorzaken dan circulair gepolariseerd licht.

We hebben een fenomenologisch model ontwikkeld dat het excitatie proces van de coherente precessie van magnetische momenten beschrijft via "*impulsieve gestimuleerde Raman verstrooiing*"(impulsive stimulated Raman scattering or ISRS). Dit is een speciaal geval van Raman verstrooiing dat op kan treden als de spectrale breedte van de excitatie puls groter is dan de frequentie van de betreffende coherente precessie (een laserpuls van 100 fs en een golflengte van 800nm correspondeert met een spectrale pulsbreedte van 45 meV, terwijl typische magnon frequenties van de orde van een paar meV zijn). We hebben de excitatie van de spin precessie ook beschreven door de, via het licht opgewekte, effectieve magnetische velden in te voeren als de drijvende krachten in de Landau-Lifschitz vergelijking. Hoewel dit al eerder was gedaan laten wij hier zien dat de situatie voor een materiaal met multi-magnetische subroosters wel wat ingewikkelder is en dat, *voor een magnetisch geordend systeem, zowel circulair als lineair gepolariseerd licht kan leiden tot effectieve magnetische velden.* Uit dit gecombineerde theoretische en experimentele werk volgt dat ISRS inderdaad het correcte microscopische mechanisme is voor de excitatie van de coherente spinprecessie in onze en enkele eerder gerapporteerde optomagnetische experimenten. Dit mechanisme is dus niet gelimiteerd tot circulair gepolariseerde pulsen, waaruit meteen volgt dat *de overdracht van draaimoment tussen fotonen en magnetische momenten niet essentieel is om de laatsten tot precessie te brengen.* Deze overdracht werd tot nu toe als noodzakelijk en daardoor ook als hinderpaal gezien om tot volledig optisch schakelen van de magnetisatie te komen. Dit laatste is inderdaad recentelijk aangetoond.

We hebben bovendien laten zien dat de efficientie van deze optische excitatie bepaald wordt door de magnetische anisotropie, en dus de ellipticiteit van de precessie en niet, zoals oorspronkelijk gedacht, uitsluitend door de magneto-opische eigenschappen. Dat betekent dat *de relatieve orientatie van de magnetische momenten en de voortplantingsrichting van het licht een essentiele parameter is voor het excitatie proces in een magnetisch geordend materiaal.* Met andere woorden, in het geval van multi-magnetische subroosters kan de juiste keuze voor deze onderlinge orientatie leiden tot zowel een flinke versterking als ook onderdrukking van de optisch geexciteerde

spin precessie. Dit laat tevens zien dat ingewikkelde, maar goed gedefinieerde magnetische structuren zoals zwakke ferromagneten en antiferromagneten interessante en veelbelovende studieobjecten zijn voor een beter begrip van optisch geinduceerde supersnelle magnetisatie dynamica.

List of Publications

[1] A. M. Kalashnikova, A. V. Kimel, R. V. Pisarev, V. N. Gridnev, P. A. Usachev, A. Kirilyuk, and Th. Rasing, "Impulsive generation of coherent magnons and phonons by subpicosecond laser pulses in the weak ferromagnet $FeBO_3$," *Phys. Rev. B*, vol. 78, p. 104301(21), September 2008.

[2] P. A. Markovin, A. M. Kalashnikova, R. V. Pisarev, and Th. Rasing, "Optical study of the electronic structure and magnetic ordering in a weak ferromagnet $FeBO_3$," *JETP Lett.*, vol. 86, pp. 712–717, December 2007.

[3] A. M. Kalashnikova, A. V. Kimel, R. V. Pisarev, V. N. Gridnev, A. Kirilyuk, and Th. Rasing, "Impulsive generation of coherent magnons by linearly polarized light in the easy-plane antiferromagnet $FeBO_3$," *Phys. Rev. Lett.*, vol. 99, p. 167205(4), October 2007.

[4] R. V. Pisarev, A. S. Moskvin, A. M. Kalashnikova, A. A. Bush, and Th. Rasing, "Anomalous optical properties of the mixed-valent lithium cuprate $LiCu_2O_2$," *Phys. Rev. B*, vol. 74, p. 132509(4), October 2006.

[5] A. M. Kalashnikova, R. V. Pisarev, L. N. Bezmaternykh, V. L. Temerov, A. Kirilyuk, and Th. Rasing, "Optical and magneto-optical studies of a multiferroic $GaFeO_3$ with a high Curie temperature," *JETP Lett.*, vol. 81, pp. 452–457, 2005.

[6] V. V. Pavlov, A. M. Kalashnikova, R. V. Pisarev, I. Sänger, D. R. Yakovlev, and M. Bayer, "Magnetic-field-induced second harmonic generation in semiconductor GaAs," *Phys. Rev. Lett.*, vol. 94, p. 157404(4), April 2005.

[7] V. V. Pavlov, A. M. Kalashnikova, R. V. Pisarev, I. Sänger, D. R. Yakovlev, and M. Bayer, "Second-harmonic generation in the magnetic semiconductor (Cd,Mn)Te," *J. Opt. Soc. Am. B*, vol. 22, pp. 168–175, January 2005.

[8] A. M. Kalashnikova, V. V. Pavlov, R. V. Pisarev, Yu. E. Kalinin, A. V. Sitnikov, and Th. Rasing, "Optical and magneto-optical properties of granular magnetic nanostructures CoFeB/SiO_2 and CoFeZr/Al_2O_3," *Phys. Solid State*, vol. 46, pp. 2163–2170, 2004.

[9] A. M. Kalashnikova, V. V. Pavlov, R. V. Pisarev, M. Bayer, and Th. Rasing, "Linear and nonlinear optical spectroscopy of gadolinium ferroborate $GdFe_3(BO_3)_4$," *JETP Lett.*, vol. 80, pp. 293–297, 2004.

[10] A. M. Kalashnikova and R. V. Pisarev, "Electronic structure of hexagonal rare-earth manganites $RMnO_3$," *JETP Lett.*, vol. 78, pp. 143–147, 2003.

This manuscript includes results published in [1, 2, 3, 5].

Curriculum Vitae

Name:
Alexandra Mikhailovna Kalashnikova
Date of birth:
12 May 1980
Place of birth:
Leningrad, USSR

1986−1997	School 129, St.-Petersburg, Russia. Graduated with distinction.
1997−2003	Student at engineering-physical faculty of St. Peterburg State Institute of Precision Mechanics and Optics (Technical University), St.-Petereburg, Russia. Engineer degree (cum laude)
2003−2007	Ph.D. studies at A. F. Ioffe Physico-Technical Institute, St.-Petersburg, Russia
2003-2004	3.5 month as the visiting researcher at the group of Prof. dr. M. Bayer, Dortmund University, Germany
October 2004-January 2005	visiting researcher at the group of Prof. dr. Th. Rasing, Radboud University Nijmegen, The Netherlands
2005−2009	Ph.D. studies at Radboud University Nijmegen, The Netherlands